ISBN 978-82-326-3902-1 (printed version)
ISBN 978-82-326-3903-8 (electronic version)
ISSN 1503-8181

NTNU
Norwegian University of
Science and Technology

Doctoral Thesis

Markus Peter Först

Doctoral theses at NTNU, 2019:152

NTNU

Doctoral theses at NTNU, 2019:152

Markus Peter Först

Effects of Flow Dynamics on Bank Erosion in Consecutive Meander Bends.

A Field Study

NTNU
Norwegian University of
Science and Technology
Faculty of Engineering
Department of Civil and Environmental Engineering

NTNU
Norwegian University of
Science and Technology

Markus Peter Först

Effects of Flow Dynamics on Bank Erosion in Consecutive Meander Bends.

A Field Study

Thesis for the degree of Philosophiae Doctor

Trondheim, May 2019

Norwegian University of Science and Technology
Faculty of Engineering
Department of Civil and Environmental Engineering

NTNU
Norwegian University of
Science and Technology

NTNU
Norwegian University of Science and Technology

Thesis for the degree of Philosophiae Doctor

Faculty of Engineering
Department of Civil and Environmental Engineering

© Markus Peter Först

ISBN 978-82-326-3902-1 (printed version)
ISBN 978-82-326-3903-8 (electronic version)
ISSN 1503-8181

Doctoral theses at NTNU, 2019:152

Printed by Skipnes Kommunikasjon as

“However difficult life may seem, there is always
something you can do, and succeed at.
It matters that you don’t just give up.”

Stephen Hawking
Cambridge symposium, January 2012

Abstract

The present dissertation describes the influence of natural alteration in the rivers flow regime on the change of morphology of a freely meandering river in Norway. It consists of a thesis and four attached research papers.

Erosion along riverbanks is an important issue due to loss of soil, wildlife habitat, pollution or reservoir-filling. The interest in the erosion processes, lies in the huge economical and environmental damage happening each year. Bank failure is mainly driven by mass failure and fluvial erosion processes.

This thesis and research has focused on two different research sites. One site is a river bend located in middle Norway with some erosion protection near infrastructure. The other site is a meandering river located in northern Norway. This river is without erosion protection. Both sites are situated in unregulated catchments. This work investigates the fluvial erosion process in natural rivers at a microscale.

Methods used, are Terrestrial Laser Scanner (TLS) in order to monitor changes in river bank morphology. The bathymetry has been mapped with Real Time Kinetic GPS (RTK-GPS) and Acoustic Doppler Current Profiler (ADCP) measurements. The sediment properties of a two layer river bank has been analyzed.

The numerical model CONservational Channel Evolution and Pollutant Transport System (CONCEPTS) has been used to model the bank retreat at the river in middle Norway. The results showed that this model is not suitable for arctic climates.

For the second site, transect across three meanders in the river have been measured with an ADCP as moving boat transects and stationary. The data has been post processed by distance averaging. This new method for post processing of flow data from an ADCP made it possible to identify different flow structures in nature. These flow structures were the high velocity cell, the secondary current and the secondary outer cell. Their behavior has been compared to the bathymetry of the river. The non-conformity between water flows and bathymetry indicates that the bathymetry is strongly influenced by the hydraulic. Later calculations of shear stress from stationary ADCP measurements confirm this assumption. These data also showed a link between the movement of the high velocity cell and the appearance of the secondary outer cell. The observation of the secondary outer cell and the erosion and sedimentation along the cut bank leads to the assumption that the secondary outer cell reduces the fluvial erosion. Observed flash floods, which had no effect on erosion, might be explained by this phenomenon.

Acknowledgements

First of all I want to thank my supervisor Dr. Nils Rüther, Associate Professor at the Department of Hydraulic and Environmental Engineering. He gave me the opportunity to move and live in Norway. He supported me with everything I needed to finish this adventure. He had the patience to accompany me through all these years and encouraged me to go to conferences all over the world.

I want to thank you all from the Institute of Environmental Engineering. For the professional discussions and at least not less important the friendship, which made it much easier to live in a country thousands of kilometers away from family and friends. Just to drop a few names: Daniela Pallischeck, Emmanuel Jjungu, Geir Tesaker, Geir Walsø, Hege Livden , Knut Alfredsen, Netra Timalsina, Nils Reidar Bøe Olsen, Peggy Zinke, Robert Feurich, Stefan Haun, Stephan Spiller, Thomas Meyn. I also want to mention the students who worked with me during summer in the field (Christian, Felix, Jake, Lydia, Tyler, Susanne).

I also would like to thank Sweco Norge AS, who give me the opportunity to finish this PhD. I was able to choose my time to work at the institute and was supported by my group leader Wolf Dietrich Marchand, and division leader Per Ivar Bergan and all my colleagues, who showed understanding.

My family, Ingunn and my daughter Senja, deserve a very special thank you as they have supported me while they have had to step back during the last month in order to give me the time and space I needed to finish this PhD. Senja was worried, that I am ill, as she was told I am working on my “doctor”.

I want to mention my friends in Germany, who stayed in touch and visited me here in Norway (Brigitte, Heike, Katharina, Kati, Patrick, Manfred).

A very special thank you to Bernhard Edmaier, whom I am a huge fan of. He allowed me to use one of his photographs from his book “Water” as cover for this thesis.

Finally, a huge thank you to Jesse Smith, who proofread this thesis.

Contents

List of Papers

Journal

A) Foerst, Markus; Ruther, Nils. (2012) Post Processing Methods of Moving Boat ADCP Measurements Time Averaging vs. Distance Averaging. Berichte des Lehrstuhls und der Versuchsanstalt für Wasserbau und Wasserwirtschaft. vol. 125.

B) Foerst, Markus; Rüther, Nils (2018): Bank Retreat and Streambank Morphology of a Meandering River during Summer and Single Flood Events in Northern Norway. Hydrology, 5(4), 68; https://doi.org/10.3390/hydrology5040068

Conference

C) Foerst, Markus; Nils Rüther, Hahn, Felix (2011): Evaluating erosion processes of a two layer river bank. River, Coastal and Estuarine Morphodynamics: RCEM, Beijing.

D) Foerst, Markus; Nils, Ruther (2012): Mean and turbulent flow structures in two consecutive meander bends. 2nd IAHR Europe Conference. TU Munich; Munich. 2012-06-27 - 2012-06-29.

Minor

E) Foerst, Markus; Ruther, Nils; Hahn, Felix. (2012) Terrestrial Laser Scan (TLS) Measurement and Acoustic Doppler Current Profilers (ADCP) – a new Method to Understand Bank Retreat in Natural River Bends?. Vannets vei i landskapet - hydrologiens betydning for miljøstatus. Norsk hydrologiråd; Ås. 2012-09-20 - 2012-09-20

F) Foerst, Markus; Ruther, Nils; Hahn, Felix. (2013) Measuring Bank Retreat in Fluvial Environments with Terrestrial Laser Scanning (TLS). RCEM; Santander. 2013-06-09 - 2013-06-13

Individual Author Contribution

The present dissertation has been funded by the Norwegian University of Science and Technology (NTNU). The authors of the attached papers have contributed to the individual publications as follows:

Paper A: Markus Foerst and Nils Rüther had the idea to process the ADCP data in a new way in order to retrieve better data from known ADCP measurements. Markus Foerst came up with a new idea for postprocessing and wrote the scripts. Markus Foerst wrote the manuscript and Nils Rüther reviewed it before submitting.

Paper B: Markus Foerst and Nils Rüther planned the field work. The final research site has been chosen by Markus Foerst. Scans in the field have been done by Markus Foerst, Felix Hahn, and Christian Mörtl (acknowledgment in the paper). Markus Foerst did the postprocessing of the laser data. Point clouds has been filtered with a script, written by Aljoscha Sander (acknowledgment in the paper). Markus Foerst analyzed the data and verified them statistically. Markus Foerst wrote the manuscript and Nils Rüther reviewed it before submitting.

Paper C: Markus Foerst and Nils Rüther had the idea and planned the field work. The ADCP and Laser measurements have been conducted by Markus Foerst with the help of Master student Felix Hahn. Felix Hahn did the postprocessing of the laser data under supervision from Markus Foerst. Markus Foerst wrote the manuscript and Nils Rüther reviewed it before submitting.

Paper D: Markus Foerst and Nils Rüther had the idea for the paper and planned the field work. Markus Foerst did the measurements and the data analyses. Markus Foerst wrote the manuscript and Nils Rüther reviewed it before submitting.

Paper E: Markus Foerst and Nils Rüther had the idea for the paper and planned the field work. Markus Foerst and Felix Hahn did the measurements, Markus Foerst did the data analyses. Markus Foerst wrote the manuscript and Nils Rüther reviewed it before submitting.

Paper F: Markus Foerst and Nils Rüther had the idea for the paper and planned the field work. Markus Foerst and Felix Hahn did the measurements, Markus Foerst did the data analyses. Markus Foerst wrote the manuscript and Nils Rüther reviewed it before submitting.

Water is the driving force of all nature

Leonardo da Vinci

Delta of river Lena, Siberia, with kind permission of Berhard Edmaier

Introduction

1.1. General Background

Hiking in nature is for many people a very enjoyable free time activity. Along rivers banks the scenery is at its best when the river curls it natural way through the landscape. Scientists have been interested in this dynamic in a river for many years. The interest in the erosion processes lies in the substantial economic and environmental damage happening each year. Understanding the lateral migration of river systems has huge economic advantages. By understanding where and how a fast river will migrate, planning of new infrastructure projects such as roads and bridges can be improved. There are also projects in landscape architecture which are dealing with renaturation of river systems. This means removing erosion control and letting the river form its natural path again. Other applications are estimating whether existing infrastructures, cabins, roads or farm land, will become victim to future river migration and need special attention for erosion control.

River migration in the context of this thesis should be understood as lateral movement of the river course over time in a floodplain. The movement happens by eroding the outside of a river bend (cut bank) and accumulating on the inside (point bar) of the riverbank. This will lead to cut offs of river bends and might give the river course a new direction. The term excludes all human intervention such as constructions along the river or regulating the water discharge.

Nowadays there is a relatively good understanding of the concept of river bank erosion. River bed erosion and bank collapse are functions of hydraulic, bed material and its susceptibility to erosion (Hanson, 2001; Simon, 2000). There are also many numerical models which are able to predict river bank erosion and bank failure in river bends. The reason, that there are so many different models is, not only that there are countless factors which are involved in the river migration process, but also that the interaction between them is complex. Most of the models work within the limits that they have been developed for. Other models are able to predict erosion for a wider scope of application, but the results are more general. Therefore, the focus in river bank erosion research has shifted into smaller sub processes to identify single controlling factors (Bathurst, 1977; Julian, 2006).

One challenging factor is the fluctuations in flow. In regulated rivers, most rivers in urban areas of Norway are regulated, fluctuations are caused by hydropower. However, in natural rivers these fluctuations are mainly driven by the climate. There are seasonal fluctuations, such as high discharge during spring because of melting snow, and weather related events such as rain storm evens. Researchers all over the world agree that these rain storms will become more severe and erratic within the next century due to global climate change. This raises the need for learning about how short, but intense flow will affect river migration.

The other challenging factor is the flow structure. As long as the river course is straight, the water flows is symmetrically distributed across the river. The highest velocities are found in the middle of the river below the surface. At the point, when the current enters a bend, the momentum of the water with high velocities, pushes the current towards the outside. This generates a flow perpendicular to the main flow direction, known as secondary flow. This flow circulates from the inside to the outside under the water surface, goes down at the outside riverbank and back to the inside above the riverbed. Fine material, taken from the outside, follows the flow and accumulates along the inside of the river bend.

So far, this is the general understanding of the flow in a curved river course. However, in some spots the secondary current is deformed and another circular current appears at the outer bank, moving the opposite direction. This feature, which came again into focus in the last years, has been first discovered by Thorne and Hey (1979) and has been described by them as the outer-bank region. The outer bank region became a study object for Blanckaert (2001b, 2004a, b). While the discoverer thought that this outer bang region is supporting the migration of the river, newer experiments suggested that it slows down the erosion process along the cut bank.

In order to combine the erosion process with a numerical model and later with the hydraulics, it was crucial to find sites where it was possible to observe the described factors. Two sites in Norway have been chosen. The first site was an unregulated river, with some erosion control and old bridge piles, in the middle region of Norway, near Trondheim. The second site was a natural river in the arctic region of northern Norway, near the town Tromsø.

This work is mainly based on field measurements. Being outside in the Norwegian arctic nature motivated me to participate in the research community. Field work also means that one does not always get the conditions for measurements one wants. Anyway, the aim of this thesis is to look as close as possible into the hydraulic of a meandering river, measure the lateral movement as exact as possible, and combine these data. The result is another hypothesis of how the hydraulics interact with the cut bank I hope to provide enough data to build on for experiments in the flume or calibrating numerical models.

1.2. Secondary outer cell

The secondary cell in the outer-bank region is supposed to occur independent of consecutive bends (Bathurst, 1977; Thorne and Hey, 1979) and is only a consequence of the geometry (figure 01). However, the influence of the bank stability and erosion rate is a function of additional parameters, such as geomorphology, sediment load, aggregate stability, and temperature (Bertrand, 2009; Cantón, 2009; Simon, 2010). Additionally, aspects like aggregate stability are functions of other soil parameters, too (Le Bissonnais, 1996; Wakindiki, 2002). The erosion triggered by the outer secondary cell has not been studied in nature so far. Further, the measurements to determine the outer cell region, which were taken by Bathurst (1977; 1979), are 40 years ago and instruments didn't give the necessary resolution. Therefore, it was not possible to measure at the crucial points and thus a high bias to determine exact values for shear stress was given. However, the evidence for the outer-bank region was given at this time.

The outer cell region has been subject for research in irregular intervals. In the beginning, flow measurements in the field were performed with mechanical instruments. More recently, intensive investigation of the outer cell region has been performed in the laboratory (Blanckaert, 2001a). Experiments with different flow regimes were conducted (figure 01). Since the investigations until now are done under two different setups, the role of the outer region cell is unclear. While Bathurst (1979) measurements of currents in a natural environment theorize an expected increase in erosion and bank retreatment, Blanckaert (2004a) supposes that the secondary outer cell creates a protective layer between the high velocity cell and the river bank. The most recent study links the secondary outer cell to an increasing secondary flow with an increasing Froude number (Farhadi et al., 2018).

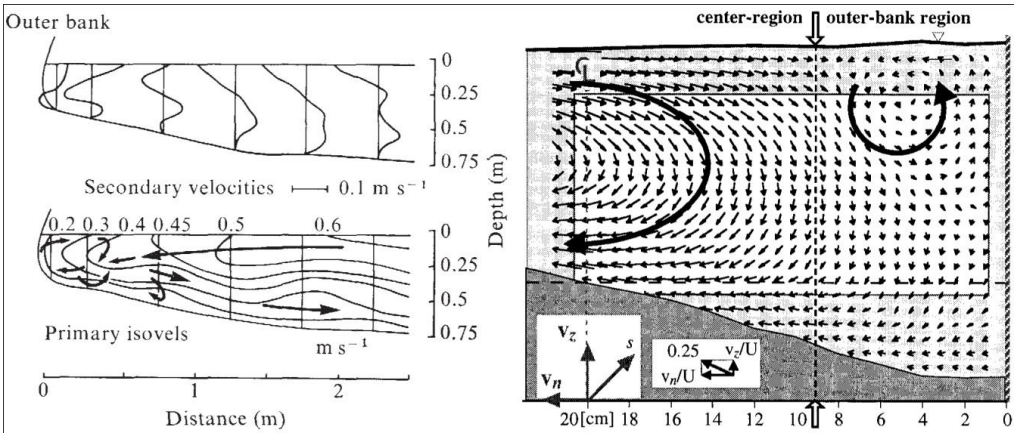

Figur 1: Outer bank region recognized in natural river bend (left in Bathurst (1977)) and laboratory (right in Blanckaert (2001b)).

All approaches to understand the complex currents in meander bends and its impact to river banks have been mainly a subject of discharge and hydraulic. The next step is to conduct investigations in combination with sediment and soil loss in natural river systems. Thereby it will be possible to quantify the bank erosion and the necessary shear stress. Additionally this thesis will determine the circumstances under which the outer cell occurs and what influence it has on erosion and bank failure.

1.3. Objectives

The objectives of the Ph. D are divided into research (a-d) and teaching duties (e):

a) Find a way to measure the secondary outer cell in a natural river.

b) Does the outer cell increase or reduce erosion and how does the outer cell influence the geometry in the river?

c) Does the bathymetry of a river determine the flow or the flow the bathymetry?

d) Provide input and test data as well as physical process description for further development of a 3D hydraulic and sediment transport model.

e) The PhD candidate did a variety of teaching, such as laboratory exercises, practical field work and supervised one master students and two bachelor students.

- **Felix Hahn (2012)**: Terrestrial Laser Scanning in short-term surveying of steep riverbanks. Master Thesis.
- **Susanne Haas (2013)**: Mean Velocity and Secondary Current in River Bends measured with Acoustic Doppler Velocimetry and Acoustic Doppler Current Profiling. Bachelor Thesis.
- **Christian Mörtl (2013)**: Groundwater Flow and River Bank Erosion. Bachelor Thesis.

- **Teaching 2012:** Headworks and Sedimentation engineering (TVM-5160)

1.4. Thesis in the framework of today's research

River migration has been subject to research for centuries. Climate change with change in weather patterns makes this topic as up to date as it has been before. The uttermost studies agree on more intense and erratic precipitation events within the next decades (Aalbers et al., 2018; Alfieri et al., 2015; Kjellström et al., 2018; Moss et al., 2010), just to name a few of them. Therefore riverine systems are coming under increasing pressure due a changing environment.

Kleinhans (2010) names different approaches in order to describe processes in nature. One is to observe the object directly in nature. This approach, however, might be limited because of dangers (e. g. drowning) or the boundary condition are not as desired (e. g. unsteady discharge). The next approach is a physical model. In a physical model the investigated process can be better isolated as it would be in nature. It is also possible to determine boundary conditions. On the downside, unknown factors which are influencing the process remain unnamed, not to mention loss of information by down scaling from nature to the model and vice versa. The third approach is numerical modelling. This has become more common with increasing calculation power of computers. Often these models are a further simplification and can only give result within the limits we create by choosing the model. Therefore it is necessary to do research with all three approaches and when the results finally converge, we will get into an understanding of natural processes.

Parker et al. (2011) observed migrating rivers over a decade and derived the idea that, numerical models have to take into account that erosion and sedimentation is not a linear process. This is something many models take account for. There have been developed many numerical models which are used to calculate river bank erosion and sediment transport, such as HEC-RAS (Song et al., 2015), CONCEPTS (Langendoen, 2000a), or BSTEM (Klavon et al., 2017),. Other authors work with more generalized models on reach (Rüther and Olsen, 2007; Yang et al., 2018) or catchment scale (Grenfell et al., 2014; Lammers and Bledsoe, 2018). These numerical approaches have in common that they need a certain amount of data, depending on how many processes and variables are included in the calculations.

The physical models have advanced with the advancement of measurement equipment. Experiments have been done in a straight flume in order to investigate sediment transport and development of channels and meanders, where laser measurements recorded changes in the geometry (Li et al., 2019; Redolfi et al., 2018). Curved flumes have been used in order to investigate flow in river bends. High precision measurements such as Acoustic Doppler Velocity meters (ADV) gave insight in the flow structure in bends (Blanckaert, 2003, 2004a; Blanckaert et al., 2012; Farhadi et al., 2018). Other experiments have been conducted in order investigate turbulence and shear stress in different kinds of setups (Biron et al., 2004).

Flow and erosion measurements in rivers have been done for a long time. Here again, the advancement of measurement devices made way to new possibilities for investigation. Erosion pins are, or have been, a very common technique to measure riverbank erosion Lawler (1993) and Couper et al. (2002). Advantages are that erosion pins can be applied in a range of different fluvial environments, and are cost-efficient. The newer versions can detect bank retreat within the order of millimetres.

Disadvantages are the spatial sampling resolution since this is a point-specific technique. Furthermore, this is an intrusive method and measurements might therefore be effected by other erosion pins. Jugie et al. (2018) combined these pins with Surface for Motion (SfM) photogrametry. Submerged pins might vibrate or generate local turbulence and pins on the riverbank might intercept eroded material which is moving downslope. The use of Light Detection And Ranging (LiDAR) in airborne survey over large areas has been applied recently (Milan et al., 2010). However, its application is limited when surveying vertical or near-vertical structures. This limitation can be overcome by using a Terrestrial LiDAR (Terrestrial Laser Scanning, TLS). As a non-intrusive method, it avoids the physical impact of the measurement device at investigated ground. Additionally, it collects a high amount of measurement points. This setup results in a dataset with a much higher resolution, compared to e.g. the above mentioned erosion pins (Day et al., 2013a, b; O'Neal and Pizzuto, 2011; Resop and Hession, 2010; Wheaton et al., 2010) and hence a more detailed insight into the sediment balance of a riverbank (Nasermoaddeli, 2008).

The Acoustic Doppler Current Profiler (ADCP) became accepted as measurement device for many different applications within hydrology. The two main companies, SonTek and RD-Instruments, build ADCP devices in different sizes and configurations. They have usually three to four ultrasound beams to measure the water velocity and direction by the sound distortion from the reflected soundwave. The so called Doppler Effect. This made it possible to measure water velocities in different depth simultaneously in the water. Therefore they were used in the beginning to measure discharge instead of mechanical measurement with a current meter. However, researches started using them to analyze the raw data and took a closer look into the flow structure (Barua and Rahman, 1998; Muste et al., 2005; Muste et al., 2004a; Muste et al., 2004b; Szupiany et al., 2007) and sediment transport (Guerrero et al., 2017).

Others methods to investigate the flow structure are Acoustic Doppler Velocimeters (ADV). They are based on the same principle as the ADCP, the Doppler Effect, to measure the water velocity. The difference is, that they have a very small sampling volume (< 1cm^2) in comparison to ADCPs, which measure the whole water column. The area of applications for ADV are therefore limited. On the other hand ADV can measure with a sampling frequency of 200Hz. Therefore, they are often used in the laboratory for near bed measurements (Groom and Friedrich, 2019) or turbulence measurements (Biron et al., 2004; Farzadkhoo et al., 2018; Leng and Chanson, 2018). But they can also be used in small rivers. Schnauder and Sukhodolov (2012) studied the turbulence around vegetation in a small river with ADVs. Sukhodolov (2012a) obtained turbulent flow characteristic for a short river reach.

Due to the changing weather patterns it will be increasingly more important to understand flood and flash flood events. Kasvi et al. (2017) conducted ADCP measurements during a nine-day long flooding period in a meandering river. It was possible to visualize the normal flow patterns such as high velocity cell and secondary cell in the bend. The outer secondary cell, however, has not been described.

This work is mainly about case studies in nature and builds on the experience and research which have been mentioned. Changes of the river bank morphology will be measured with a Terrestrial Laser Scanner in order to avoid disturbance by the measurement method itself. This work will provide a new methods for analysis of ADCP data in order to get better insight in the flow structure of natural river bends. These two methods will be combined in order to explain erosion patterns. Some of these

structures seem to prevent erosion during single flood events. Results from flow data and erosion will can be used in different numerical models.

1.5. Outline of the Thesis

The thesis divided into 5 chapters plus references and the appendix. Chapter 1 gives an introduction, explains the objectives of this work, and puts it into place between other researches done. Chapter 2 gives an overview over the research sites and explains the methods used to gain the data. Chapter 3 gives a summary of published papers during the PhD. In chapter 4 the conclusions will be presented. Chapter 5 describes ongoing work and gives an outlook into future research possibilities based on this work. In appendix A, a copy of the publications is presented. Appendix B presents all transects measured during the field work to give a complete insight in the flow structure of three consecutive river bends.

2. Research Methods

2.1. Research Campaigns

There have been conducted four research campaigns. The first one in middle Norway from autumn 2010 to spring 2011. The other three have been conducted in northern Norway during the short summer period in 2011, 2012, and 2013. The last one was the shortest and lasted only three weeks. Both sites are shown in figure 02.

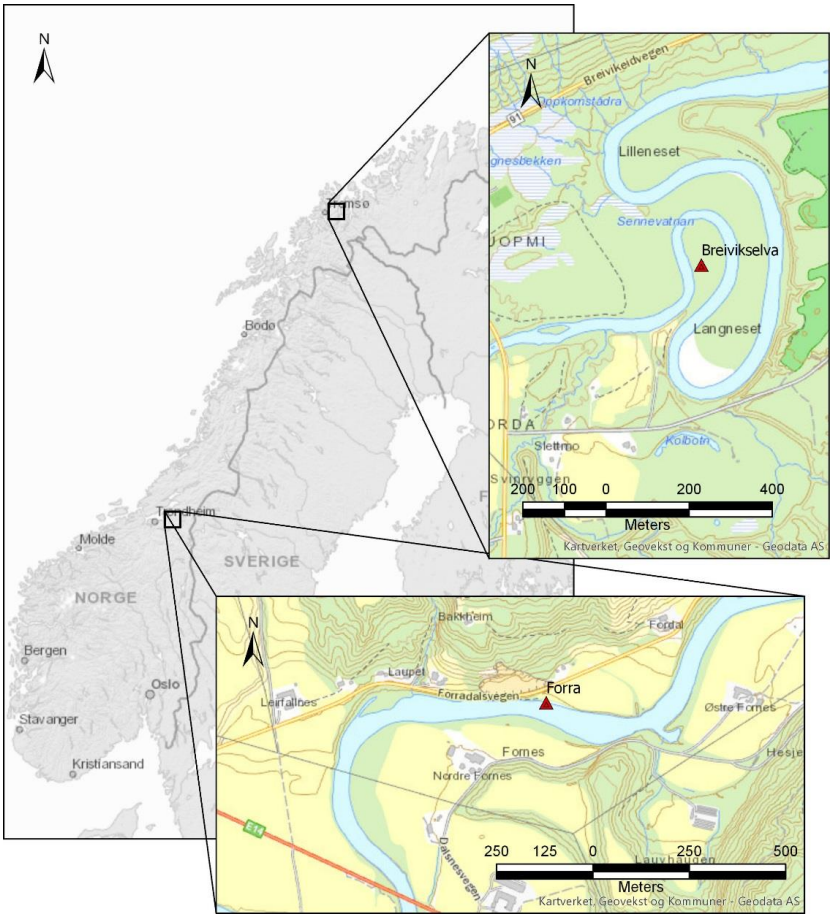

Figure 2: Map over Research sites. Breivikselva in Northern Norway and Forra River in Middle Norway.

2.2. Description of the research sites

This thesis contains investigations at two different sites in Norway. The first one is located in middle Norway near Trondheim, the second one is located in the northern part near Tromsø. Both rivers are unregulated. However, while the river Forra near Trondheim has some erosion control, the course of river Breivikselva near Tromsø is natural with no erosion control.

The river Forra (catchment nr. 124.AA0) is a tributary to Stjørdalselva, which has a couple of tributaries itself. The catchment area covers around 600 km2 with a field length of 49 km. The land use around is mainly farm land and some urban infrastructure, which made it necessary to protect parts of the river bank against erosion. The climate is subpolar (Cfc) with less extreme temperatures between summer and winter.

The valley infill is post glacial stratified fine-grained sediment which was deposited since the last glacial maximum (Lysså et al., 2008). The discharge is continuously monitored by the Norwegian Water Resources and Energy Directorate (NVE) at Høggås Bridge, which is located about 10 km upstream from the investigated river bank. The discharge has been scaled to fit the larger catchment. The measured discharge and the scaled discharge are shown in figure 03. The data shows that from mid-November to end of January, the discharge is very low. This is due to snow where the precipitation is stored and released in spring during snow melting. This happens for a short time end of January and later on form mid-March.

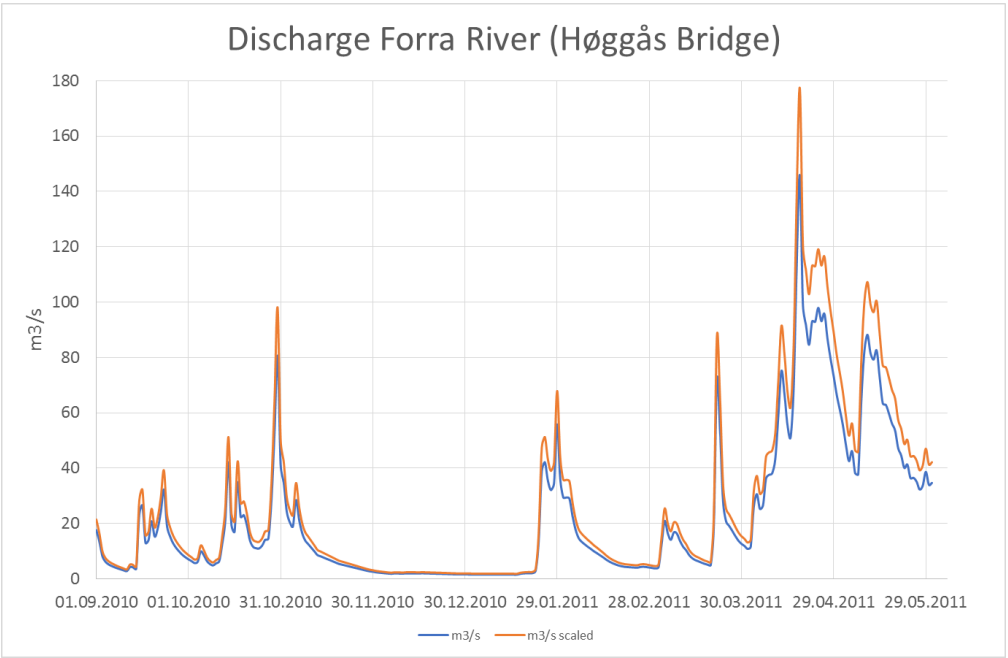

Figure 3: Discharge for Forra river between September 2010 and April 2011. The blue line shows data from the station Høggås Brigde, the orange line are scaled discharge at the research site.

The river Breivikselva (catchment nr 203.2B) drains to the sea about 4 km downstream from the investigated reach at Breivikseidet. The catchment is 164 km2 with a field length of 19 km. Nearly 60 % of the catchment are barren mountain areas. This makes the discharge sensitive to water input such as rain events or increased snow melting when the sun faces rocky areas. The climate is subarctic (Dfc) and therefore the temperature difference between summer and winter more extreme.

Breivikeidet is a typical fjord valley which has a thick layering of sediments that were formed by infilling, emergence, incision, and terracing during the last deglacial-postglacial period. The contribution of sediment to fjord valleys in northern Norway is driven by the glaciation and deglaciation. During the

glaciation stage, the fjord-valley stage, the sediment distribution was steered by a fjord-glacier and the sediments, composed of till and glaciofluvial sand and gravel, were deposited at or close to the glacier margin. At this stage the glacier is an outlet glacier with direct contact to a marine environment and fine sand, silt, and clay are deposited on the fjord floor beyond the glacier margin. During the deglaciation, the retreat of the glacier, sediments composed of sand and gravel were delivered to the head of the fjord by glacier-fed rivers (Corner, 2006).

The low relief and fine sediment supports the development of meanders. Bayous of different age can be seen as residuals of former river movement. River bed sediment samples and under water observations showed that the upstream part of the reach was dominated by smaller gravels whereas the downstream part was exposed to three dimensional bed forms.

The water level has been measured by two water loggers at the investigated reach. One upstream of the investigated reach and one downstream. The logger have been installed each year to begin the campaign and removed over winter time. In 2012 there were technical problems, which resulted in just one logger (upstream) for the first half of the campaign. The water level from the upstream logger is shown in figure 04. One can see that in the beginning of June during the 2011 campaign the snow from the surrounding mountains is still melting. This leads on one hand to a rather high water level early in the campaign. On the other hand, it shows a daily fluctuation, which degrease over the summer. These small fluctuations are caused by increased snow melting when the sun heats the rocks during the day. The year after, the main snow melting was earlier and the river, Breivikselva, had a constant lower water level. Again, the fluctuations from snow melting during the day are recorded.

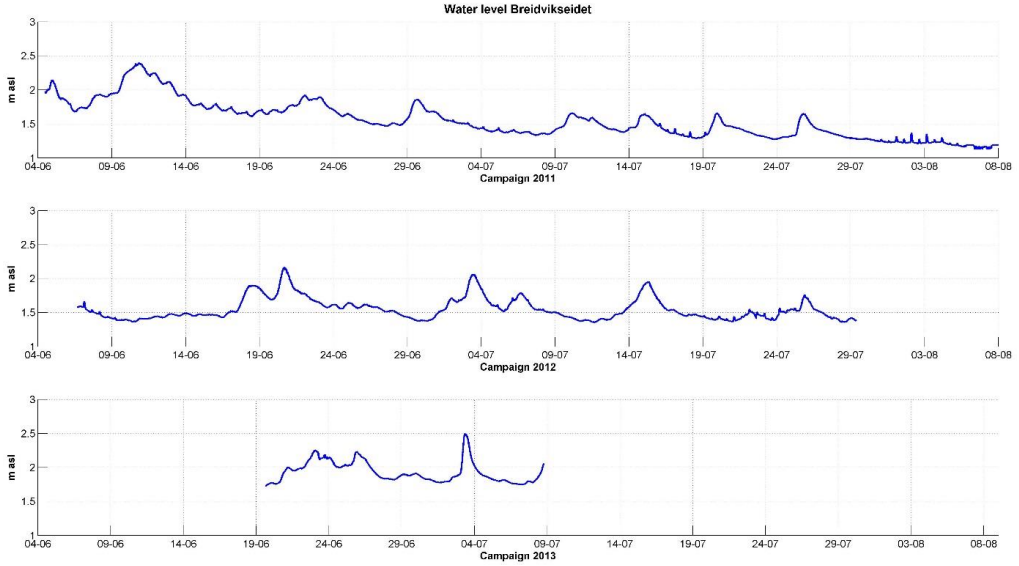

Figur 4: Water level during the field campaigns in 2011, 2012, and 2013.

The discharge has been measured during the first campaign in 2011 for different water levels in order to create a rating curve (figure 05).

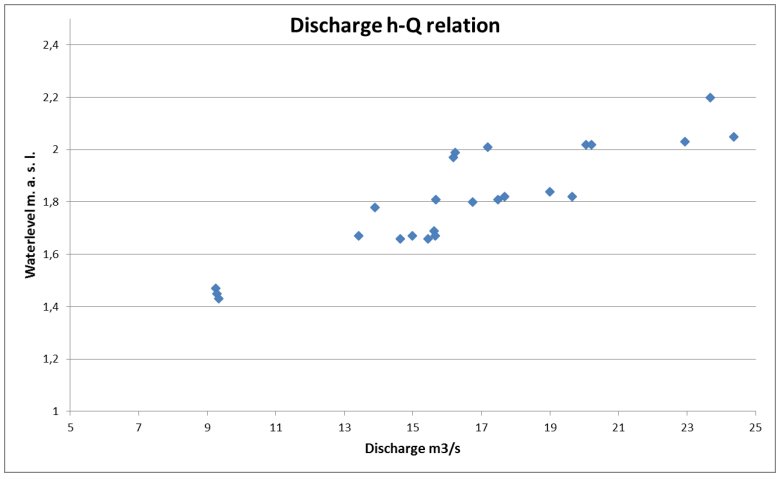

Figur 5: Discharge rating curve created during the first field campaign in 2011.

2.1. Setup of Field Measurement

All research was conducted in the field, in natural rivers. This makes the setup of the measurements the first challenge. While some measurements are just well known methods, such as taking and analyzing sediment samples, others are more challenging such as fixed measurements with an ADCP or even three ADVs simultaneously.

2.1.1. Sediment properties

For the first campaign soil samples have been taken for analyses of critical shear stress, texture, and total organic content (TOC). For the measurement of critical shear stress, a vane shear stress meter H-60 from GEONOR has been used. The sampling has been done direct in the field.

For further analyses of soil properties, the samples were sieved down to 2 mm grainsize. Sieving showed that there were nearly no grains (3 – 5 per 140 g sample) larger than 2 mm. Afterwards, 10 g of air dried material were taken for further processing. Each sample was treated with H_2O and 35 % hydrogen peroxide solution (H_2O_2) and heated to 50° C in order to remove organic matter. In preparation for further grain size analysis samples were dissolved in H_2O and 50 ml of sodium hexametaphosphate $(NaPO_3)_6$. This solution was shaken for at least twelve hours at 160 rpm. For the final texture analyses the laser diffractometry was chosen as method, due to better reproducibility (Beuselinck, 1998). For the analyses a Coulter LS 230 was used with a particle size analysis range from 0.04 µm to 2000 µm. Three runs, each 120 sec for each sample were done using the Fraunhofer optical model.

2.1.2. Terrestrial Laser Scanning

For all erosion measurements a terrestrial laser scanner (TLS), Topcon GLS-1000, has been used (Momm et al., 2011). The scanner has a range up to 330 m with a single point accuracy of minimum 4 mm at a range up to 150 m. There has been used four georeferenced targets during the scans in order to get the lowest georeferencing error (Coveney and Stewart Fotheringham, 2011). Every site was

scanned from at least two angels to cover also areas which were out of sight, due to a shadow effect from obstacles. These scans were put together with the standard software for this laser scanner (Topcon ScanMaster) and exported as point cloud.

These point clouds showed single points which have to be regarded as artefacts. These single points created during the scan have been removed by a density filter. The basis of the filter has been provided by Point Cloud Library (PCL 2013). The filter projected a sphere with the radius R around each point and counted the amount of points within this sphere. If there has been a certain amount of neighbour points N within this sphere, then it was defined as good point, otherwise it was regarded as outlier (Brodu and Lague, 2012; Lague et al., 2013). After a manually inspection whether the point cloud was still coherent, it became clear that larger part of vegetation and dead wood also met the criteria for valid points. Some parts of vegetation could be removed by a colour filter. However, most part of it needed to be removed manually. This has been done with ArcScene©.

2.1.3. Bathymetry

Bathymetry measurements were conducted with the ADCP from Sontek (M9). This has been equipped with a differential GPS. The measurement range for the M9 is between 0.3 and 60 meters. Parts of the river, which were shallower than 0.3 m were measured with a RTK-GPS. Also, all nearly horizontal areas were measured with a RTK-GPS, such as the point bars. The riverine geometry was measured with a terrestrial laser scanner. The combination of the three data sets led to a detailed DTM of the river reach.

2.1.4. Moving ADCP

In order to get reproducible transects, a cable way was rigged up. The cableway consisted of a rope which was fixed in pulleys on either side of the river. The pulleys itself were fastened with a tension belt over a wooden support system at the ground (figure 06).

The Streampro© ADCP was mounted in the middle. Thus it was possible to pull the ADCP steady over the river. For each transect the ADCP was pulled over the reach four times, two times from left to right and two times from right to left. In order for a measurement to be valid, it had to have less than 5 % of invalid bins.

All transects have been georeferenced at the mounting point for the cable lines. Thus it is possible to measure the same positions with changing environmental parameters.

Figure 6: Setup of the moving boat cableway.

2.1.5. Stationary Measurement Setup (ADCP and ADV)

A platform system was built to make it possible for fixed measurements with the ADCP and later with ADVs in the river. In order to make the platform mobile, to measure different transect and stable at the same time, the platform was mounted on a double rope system. The ends of the guiding ropes were fixed in the ground with tension belts and adjusted in height with the wooden support system (figure 07). On the platform, the RTK-GPS was mounted direct above the ADCP sensor. The ADCP housing and the sensor were mounted onto moveable rods. So it was easy to adjust the height, to get the sensor only 2-3 cm into the water. Just enough to keep it under water during the measurement by having least drag from the water. This kept the measurement station extremely stable.

This setup worked so well, that this platform was also used in a later campaign for ADV measurements. The platform had to be modified to mount two down looking and one side looking ADV (figure 08). The ADVs were mounted on vertical rods. These three rods were fixed in place in guide fillets at one side of the platform. Holes in the rods with a distance of 10 cm to each other and a screw through one of the holes stopped the bars in the wanted depth. The distance between rods on the platform were adjusted so the ADV measuring volumes were 0.5 m apart. Additionally, the rods with the probes were fixated with attached slanted rods connecting them to the downstream side of the platform. The fixation through the slanted bars helped to minimize the vibrations the probes experienced due to increasing drag with depth. Another mounting point with a cantilever connected to the ground reduced swinging from the platform itself.

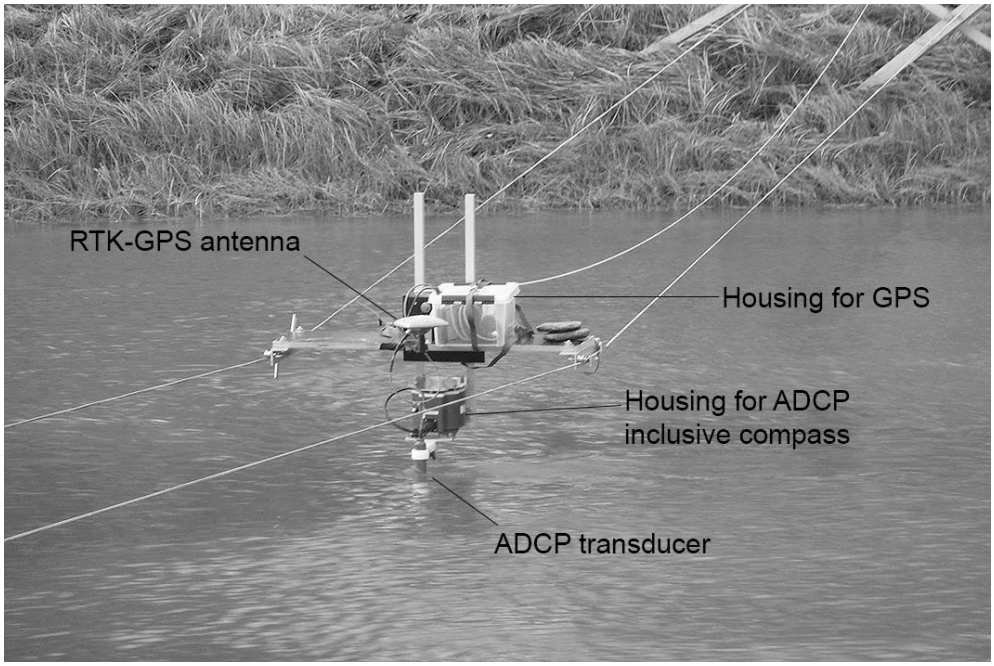

Figure 7: Streampro© ADCP mounted on a platform for fixed boat measurements. RTK-GPS is mounted above the ADCP sensor.

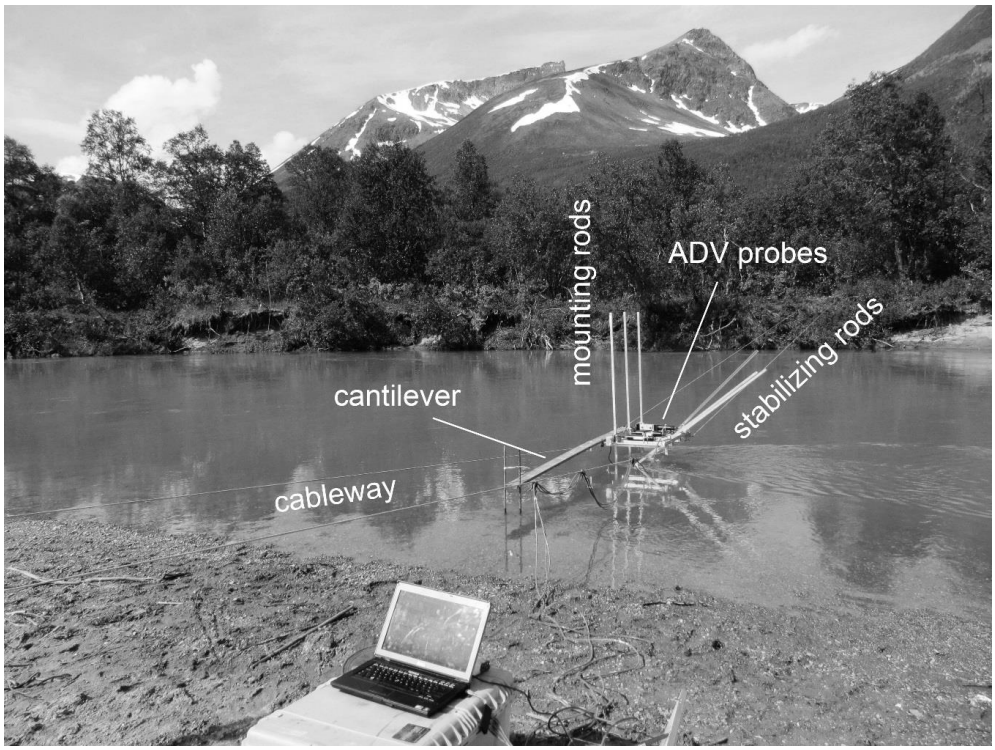

Figure 8: Field setup for ADV measurements. Three vertical rods, where the ADVs are attached to. Three slanted rods eliminate vibrations at the probe. Mounting platform with ADVs are additionally stabilized with a cantilever beam.

2.1.6. Stationary ADCP Measurements

For stationary ADCP measurements the ADCP (Streampro©) was mounted on the platform (figure 07). The ADCP has a sampling rate of 1 Hz. The measurements were taken for a duration of minimum 600 sec to ensure that enough data was collected to calculate a reliable average (Barua and Rahman, 1998; Guerrero and Lamberti, 2012; Muste et al., 2004a). This amount of data was reached after about 570 sec by the approach of the normalized mean square error (NMSE) to 0 (figure 09). This is necessary to filter noise which is produced by vibrations of rolling, pitching and rotating of the ADCP.

Further post processing is described in the respective chapters. Stabilizing

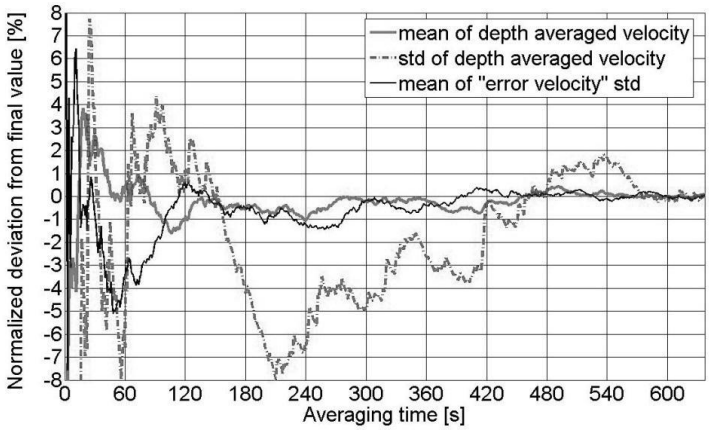

Figure 9: Variability of average velocity over time

2.1.7. Fixed ADV measurements

Velocity and current measurements in Breivikelva were carried out with three synchronized ADVs. Each positon of the ADV probe has been measured with an RTK-GPS.

The probes where connected via serial-USB adapter and an USB hub to the computer. This limited the data transfer. Therefore, the sampling frequency was at set 50 Hz, since higher sampling frequencies leaded to gaps in the data. The sampling period was three minutes, which resulted in datasets of 9000 values for each probe and measurement.

The goal was to measure complete transects with the ADVs. However, the current in the river created so much drag, that measurements were not possible. This was due to both safety reasons, and that is would have been impossible to stabilize the platform. Therefore, the transects are incomplete. It is for the same reason that measurement deeper than 1 meter below water level don't exist.

2.2. Post processing of point clouds

The post processing of the point cloud has been a challenge. The first challenge has been vegetation. To avoid problems with the cover vegetation the TLS data have been cut at the soil horizon, which is

about 15 cm below the upper surface. The dimensions of the point clouds have been defined by a vertical cut at 2.8 m a. s. l. as the upper limit. The lower limit is the water line at that moment when the scan has been taken. The point clouds showed single points which have to be regarded as artefacts. These single points created during the scan have been removed by a density filter. The basis of the filter has been provided by Point Cloud Library (PCL 2013). The filter projected a sphere with the radius R around each point and counted the amount of points within this sphere. If there has been a certain amount of neighbour points N within this sphere, then it was defined as good point, otherwise it was regarded as outlier (Brodu and Lague 2012). The filter has been applied with radiuses R from 0.01 to 0.15 m in steps by 0.015 m. The amount of neighbour points have been defined for N = [5 10 5 20 25]. Points with less than N neighbour points have been deleted. In this way for each point cloud, 50 filtered point clouds have been created. These point clouds have been plotted. Afterwards they have been visually inspected whether enough outliers have been removed and whether the point cloud was still coherent. The result was very different and no special pattern concerning the settings was visible. Vegetation and dead wood has been removed manually. This has been done first in the 2D view of ArcGIS© and 3D of ArcScene©.

Further post processing has been done in Matlab©. For each patch, a mesh has been created with a cell size of 0.005 m. On this mesh, the point clouds have been projected and a digital elevation model (DEM) has been created. From this DEM the slope gradient in degree, has been calculated and plotted (figure 04). The slope gradient ∇F is defined by

$$\nabla F = \frac{\partial F}{\partial x}\hat{\imath} + \frac{\partial F}{\partial y}\hat{\jmath}$$

Thus, the gradient in degree (Gdeg) has been calculated with

$$G_{deg} = \operatorname{atan}\left(\sqrt{(\nabla Fx)^2 + (\nabla Fy)^2}\right) * \frac{180}{\pi}$$

2.3. Post Prosessing ADCP

All ADCP measurements have been conducted with the Streampro© from RD-Instruments. The in-house software, WinRiver, from RDI does not provide much post processing. WinRiver II allows to change environmental parameters, in case they have been forgotten or wrong during the setup of the measurement. Therefore, a Matlab script has been written in order to import raw data into 3d-variables. After reprocessing with ASCI-mode enabled in WinRiver II (classic mode) Data contains raw data, header contains filename, date and columns output will be a 3d variable with each ping on the next level.

Stationary measurements have been georeferenced with the GPS coordinates which were taken during measurement (Chapter 2.1.5). The further post processing in Matlab is described in more detail within the published papers.

3. Summary of Papers

The research was planned to start with the geomorphological features to the hydraulic of the river. Therefore, the summary of the papers is presented in chronological order.

3.1. (C) Markus Foerst, Nils Rüther, Felix Hahn, 2011: Evaluating erosion processes of a two layer river bank.

This paper focuses on the numerical modelling of a river bank in the middle part of Norway, Trøndelag. The riverbank consists of two layers with different properties. This site has been chosen, since a layered riverbank is quite common along lowland rivers in Norway. The lower part is fine layered material, deposited during the retreat of the ice sheets, which covered Scandinavia during the last Ice Age. (Corner, 2006; Solberg et al., 2008). The layers have been analyzed for texture and shear stress. The riverbed was characterized by hollows and bars, which were covered by pebbles. These properties have been used in the Model CONCEPTS (CONservational Channel Evolution and Pollutant Transport System), which has been developed by Langendoen (2000a). This model was chosen due to a focus on soil texture, shear stress and erodibility within the soil layers. Additionally it allows different vertical soil layers within a riverbank. The intention was to model and evaluate stream-corridor restoration designs, especially to evaluate the long-term stability of stream corridors (Langendoen, 2000b). It is made to compute one-dimensional flow simulations of straight channels. The bathymetry has been smoothed out, since the model has difficulties to model river with bars and multiple channels. To verify the results from CONCEPTS the actual erosion has been measured with a Terrestrial Laser Scanner. The first scan were done in autumn 2010 and the second scan in spring 2011. This means, that there has been a thick layer of ice during the winter following with snow smelting and high discharge in spring 2011. The laser scan measurements showed erosion all along the river bank (figure 10). The results showed, that the model strongly underestimated the erosion in this reach. The main reason for that is that CONCEPTS does not take into account the erosion due to freezing and thawing process (Bertrand, 2009). Processes which play a huge role in Scandinavia, where ice covered rivers during winter season are common. One other reason might be the fact, that a smoothed riverbed neglects the fact that higher current in channels along the river bank occur and therefore the shear forces are underestimated. The outcome from this paper lead to two main conclusions for the ongoing work: First, comparison of erosion over winter time will be excluded and second this numerical model is not suitable for rivers in cold climates.

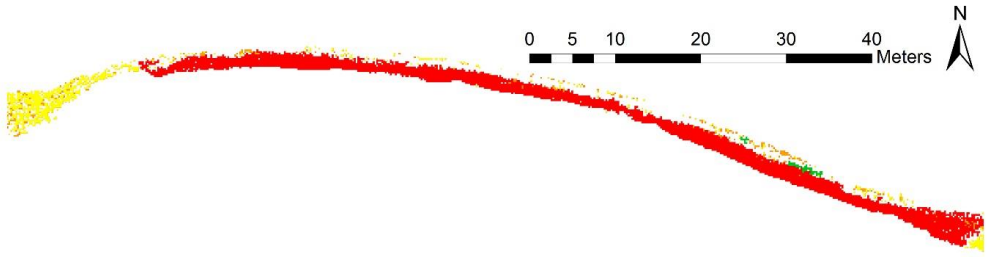

Figure 10: Showing the erosion along the northern river bank of Forra river, which occurred between autumn 2010 and spring 2011. Green is vegetation, yellow are stone blocks from erosion control and red is erosion.

3.2. (A) Markus Foerst, Nils Rüther, 2012: Post Processing Methods of Moving Boat ADCP Measurements Time Averaging vs. Distance Averaging.

This paper describes a new method for post processing of Acoustic Doppler Current Profilers (ADCP) data. The most common use for ADCP instruments is the measurement of discharge. Thereby the instrument measures the water flow in different depth in the water column one time per second (1 Hz). The result is depth of the water, the flow velocity and the flow direction in the water body. From these information the discharge is calculated. Since these data also contain information about the flow structure it is possible to map the secondary flow in a river bend. The procedure for discharge measurement is to measure the same transect four times. In the beginning and the end of each transect, the measurement should be stationary for 10 to 15 seconds to get an estimate of the discharge at the edges. Additionally, the velocity of the moving ADCP is normally varying with the position along the transect. However, water flow in natural rivers can always be regarded as turbulent. This leads to the problem that point measurements along a transect will not reveal the general flow structure across the river (figure 11). Therefore, it is necessary to average single pings in order to remove outliers. This paper describes different methods how to post process the measured data in order to get a picture of the averaged flow structure.

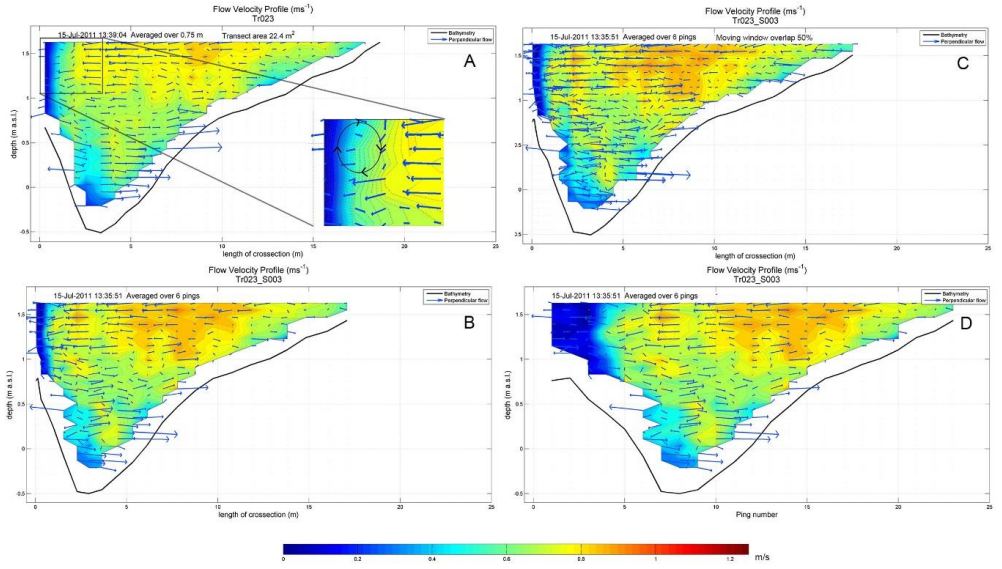

Figure 11: Results of different post processing methods. A: distance averaging, B: time averaging, C: time averaging with moving window 50 % overlap, D: time averaging plotted against ping number.

This new method made it possible to discover the outer secondary cell in a natural river. The investigated reach at Breivikelva has been measured by that method. There has been taken 72 transects along three meanders. The complete set of results are shown in appendix B.

3.3. (D) Markus Foerst, Nils Rüther, 2012: Mean and Turbulent Flow Structures in Two Consecutive Meander Bends.

This paper focuses on the flow structure, which became more visible due to the post processing method described in the preceding paper. All 72 transects, which have been measured with the ADCP, have been evaluated based on the existence of secondary flow, high velocity cell, and erosional channel in the bathymetry. Based on this, the behavior of the mean velocity cell and the secondary current has been described in relation to change in bathymetry along the reach. The location of change in flow is shown in figure 12. It shows that the high velocity cell, secondary current and the river channels don't adapt simultaneously. Additionally, the paper shows also that it was possible to detect the secondary outer cell in a natural river. Comparison of the occurrence of the secondary outer cell and the high velocity cell suggested that the outer cell is more likely to appear, when the position of the high velocity cell is more towards the point bar. The most relevant transects have been presented in this paper. The complete set of transects along the reach is presented in appendix B.

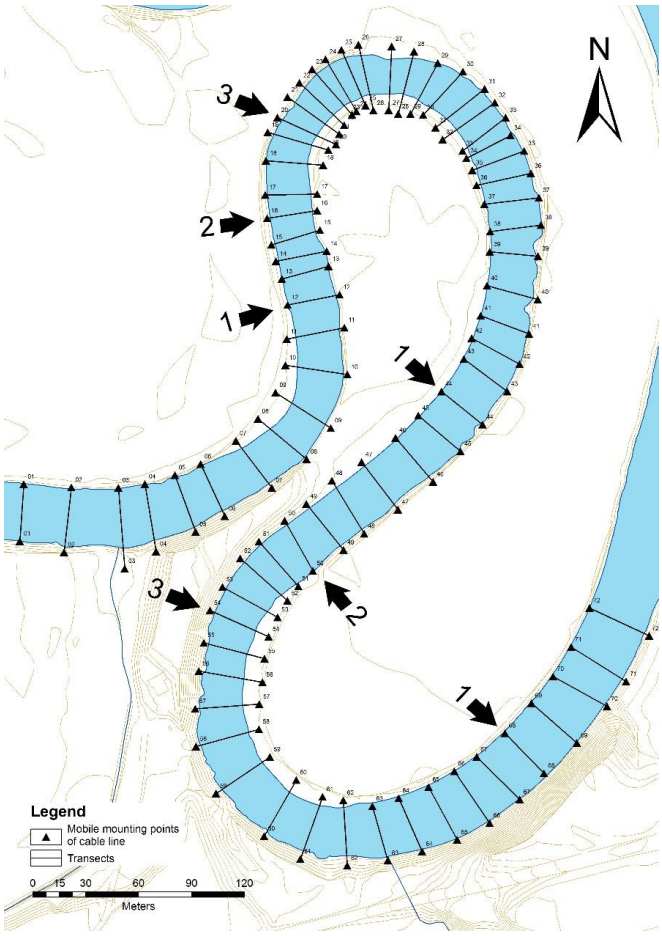

Figur 12: Changing of flow characteristics: 1) disintegration of secondary current (end of bend), 2) bathymetry – shift of channel (after inflection point), 3) movement of high velocity cell (after beginning of bend).

3.4. (B) Markus Foerst, Nils Rüther, 2018: Bank Retreat and Streambank Morphology of a Meandering River during Summer and Single Flood Events in Northern Norway.

This paper combines the erosion measurements along the outer river bank with the terrestrial laser scanner and the flow measurements with the ADCP. The erosion has been measured over three years at the beginning and the end of each summer. The water level has been monitored continuously. The river had eight moderate high water events in between the scans of the river bank. During the measurement campaign in the second year, we had six moderate high water events in between the scans. During the third campaign, the river had one moderate high water event and one extreme high water event. It was possible to get a scan just before the first and the second high water event and directly after the second high water event. The significance of bank retreat has been statistically verified. In the first two years, both times, the results showed a bank retreat up to 0.5 meters. The analyses of the scans in the third year, showed little retreat during the first high water event and no significant change after the extreme high water event. A possible explanation came up by looking into the hydraulics. The formation and existence of an outer secondary cell has been observed and documented in a natural meandering river at bends with high curvature and relatively steep riverbanks. Based on the observations and calculations from Blanckaert (2004a) the secondary outer cell seems to have a dampening effect on river migration. This effect can be explained in three steps (figure 13) of erosion and sedimentation. First (I), one can observe a steepening of the riverbank, which leads to an appearance of the outer secondary cell. At the second step (II), bank material is falling from the top due to the dampening effect and is accumulating in front of the bank toe. This flattening leads to the decay of the outer secondary cell and the dampening effect disappears. During the third step (III), this accumulated material is eroded, returning the riverbank back to its vertical shape, restarting the cycle in step I.

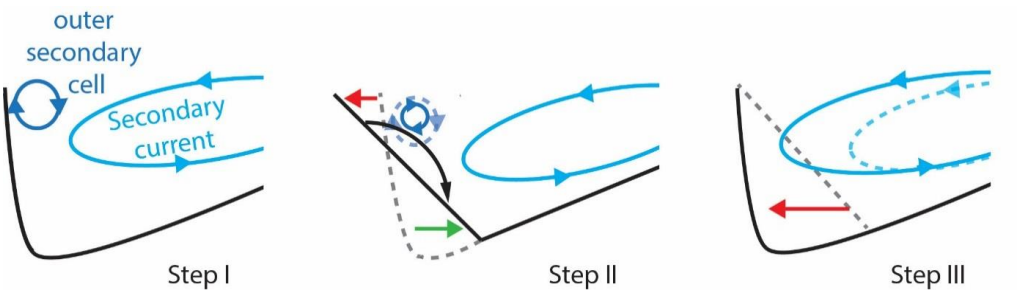

Figure 13: Schematic drawing of the three steps of the erosion process. Step I shows a steep riverbank, triggering the secondary outer cell. Step II falling material flattens the riverbank and destroys the secondary outer cell. Step III eroding the fallen material and creating a steep riverbank.

4. Conclusions

This PhD has been planned and conducted as a field work. Two sites have been chosen as research objects. The first site, Forra, is an unregulated river but has partial erosion control and other constructions along its bank. It was chosen as it had a two-layered river bank, which is common for a lowland river in Norway. Hydraulic data was collected with an ADCP and the bathymetry was mapped with an RTK-GPS and ADCP. The cut bank was carefully mapped with a Terrestrial Laser Scanner two times for comparison. The first time in autumn 2010 and the second time in spring 2011. Additionally, the soil has been analyzed for its structure and stability. These data have been used as input to the channel evolution model "CONCEPTS".

The second site, Breivikselva, has been chosen as it is unregulated and the river course dynamic is not altered by any constructions. The change of the river bank has been measured seven times with a Terrestrial Laser Scanner over three years. The bathymetry has been mapped with an RTK-GPS and ADCP. The change of water level has been monitored by two water loggers, one upstream and one downstream of the research site. The structures in the flow have been measured by moving ADCP measurements at 72 transects. In addition, 102 stationary ADCP measurements along 21 of these transects were taken. For the analyses of these moving boat transects, a new post processing method has been developed in order to visualize details of the flow structure. From the stationary measurements, the shear stress at the riverbed has been calculated. The conclusions of this thesis can be summarized by the following:

a) The secondary outer cell has been recognized by Bathurst (1977) in a natural river bend. This cell has been measured decades later by Blanckaert (2001b) in a flume in the laboratory. It has never been measured directly with an ADCP in nature. The developed method of distance averaged ADCP data, made it possible to visualize these flow structures.
b) Besides the outer secondary cell, the course of the high velocity cell and the secondary current has been mapped along the meander bends. These structures are not conforming to the bathymetry of the river. Shear stress values showed an increase where erosion features are present and a decrease in areas where no erosion is recognized. This leads to the assumption that the flow structure is forming the river morphology, rather than that the river morphology is creating flow structures.
c) Data analyses of change in river bank morphology and change of water level showed that single, rapid flood events have little influence on bank erosion in river bends.
d) This can be explained by the existence of the secondary outer cell. As Blanckaert (2011) predicted, the secondary outer cell creates a protective layer between the high velocity cell and the river bank. When the secondary outer cell starts to decay, the high velocity cell moves outwards (Farhadi et al., 2018) and erodes material from the river bank. Data from this field work are therefore in agreement with the experimental data.
e) The attempt to model river bank erosion in Norway with CONCEPT was in vain. The results showed that the amount of snow during winter has too many variables for a channel evolution model, which has been developed for warmer climates.
f) In addition to the detailed flow data, a detailed digital terrain model has been created. These data can be used for calibration and developing numerical models.

g) Measuring river bank dynamics with laser scanning is time consuming and has its limits when a lot of vegetation exists. However, laser scanning creates the possibility to measure changes in morphology to under a centimeter in accuracy.

This thesis does not answer all questions but has rather created additional islands of knowledge in the sea of uncertainty, from which others will continue to explore.

5. Recommendations and further research

This PhD leaves room for further and more detailed investigation in the future. This chapter presents unpublished work (5.1 and 5.2) as well as ideas for further research by others.

5.1. Further analysis of ADCP data

In Foerst and Rüther (2012b), it has been shown that averaging ADCP data over distance yields in better results for flow structure analysis. The post processing method for Moving Boat ADCP measurements have been refined. For each transect it has been calculated the optimal averaging distance. This has been done by calculating standard deviation σ for east and north vector for each transect. Both standard deviations have been added. This has been plotted for each distance averaged figure (14). Additionally the figures shows the amount of averaged pings for the respective averaging distance.

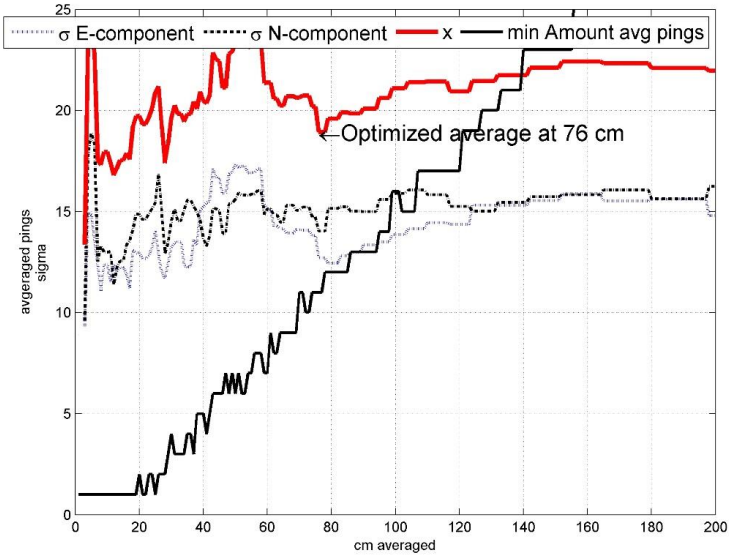

Figure 14: Determination of optimal averaging distance.

The minimum error for distance averaging has been calculated by

$$x = \sqrt{(\sigma_{east}^2 + \sigma_{north}\text{^}2)}$$

The optimal averaging distance has been determined

when

x = minimum

and

amount of averaged pings > 6

Though, this approach might yield in a statistically optimal distance, it has not been used for the search for the secondary outer cell. Therefore, it is necessary to evaluate whether the averaging is appropriate to the flow structure one wishes to study. For this research, an average distance of 0.75 m has been used.

5.2. Stationary paper: Flow characteristics in two consecutive meander bends of a low land river with focus on shear stresses by stationary ADCP measurements. (in prep.)

5.2.1. Introduction and Aims

The understanding of erosion and sediment transport is important to understand the migration of a river in space and time (Couper et al., 2002). This migration process is a complex coaction between many different processes such as hydraulic (Abad et al., 2008; Afzalimehr and Rennie, 2009; Bathurst, 1979), freezing and thawing (Bertrand, 2009; Couper et al., 2002; Lawler, 1993), stratigraphy (Langendoen, 2008), and pore water pressure (Fox et al., 2007; Luchi et al., 2011). The migration can be observed at different scales, such as bend, reach, or river scale (Couper et al., 2002; Kavvas, 1999; Kleinhans, 2010).

Within the last decade the measurements methods of fluvial systems have significantly improved. Moving boat and stationary Acoustic Doppler Current Profiler (ADCP) measurements have been conducted in large rivers to understand the water flow and its influence in erosion and sediment transport (Guerrero and Lamberti, 2012; Sime et al., 2007; Szupiany et al., 2007; Thorne, 1981; Thorne and Hey, 1979; Thorne et al., 1985). The water flow is influenced by different and complex factors such as bathymetry, discharge variability, or submerged vegetation (Langendoen et al., 2005; Schnauder and Sukhodolov, 2012; Sukhodolov and Sukhodolova, 2010). Further, the water flow determines the shear stress (τ) (Biron et al., 2004). Shear stress is the force, which affects the particles. If the force is big enough, the particles break from the riverbed and get in suspension. Therefore, the water flow just above the riverbed, the shear layer, is a driving factor for erosion and river migration. Shear stress cannot be measured directly. However, the shear stress can be calculated from a variety of methods (Biron et al., 2004) such as reach average shear stress (Babaeyan-Koopaei et al., 2002), by log law of the wall (Rodríguez et al., 2013; Schlichting, 1979), turbulent kinetic energy (Kim et al., 2000) or with the Reynolds number (McLelland and Nicholas, 2000). Shear stress is the force, which attacks material and if the force it big enough, the material will be removed, called erosion. A result of erosion are scours due to local increase of energy (Ardies et al., 2002). Main focus on this has been within constructions where scouring can end in fatal results (Fisher et al., 2013). Therefore, the number of investigations of scouring in natural river systems has been limited. Some work has been done by (Wooldridge and Hickin, 2005) in braided rivers and in delta channels by (Beltaos et al., 2011; Eilertsen and Hansen, 2008).

The aim of this paper is to investigate the shear stress, estimated by stationary ADCP measurements. Furthermore, the flow characteristics in two consecutive meander bends of a lowland river in northern

Norway in detail will be described and its influence on the geomorphology and scour development (Eilertsen and Hansen, 2008; Wooldridge and Hickin, 2005). This paper will also present further possibilities of moving boat ADCP measurements and stationary ADCP measurements and discussing this two methods for spatial scaling of the water flow (Couper et al., 2002).

5.2.2. Research site and measuring instruments

The river Breidvikelva is located in a glacial affected valley in northern Norway, Troms. This part of the river has no artificial embankment and high migration activity. The reach consists of three consecutive meander bends with a straight inflow (Foerst and Rüther, 2012a). The first bend has a radius of curvature (RC) of 110 m. The RC of the second and third bend are 60 m and 85 m respectively (table 01). The sinuosity for second and third bend is 4.7. The second and third meander bend form meanders of high-amplitude (Abad and Garcia, 2009; Parker et al., 1983). The investigated reach has a length of 1100 m and a slope of S_w=0.36 ‰. The location beyond the Arctic Circle within a mountainous area, combined with the proximity to the sea makes it behave like a mountain river (McKean and Tonina, 2013), with sediments, expected for a low land river. The riverbed consists mainly of loose silt and sand. Cobbles appear in lower layers. They built the surface on some spots along the slip-off slope and upstream the first bend. The river cuts into a system of former alluvial terraces of different heights. The riverbanks show therefore different altitudes from 3 m a. s. l. up to 25 m a. s. l. Though the proximity to the ocean is given, no backwater effect from the tides has been observed. The lower banks, the left side and partly the right side of the river, are covered with vegetation: birches, scrubs and fern. The dead and living vegetation disrupt the water flow in these areas. Additionally have pockets developed along the erosion slope. The higher banks are located at the right side in the beginning of the first bend and all along the outer bend in the third bend. They consist of loose material without stabilizing vegetation. These riverbanks are strongly affected by erosion.

The geometry has been recorded with a Topcon® RTK-GPS system. The submerged riverbed has been measured with the Sontek© M9 ADCP. In a first step, points in between the measured M9 ADCP transects have been created by interpolation. This was necessary to calculate the riverbed. In a second step, the GPS data have been added and the geomorphology has been calculated by linear interpolation.

The water flow has been recorded with moving and stationary ADCP measurements. The ADCP used in this study for the measurement of the hydraulics is a Streampro© ADCP from RDInstruments. The basic functions of an Acoustic Doppler Current Profiler (ADCP) are described in various papers such as Muste et al. (Muste et al., 2004a), Szupiany (Szupiany et al., 2007), RDInstruments (RDInstruments, 2011), and Shields Jr et al. (Shields Jr et al., 2003). The Streampro© ADCP has been equipped with a pitch and roll sensor as well as a compass to compensate all movements and to have a site wide orientation. The sample frequency, the so-called ‘ping’, has been about 1 Hz. Each ping gets velocity data over the depth and consists of up to 30 vertical measurement points (bins). The size of the bins has been between 3 and 6 cm in depth, depending on the maximal depth of the water level and the amount of valid bins.

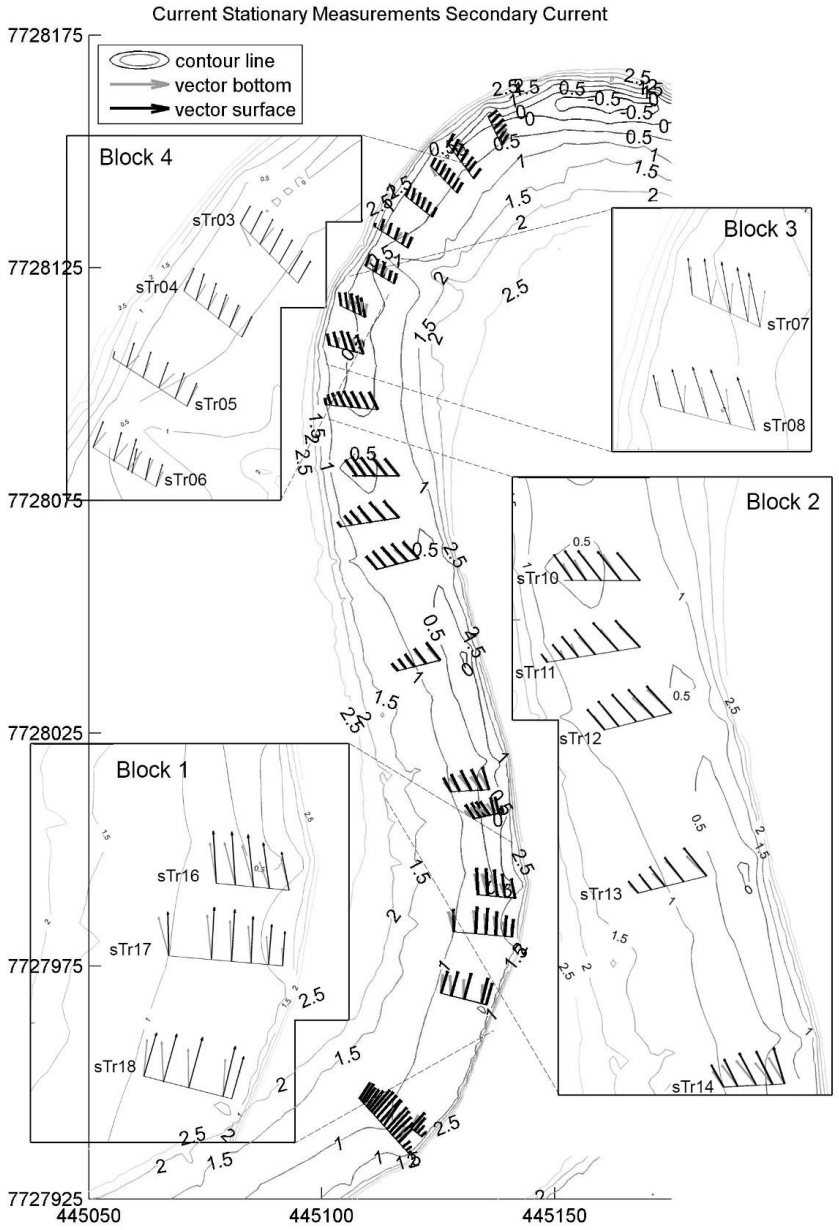

Figure 155: Location of analyzed blocks and measured flow.

Stationary measurements have been conducted with the Streampro© ADCP. The ADCP has been mounted on a platform, which was strained on a double cableway over the river (figure 07). Measurements have been done at 20 transects (sTr01 – sTr20) containing 5 to 8 measurement points, overall 131 stationary ADCP measurements. The distance between transects were in average about 10 m and the distance between the stationary measurements 2 m. These measurements have been

conducted in the first and second bend and the transition between them (figure 15). This mounting made the system flexible enough to move the platform along the cables and move the complete mounting system to the next transect within a short time. Another advantage is that there is no disruption of the water flow or riverbed by mounting it on piles in the river. Additionally, the cableway has been stable enough to hold the transducer without movements. The position of the ADCP was determined with the Topcon© RTK-GPS system, mounted over the transducer on the platform. This RTK-GPS, which gives an absolute accuracy of less than 1 cm horizontally and 1.5 cm vertically. The GPS was programmed to record every 60 seconds the position. All records at one measurement point show the same coordinates clearly within the accuracy. Additional visual performed checks did not show any movements. The stationary ADCP setup can be regarded as stable and therefore no corrections for a swinging ADCP during the post processing are needed (Guerrero and Lamberti, 2012). On a single station, the water flow was recorded for at least 600 pings. The analyses of the normalized mean square error shows (figure 09), that this is enough time to eliminate single fluctuations for averaged flow characteristics (Barua and Rahman, 1998; Guerrero and Lamberti, 2012; Muste et al., 2004a).

5.2.3. Analysis and Results

5.2.3.1. Bathymetry

The bathymetry shows typical point bars and deposition banks in all three meander bends. The thalweg is about 1.1 m a. s. l. at the beginning of the reach and 0.7 at the end. Along the outer bend of all three meanders, the bathymetry shows 5 distinct scours. While in the first bend only 1 scour developed bend 2 and 3 have each 2 scours (figure 16). They depth of the scours reach from -0.5 to 0.5 m a. s. l. The deepest scour is at the apex of the second bend. This is also the only scour, which lies at the apex. In the first bend, the scour appear near the inflection point to the second bend and in bend 3 the scours appear before and after the apex.

The scour in the first bend begins after the apex of the bend and it takes course along the outer bend until the inflection point. There it has its maximum depth at 0.5 m a. s. l. It is weakly developed in comparison to the second bend, which has its maximum depth below -0.5 m a. s. l. In contrast to the upstream bend the scour of the second bend is stronger developed and begins after the apex. There the channel of the second bend begins in the apex and ends about 30 m after the apex, where the channel becomes shallower again. At the inflection point between the bends, the riverbed becomes symmetric with similar slope angles on both riverbanks.

For each scour has been the scour/reach ratio (S/R) calculated (Eilertsen and Hansen, 2008). The S/R has been calculated for mean water level (WL) at this reach (Table 01). Galay (1987) states that the S/R ratio should not exceed 2.5. This is valid for the mean WL. Similar results have been yielded from Eilertsen and Hansen (2008). This publication, however, shows differences in the depth of the thalweg. Since the thalweg in this reach shows a linear slope and the dune development is negligible in this calculation, the S/R is direct proportional to the scour depth. Comparing the RC with the scour depth, it becomes obvious that the deepest scours appear at the bends with the smallest RC.

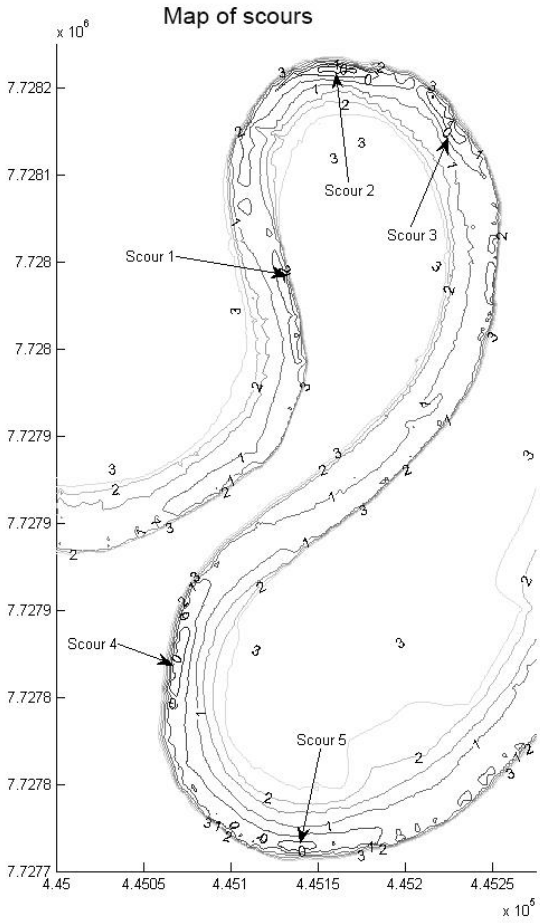

Figure 166: Overview of scours.

Table 1: Overview over scours (figure 16).

Scour Number	**1**	**2**	**3**	**4**	**5**
Scour depth under mean WL (m)	1,45	2,49	2,34	1,89	1,74
Thalweg under mean WL (m)	1,15	1,15	1,15	1,15	1,15
Scour/reach ratio mean WL	1,3	2,2	2,0	1,6	1,5
RC	110	60	60	85	85

5.2.3.2. Stationary Measurements

The amount of collected data made it necessary to measure over a period of 3 week. This leads to alternating water levels during the measurement period. To keep the alternating effect on measurements as low as possible and since the focus has been on the outer bend no measurements

at the point bar side of the river bends have been conducted. For the analyses it was necessary to create blocks of consecutive transects with similar hydraulic conditions. The transects have been analyzed block wise (figure 15). Within each block, the hydraulic conditions (table 2) have been similar.

Table 2: Water level at the moment of stationary measurements.

Block Number	Transects	Water Level
1	16, 17, 18	1.38 masl
2	10, 11, 12, 13, 14	1.34 masl
3	7, 8	1.41 masl
4	3, 4, 5, 6	1.28 masl

The shear stress (τ) has been calculated for the transects by extrapolating the vertical velocity profile to the bottom, using the log law of the wall (Dittrich, 1998; Eilertsen and Hansen, 2008; Rodríguez et al., 2013). The log law of the wall states, that the velocity shows a logarithmic gradient within the last 20 % of the distance from the wall. For this reason, only those stations have been analyzed and compared, if at least 2 bins have been measured within this 20 % distance from the riverbed. Stationary measurements, where the blanking zone at the bottom was bigger than 20 % of the total depth, have been ignored for the calculation of the shear stress. The shear stress (τ_{bed}) has been calculated with the "log law of the wall" by

$$\tau_{bed} = \rho u_*^2 = \rho \left(\frac{u_{bed}\mathrm{K}}{ln\left(\frac{30y}{ks}\right)} \right)^2 \text{ N m}^{-2}$$

with karman constant (K) = 0.41, density (ρ) = 1000 kgm^3, distance from river bed (y) , roughness (ks), and near bed velocity (u_{bed}) (Schlichting, 1979). The roughness (ks) has been calculated by

ks = 3*d90

with

$$d90 = \left(\frac{26}{Strickler\ k} \right)^6$$

with Strickler k = 12.

Block 1: The hydraulic at block 1 has been recorded by a water level of 1.38 m. a. s. l. This corresponds to a discharge of about 12 m^{3}s^{-1}.The bathymetry at the end of the first meander shows a steady, flat-angled slope toward the erosion bar. A 50 m long channel has developed from stationary transect 16 (sTr 16) downstream. The high velocity cell moves from the outer side (sTr 18) towards to the point bar (sTr 16). The secondary current is well-developed and clear visible (figure 15). The stations closest to the outer bank show much weaker secondary currents and a significant drop in water velocities. The magnitude of the secondary current decreases with the outflow of the bend. Short after the apex at transect 18 the average angle between the upper layer (black) and the lower layer (grey) has been 11.3°, and had a value of 9.2° at transect 17 and 8.9° at transect 16. The shear stress (τ) at the outer

stations (transects 16 and 18) show values of 1.65 N m^{-2} and 0.2 N m^{-2} while towards the point bar the value is 2.72 N m^{-2} (figure 17).

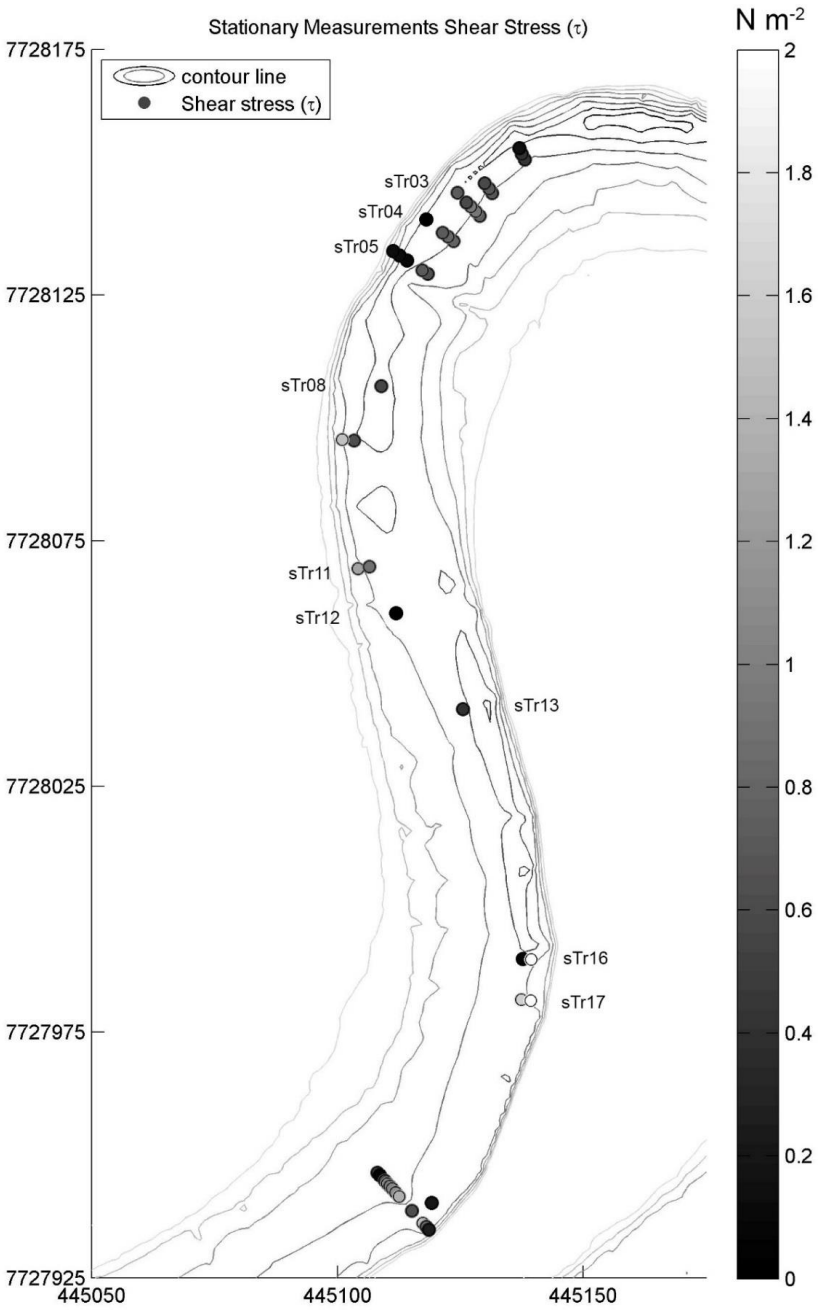

Figure 177: Calculated shear stress.

Block 2: These transects cover the transition between bend 1 and bend 2. At transect 14 it bathymetry gets steeper towards the erosion side and is the channel which developed downstream of block 1. It shows a wide high velocity cell, which stays on the right side. A shift to the left side begins in transect 10, just before the flow enters the second bend. At this time, the thalweg has already moved longer to the left, so that the high velocity cell is not aligned with the bathymetry. While the secondary current is still clear visible at the beginning of the transition (transect 14), it nearly disappears at the inflection point (transect 13) and remains very weak within this block. At transect 11 in this transition zone the shift occurs from a clockwise secondary current to the counter clockwise secondary current (figure 3). In this transect, stations 1 to 3 show a weak, but clear counter clockwise current, while the outer stations 4 to 5 still show residues in the current from the first bend. Such a splitting is, however, not visible in the high velocity cell (figure 2). The shear stress (τ) has been calculated at the same position at transect 11 and transect 10. It increased from 0.9 N m^{-2} at transect 11 to 2.83 N m^{-2} at transect 10.

Block 3: The water level has been at 1.48 m a. s. l. during these measurements. The bathymetry shows that the channel along the erosion bar is slightly wider as it is 25 m further downstream. The highest velocities have been measured above the deepest position of the transect. The secondary current is well developed in both transects. Transect 7, which lies further downstream the bend than transect 8, has a stronger secondary drift (figure 3). The average angle in transect 7 (α=12.3°) is about 1.5° more open as it is in transect 8 (α=10.7°). The shear stress (τ) has been calculated only at the stations upstream of the channel (τ=1.02 N m^{-2} and 0.57 N m^{-2}) and in the beginning of the channel (τ=0.55 N m^{-2}) (figure 17).

Block 4: The bathymetry in this block shows a more distinguished channel as it has been in bend 1. Downstream of transect 3 this channels deepen and get their maximum depth at the head of the bend. The mean velocity has it maximum above the thalweg in transects 4-6. In transect 3 the high velocity cell moved towards the point bar. The maximum velociy lies at between 0.45 and 0.49 ms^{-1} (figure 15). The secondary current exists, however, there is a change in the magnitude from transect 6 to 3. In figure 15 shows the transects 6 and 5 having an average angle between surface and bottom direction of 7.1° and 7.65° while in transect 5 the angle reduces to 5.8° and is nearly disappeared in transect 3 with only 2.3°. The outer position in transect 3 shows values which do not fit into the pattern of the transect. This is due to the location in an out washed pocket. The bed shear stress (τ) decreases from the point bar side to the outer bank. The exception is station 6 in transect 3, which is located directly upstream of the narrow, deep channel. At this position, shear stress (τ) increases again (figure 17).

4. Discussion

This paper analyses the flow structure with stationary ADCP measurements over a reach of 250 m which contains two consecutive meander bends. The river is not regulated and due to the landscape and catchment properties, the water level reacts quickly (Foerst and Rüther, 2012a). This made it impossible to monitor the flow under the same conditions for all measurements. The measurements have been classified into 4 blocks were the water level has been at the same level. Block 1 shows the outflow of the first meander, block 2 shows the crossover from the first to the second meander. Blocks 3 and 4 show the first third of the second meander bend. The shear stress (τ) has been calculated with the logarithmic law of the wall.

The water cuts a channel in the riverbed. It reaches from the end of bend 1 along the transition zone over the inflection point. Another channel has been cut at the beginning of bend 2 and is considerable deep around the apex. Such scours have been reported before in natural rivers, e. g. Thompson (1986), or in flumes e. g. Rodríguez (2013). The high velocity cell before both cases has moved out of the thalweg toward the inner bank and is therefore not aligned with the channel. The high velocity crosses the river at the transition, while the thalweg continuous at the right side (block 2). An alignment of high velocity cell and thalweg happens after the inflection point. Before the flow enters the second bend, another channel is formed on the outer side. A similar phenomena, however, has been measured with the moving boat ADCP (Foerst and Rüther, 2012a) at this position. That the main flow is not aligned with the bathymetry has been described in flumes (Blanckaert, 2001b) and natural rivers (Sukhodolov, 2012b) before.

5.2.4. Conclusion

In this study, the bathymetry has been measured with RTK GPS and ADCP. The water flow has been measured with stationary ADCP. The amount of averaged data (570 pings) makes the stationary measurements less susceptible to outliers. From the stationary measurements the shear stress has been calculated with the log law of the wall. In addition the flow at each measurement station has been plotted.

The water flow is aligned with the bathymetry (transect 18 and 17) and creates low shear stress (τ=0.2 N m^{-2}) at the outer station in transect 18). In transect 16 the main water flow leaves the thalweg and the shear stress (τ=1.65 N m^{-2} at the outer station in transect 16) increases. The same happens later before bend 2 at transect 11 and transect 10. The highest shear stresses occur where the bathymetry deepens ($s_0 < s_{bed}$).

The flow structure showed all expected features, such as high velocity cell and secondary current. It was not possible to visualize the secondary outer cell. For smaller flow structures such as the outer cell circulation (Blanckaert, 2004a; Thorne, 1981) a spatial resolution of minimum half of the expected structure is necessary. This is the advantage of moving boat measurements, as described in chapter 3.2. and 3.3. The stationary ADCP measurements confirm the observations from the moving boat ADCP measurements, that the bathymetry, high velocity cell, and secondary current are not aligned during the transition between two meander bends (Foerst and Rüther, 2012a).

Two observations were made. Firstly, the features of the flow, secondary current and high velocity cell are not always aligned with the bathymetry. Secondly, the shear stress is lowest when the flow is aligned with the bathymetry and vice versa. This leads to the assumption that the bathymetry is rather a result of the flow conditions, rather than the flow is a result of the bathymetry.

5.3. ADV measurements

It has been shown that ADV measurements in natural rivers are limited due to the sensitivity to movements. While Schnauder and Sukhodolov (2012) did measurements in a narrow river, it was possible to use a fixed bridge. As this work shows, the effort on already slightly larger rivers is much higher. Nevertheless, the higher sampling frequency and the much smaller sampling volume yields in much more detailed information about turbulence. Focusing in the future on areas close to the river bank will give a better understanding of which processes occur in boundary layers.

5.4. Ground Water Connections

Part of the objective of this thesis was to supervise a bachelor student regarding ground water flow towards these meanders. This work neglected this topic, even it is known as another, important feature for sediment transport (Eekhout et al., 2013; van Balen, 2008). It would also have gone beyond the scope of this thesis. However, groundwater seeping into the riverbank is a major factor to destabilize a riverbank.

6. Literature

Aalbers, E. E., Lenderink, G., van Meijgaard, E., and van den Hurk, B. J. J. M., 2018, Local-scale changes in mean and heavy precipitation in Western Europe, climate change or internal variability?: Climate Dynamics, v. 50, no. 11, p. 4745-4766.

Abad, J. D., and Garcia, M. H., 2009, Experiments in a high-amplitude Kinoshita meandering channel: 2. Implications of bend orientation on bed morphodynamics: Water Resources Research, v. 45.

Abad, J. D., Rhoads, B. L., Guneralp, I., and Garcia, M. H., 2008, Flow structure at different stages in a meander-bend with bendway weirs: Journal of Hydraulic Engineering-Asce, v. 134, no. 8, p. 1052-1063.

Afzalimehr, H., and Rennie, C. D., 2009, Determination of bed shear stress in gravel-bed rivers using boundary-layer parameters: Hydrological Sciences Journal, v. 54, no. 1, p. 147-159.

Alfieri, L., Burek, P., Feyen, L., and Forzieri, G., 2015, Global warming increases the frequency of river floods in Europe: Hydrol. Earth Syst. Sci., v. 19, no. 5, p. 2247-2260.

Ardies, G. W., Dalrymple, R. W., and Zaitlin, B. A., 2002, Controls on the geometry of incised valleys in the basal quartz unit (Lower Cretaceous), western Canada sedimentary basin: Journal of Sedimentary Research, v. 72, no. 5, p. 602-618.

Babaeyan-Koopaei, K., Ervine, D. A., Carling, P. A., and Cao, Z., 2002, Velocity and turbulence measurements for two overbank flow events in River Severn: Journal of Hydraulic Engineering, v. 128, no. 10, p. 891-900.

Barua, D. K., and Rahman, K. H., 1998, Some aspects of turbulent flow structure in large alluvial rivers: Journal of Hydraulic Research, v. 36, no. 2, p. 235-252.

Bathurst, J. C., 1977, Direct measurements of secondary currents in river bends: Nature, v. 269, no. 5628, p. 504-506.

-, 1979, Secondary flow and shear stress at river bends: Journal of the Hydraulics Division, ASCE, v. 105, no. HY10, Proc.Paper, 14906, p. 1277-1295.

Beltaos, S., Carter, T., and Prowse, T., 2011, Morphology and genesis of deep scour holes in the Mackenzie delta: Canadian Journal of Civil Engineering, v. 38, no. 6, p. 638-649.

Bertrand, F., 2009, Effects of freezing and thawing processes on bank stability: Proceedings of World Environmental and Water Resources Congress 2009 - World Environmental and Water Resources Congress 2009: Great Rivers, v. 342, p. 6480-6488.

Beuselinck, L., 1998, Grain-size analysis by laser diffractometry: Comparison with the sieve-pipette method: Catena, v. 32, no. 3-4, p. 193-208.

Biron, P. M., Robson, C., Lapointe, M. F., and Gaskin, S. J., 2004, Comparing different methods of bed shear stress estimates in simple and complex flow fields: Earth Surface Processes and Landforms, v. 29, no. 11, p. 1403-1415.

Blanckaert, K., 2001a, Bend-flow simulation using 2D depth-averaged model: Journal of Hydraulic Engineering, v. 127, no. 2, p. 166-167.

-, 2001b, Mean flow and turbulence in open-channel bend: Journal of Hydraulic Engineering, v. 127, no. 10, p. 835-847.

-, 2003, Nonlinear modeling of mean flow redistribution in curved open channels: Water Resources Research, v. 39, no. 12, p. ESG61-ESG614.

-, 2004a, Secondary flow in sharp open-channel bends: Journal of Fluid Mechanics, no. 498, p. 353-380.

-, 2011, Hydrodynamic processes in sharp meander bends and their morphological implications: Journal of Geophysical Research: Earth Surface, v. 116, no. 1.

Blanckaert, K., and Graf, W. H, 2004b, Momentum transport in sharp open-channel bends: Journal of Hydraulic Engineering, v. 130, no. 3, p. 186-198.

Blanckaert, K., Duarte, A., Chen, Q., and Schleiss, A. J., 2012, Flow processes near smooth and rough (concave) outer banks in curved open channels: Journal of Geophysical Research F: Earth Surface, v. 117, no. 4.

Brodu, N., and Lague, D., 2012, 3D terrestrial lidar data classification of complex natural scenes using a multi-scale dimensionality criterion: Applications in geomorphology: ISPRS Journal of Photogrammetry and Remote Sensing, v. 68, no. 1, p. 121-134.

Cantón, Y., 2009, Aggregate stability in range sandy loam soils Relationships with runoff and erosion: Catena, v. 77, no. 3, p. 192-199.

Corner, G. D., 2006, A transgressive-regressive model of fjord-valley fill: stratigraphy, facies and depositional controls: Society for Sedimentary Geology, v. 85, p. 161-178.

Couper, P., Stott, T., and Maddock, I., 2002, Insights into river bank erosion processes derived from analysis of negative erosion-pin recordings: Observations from three recent UK studies: Earth Surface Processes and Landforms, v. 27, no. 1, p. 59-79.

Coveney, S., and Stewart Fotheringham, A., 2011, Terrestrial laser scan error in the presence of dense ground vegetation: Photogrammetric Record, v. 26, no. 135, p. 307-324.

Day, S. S., Gran, K. B., Belmont, P., and Wawrzyniec, T., 2013a, Measuring bluff erosion part 1: Terrestrial laser scanning methods for change detection: Earth Surface Processes and Landforms, v. 38, no. 10, p. 1055-1067.

-, 2013b, Measuring bluff erosion part 2: Pairing aerial photographs and terrestrial laser scanning to create a watershed scale sediment budget: Earth Surface Processes and Landforms, v. 38, no. 10, p. 1068-1082.

Dittrich, A., 1998, Wechselwirkung Morphologie/Strömung naturnaher Fliessgewässer, Karlsruhe, Wasserwirtschaftsverband Baden-Württemberg e. V., Mitteilungen des Institutes für Wasserwirtschaft und Kulturtechnik der Universität Karlsruhe (TH).

Eekhout, J. P. C., Hoitink, A. J. F., and Makaske, B., 2013, Historical analysis indicates seepage control on initiation of meandering: Earth Surface Processes and Landforms, v. 38, no. 8, p. 888-897.

Eilertsen, R. S., and Hansen, L., 2008, Morphology of river bed scours on a delta plain revealed by interferometric sonar: Geomorphology, v. 94, no. 1-2, p. 58-68.

Farhadi, A., Sindelar, C., Tritthart, M., Glas, M., Blanckaert, K., and Habersack, H., 2018, An investigation on the outer bank cell of secondary flow in channel bends: Journal of Hydro-environment Research, v. 18, p. 1-11.

Farzadkhoo, M., Keshavarzi, A., Hamidifar, H., and Javan, M., 2018, A comparative study of longitudinal dispersion models in rigid vegetated compound meandering channels: Journal of Environmental Management, v. 217, p. 78-89.

Fisher, M., Khan, A. A., and Atamturktur, S., 2013, The state of the art in scour monitoring, p. 37-72.

Foerst, M., and Rüther, N., 2012a, Mean and Turbulent Flow Structures in two Consectutive Meander Bends, IAHR Europe, Proceeding 2012: Munich, Germany, Proc. 2nd European Congress of the IAHR.

Foerst, M., and Rüther, N., 2012b, Post Processing Methods of Moving Boat ADCP Measurements: Time Averaging vs. Distance Averaging., 14. Treffen junger WissenschaftlerInnen an Wasserbauinstituten. Beiträge zum JuWi-Treffen am 25. und 26. Juni 2012 an der Technischen Universität München.: Munich, TU Munich, p. 216.

Fox, G. A., Wilson, G. V., Simon, A., Langendoen, E. J., Akay, O., and Fuchs, J. W., 2007, Measuring streambank erosion due to ground water seepage: correlation to bank pore water pressure, precipitation and stream stage: Earth Surface Processes and Landforms, v. 32, no. 10, p. 1558-1573.

Galay, V. J., Yaremko, E.K., Quazi, M.E., 1987, River bed scour and construction of stone riprap protection., *in* Thorne C.R., B. J. C., and Hey R.D., ed., Sediment Transport in Gravel-bed Rivers: Chichester, United Kingdom, Wiley and Sons, p. 353-379.

Grenfell, M. C., Nicholas, A. P., and Aalto, R., 2014, Mediative adjustment of river dynamics: The role of chute channels in tropical sand-bed meandering rivers: Sedimentary Geology, v. 301, p. 93-106.

Groom, J., and Friedrich, H., 2019, Spatial structure of near-bed flow properties at the grain scale: Geomorphology, v. 327, p. 14-27.
Guerrero, M., and Lamberti, A., 2012, Flow field and morphology mapping using ADCP and multibeam techniques: Survey in the po river: Journal of Hydraulic Engineering, v. 137, no. 12, p. 1576-1587.
Guerrero, M., Rüther, N., Haun, S., and Baranya, S., 2017, A combined use of acoustic and optical devices to investigate suspended sediment in rivers: Advances in Water Resources, v. 102, p. 1-12.
Hanson, G. J. a. S., A., 2001, Erodibility of cohesive streambeds in the loess area of the midwestern USA: HYDROLOGICAL PROCESSES, v. 15, p. 23-28.
Jugie, M., Gob, F., Virmoux, C., Brunstein, D., Tamisier, V., Le Coeur, C., and Grancher, D., 2018, Characterizing and quantifying the discontinuous bank erosion of a small low energy river using Structure-from-Motion Photogrammetry and erosion pins: Journal of Hydrology, v. 563, p. 418-434.
Julian, J. P., 2006, Hydraulic erosion of cohesive riverbanks: Geomorphology, v. 76, no. 1-2, p. 193-206.
Kasvi, E., Laamanen, L., Lotsari, E., and Alho, P., 2017, Flow Patterns and Morphological Changes in a Sandy Meander Bend during a Flood—Spatially and Temporally Intensive ADCP Measurement Approach: Water, v. 9, no. 2, p. 106.
Kavvas, M. L., 1999, On the coarse-graining of hydrologic processes with increasing scales: Journal of Hydrology, v. 217, no. 3-4, p. 191-202.
Kim, S. C., Friedrichs, C. T., Maa, J. P. Y., and Wright, L. D., 2000, Estimating bottom stress in tidal boundary layer from acoustic doppler velocimeter data: Journal of Hydraulic Engineering, v. 126, no. 6, p. 399-406.
Kjellström, E., Nikulin, G., Strandberg, G., Christensen, O. B., Jacob, D., Keuler, K., Lenderink, G., van Meijgaard, E., Schär, C., Somot, S., Sørland, S. L., Teichmann, C., and Vautard, R., 2018, European climate change at global mean temperature increases of 1.5 and 2 °C above pre-industrial conditions as simulated by the EURO-CORDEX regional climate models: Earth Syst. Dynam., v. 9, no. 2, p. 459-478.
Klavon, K., Fox, G., Guertault, L., Langendoen, E., Enlow, H., Miller, R., and Khanal, A., 2017, Evaluating a process-based model for use in streambank stabilization: insights on the Bank Stability and Toe Erosion Model (BSTEM): Earth Surface Processes and Landforms, v. 42, no. 1, p. 191-213.
Kleinhans, M. G., 2010, Sorting out river channel patterns: Progress in Physical Geography, v. 34, no. 3, p. 287-326.
Lague, D., Brodu, N., and Leroux, J., 2013, Accurate 3D comparison of complex topography with terrestrial laser scanner: Application to the Rangitikei canyon (N-Z): ISPRS Journal of Photogrammetry and Remote Sensing, v. 82, p. 10-26.
Lammers, R. W., and Bledsoe, B. P., 2018, A network scale, intermediate complexity model for simulating channel evolution over years to decades: Journal of Hydrology, v. 566, p. 886-900.
Langendoen, E. J., 2000a, CONCEPTS - Conservational Channel Evolution and Pollutant Transport System, *in* Laboratory, U.-A. N. S., ed., Guidline NSL Technical Report: Oxford, MS, p. 180.
-, 2008, Modeling the Evolution of Incised Streams. II: Streambank Erosion: J. Hydraul. Eng., v. 134, no. 7, p. 905.
Langendoen, E. J., and Simon, A., 2000b, Stream channel evolution of Little Salt Creek and North Branch West Papillion Creek, eastern Nebraska.: National Sedimentation Laboratory, .
Langendoen, E. J., Lowrance, R. R., Williams, R. G., Pollen, N., and Simon, A., Modeling the impact of riparian buffer systems on bank stability of an incised stream2005, p. 591.
Lawler, D. M., 1993, Needle ice processes and sediment mobilization on river banks: the River Ilston, West Glamorgan, UK: Journal of hydrology, v. 150, no. 1, p. 81-114.
Le Bissonnais, Y., 1996, Aggregate stability and assessment of soil crustability and erodibility: I. Theory and methodology | Stabilite structurale et evaluation de la sensibilite des sols a la

battance et a l'erosion: I: Theorie et methologie: European journal of soil science, v. 47, no. 4, p. 425-437.
Leng, X., and Chanson, H., 2018, Transverse velocity profiling under positive surges in channels: Flow Measurement and Instrumentation, v. 64, p. 14-27.
Li, Z., Wu, X., and Gao, P., 2019, Experimental study on the process of neck cutoff and channel adjustment in a highly sinuous meander under constant discharges: Geomorphology, v. 327, p. 215-229.
Luchi, R., Zolezzi, G., and Tubino, M., 2011, Bend theory of river meanders with spatial width variations: Journal of Fluid Mechanics, v. 681, p. 311-339.
McKean, J., and Tonina, D., 2013, Bed stability in unconfined gravel bed mountain streams: With implications for salmon spawning viability in future climates: Journal of Geophysical Research F: Earth Surface, v. 118, no. 3, p. 1227-1240.
McLelland, S. J., and Nicholas, A. P., 2000, A new method for evaluating errors in high-frequency ADV measurements: Hydrological Processes, v. 14, no. 2, p. 351-366.
Milan, D. J., Heritage, G. L., Large, A. R. G., and Entwistle, N. S., 2010, Mapping hydraulic biotopes using terrestrial laser scan data of water surface properties: Earth Surface Processes and Landforms, v. 35, no. 8, p. 918-931.
Momm, H. G., Bingner, R. L., Wells, R. R., and Dabney, S. M., Application of ground-based lidar for gully investigation in agricultural landscapes, *in* Proceedings American Society for Photogrammetry and Remote Sensing Annual Conference 20112011, p. 331-340.
Moss, R. H., Edmonds, J. A., Hibbard, K. A., Manning, M. R., Rose, S. K., van Vuuren, D. P., Carter, T. R., Emori, S., Kainuma, M., Kram, T., Meehl, G. A., Mitchell, J. F. B., Nakicenovic, N., Riahi, K., Smith, S. J., Stouffer, R. J., Thomson, A. M., Weyant, J. P., and Wilbanks, T. J., 2010, The next generation of scenarios for climate change research and assessment: Nature, v. 463, p. 747.
Muste, M., Kim, Y., Kruger, A., Krajewski, W., Bradley, A., and Papanicolaou, T., Watershed-scale cybertools: Real-time stream monitoring at ungaged sites, Williamsburg, VA, 2005, p. 169-175.
Muste, M., Yu, K., Pratt, T., and Abraham, D., 2004a, Practical aspects of ADCP data use for quantification of mean river flow characteristics; Part II: Fixed-vessel measurements: Flow Measurement and Instrumentation, v. 15, no. 1, p. 17-28.
Muste, M., Yu, K., and Spasojevic, M., 2004b, Practical aspects of ADCP data use for quantification of mean river flow characteristics; Part I: moving-vessel measurements: Flow Measurement and Instrumentation, v. 15, no. 1, p. 1-16.
Nasermoaddeli, M. H., Pasche, E., Application of terrestrial 3D laser scanner in quantification of the riverbank erosion and deposition, *in* Proceedings Proceedings of International Conference on fluvial Hydraulics, Cesme-Ismir,Turkey, Sep. 3-5 2008, Volume 3, p. 10.
O'Neal, M. A., and Pizzuto, J. E., 2011, The rates and spatial patterns of annual riverbank erosion revealed through terrestrial laser-scanner surveys of the South River, Virginia: Earth Surface Processes and Landforms, v. 36, no. 5, p. 695-701.
Parker, G., Diplas, P., and Akiyama, J., 1983, MEANDER BENDS OF HIGH AMPLITUDE: Journal of Hydraulic Engineering, v. 109, no. 10, p. 1323-1337.
Parker, G., Shimizu, Y., Wilkerson, G. V., Eke, E. C., Abad, J. D., Lauer, J. W., Paola, C., Dietrich, W. E., and Voller, V. R., 2011, A new framework for modeling the migration of meandering rivers: Earth Surface Processes and Landforms, v. 36, no. 1, p. 70-86.
RDInstruments, 2011, Acoustic Doppler Current Profiler Principles of Operation A Practical Primer: Poway, CA, USA.
Redolfi, M., Bertoldi, W., Tubino, M., and Welber, M., 2018, Bed Load Variability and Morphology of Gravel Bed Rivers Subject to Unsteady Flow: A Laboratory Investigation: Water Resources Research, v. 54, no. 2, p. 842-862.
Resop, J. P., and Hession, W. C., 2010, Terrestrial laser scanning for monitoring streambank retreat: Comparison with traditional surveying techniques: Journal of Hydraulic Engineering, v. 136, no. 10, p. 794-798.

Rodríguez, J. F., García, C. M., and García, M. H., 2013, Three-dimensional flow in centered pool-riffle sequences: Water Resources Research, v. 49, no. 1, p. 202-215.
Rüther, N., and Olsen, N. R. B., 2007, Modelling free-forming meander evolution in a laboratory channel using three-dimensional computational fluid dynamics: Geomorphology, v. 89, no. 3-4, p. 308-319.
Schlichting, H., 1979, Boundary Layer Theory, New York, McGraw-Hill.
Schnauder, I., and Sukhodolov, A. N., 2012, Flow in a tightly curving meander bend: Effects of seasonal changes in aquatic macrophyte cover: Earth Surface Processes and Landforms, v. 37, no. 11, p. 1142-1157.
Shields Jr, F. D., Knight, S. S., Testa Iii, S., and Cooper, C. M., 2003, Use of Acoustic Doppler current profilers to describe velocity distributions at the reach scale: Journal of the American Water Resources Association, v. 39, no. 6, p. 1397-1408.
Sime, L. C., Ferguson, R. I., and Church, M., 2007, Estimating shear stress from moving boat acoustic Doppler velocity measurements in a large gravel bed river: Water Resources Research, v. 43, no. 3.
Simon, A., 2000, Bank and near-bank processes in an incised channel: Geomorphology, v. 35, no. 3-4, p. 193-217.
Simon, A. a. D., S., 2010, It's Not All About Discharge and Hydraulics: The Role of Shear Strength and Streambank Composition in Controlling Channel Width, EGU 2010, Volume 12: Vienna, p. 1.
Solberg, I. L., Hansen, L., Rokoengen, K., Sveian, H., and Olsen, L., 2008, Deglaciation history and landscape development of fjord-valley deposits in Buvika, Mid-Norway: Boreas, v. 37, no. 2, p. 297-315.
Song, S., Schmalz, B., and Fohrer, N., 2015, Simulation, quantification and comparison of in-channel and floodplain sediment processes in a lowland area – A case study of the Upper Stör catchment in northern Germany: Ecological Indicators, v. 57, p. 118-127.
Sukhodolov, A. N., 2012a, Structure of turbulent flow in a meander bend of a lowland river: Water Resources Research, v. 48, no. 1.
Sukhodolov, A. N., 2012b, Structure of turbulent flow in a meander bend of a lowland river: Water Resources Research, v. in press.
Sukhodolov, A. N., and Sukhodolova, T. A., 2010, Case study: Effect of submerged aquatic plants on turbulence structure in a lowland river: Journal of Hydraulic Engineering, v. 136, no. 7, p. 434-446.
Szupiany, R. N., Amsler, M. L., Best, J. L., and Parsons, D. R., 2007, Comparison of fixed- and moving-vessel flow measurements with an aDp in a large river: Journal of Hydraulic Engineering, v. 133, no. 12, p. 1299-1309.
Thompson, A., 1986, Secondary flows and the pool-riffle unit: a case study of the processes of meander development: Earth Surface Processes & Landforms, v. 11, no. 6, p. 631-641.
Thorne, C. R., 1981, Direct measurements of secondary currents in natural meander: Wasserwirtschaft, v. 71, no. 10 , Oct. 1981, p. 283-288.
Thorne, C. R., and Hey, R. D., 1979, Direct measurements of secondary currents at a river inflexion point [8]: Nature, v. 280, no. 5719, p. 226-228.
Thorne, C. R., Zevenbergen, L. W., Pitlick, J. C., Rais, S., Bradley, J. B., and Julien, P. Y., 1985, Direct measurements of secondary currents in a meandering sand-bed river: Nature, v. 315, no. 6022, p. 746-747.
van Balen, R. T., 2008, Impact of groundwater flow on meandering; example from the Geul River, The Netherlands: Earth Surface Processes and Landforms, v. 33, no. 13, p. 2010-2028.
Wakindiki, I. I. C. I. I. C., 2002, Soil mineralogy and texture effects on crust micromorphology, infiltration, and erosion: Soil Science Society of America Journal, v. 66, no. 3, p. 897-905.
Wheaton, J. M., Brasington, J., Darby, S. E., and Sear, D. A., 2010, Accounting for uncertainty in DEMs from repeat topographic surveys: Improved sediment budgets: Earth Surface Processes and Landforms, v. 35, no. 2, p. 136-156.

Wooldridge, C. L., and Hickin, E. J., 2005, Radar architecture and evolution of channel bars in wandering gravel-bed rivers: Fraser and Squamish rivers, British Columbia, Canada: Journal of Sedimentary Research, v. 75, no. 5, p. 844-860.
Yang, H., Lin, B., and Zhou, J., 2018, Avulsions in a Simulated Large Lowland Braided River: Water Resources Management, v. 32, no. 7, p. 2301-2314.

7. Appendix

7.1. Appendix A: Publications

PAPER I

River, Coastal and Estuarine Morphodynamics: RCEM2011
© 2011 Tsinghua University Press, Beijing

Evaluating erosion processes of a two layer river bank

Markus FOERST, Nils RÜTHER
Norwegian University of Science and Technology,
Department of Hydraulic and Environmental Engineering,
S.P. Andersensveg 5, 7491 Trondheim, Norway

Felix HAHN
Eberhard Karls University of Tuebingen
Department of Geography, Tuebingen, Germany

ABSTRACT: The present study presents data of a strongly erosive reach in a river in central Norway. It gives insight in the erosional behavior of river bank sediments which consist of two different layers of typical fjord valley infillings (Hansen et al., 2009). The river, Forra, in the east of Trondheim, Norway, is a meandering river with relicts of infrastructural buildings. The side-slope of the riverbank is partly protected by trees and anthropogenic positioned rocks. The investigated part of the side- slope adjoins over most of its length to farmland. The investigated reach is located after a geometrical contraction due to bridge piers and characterized by severe bank erosion. At this location, the side erosion rate reaches 0.5 - 1 ma-1. The erosion processes at this site are very complex and a combination of freezing and thawing triggered erosion, bank mass failure and seepage erosion. The geological setup of the riverbank is divided into two different layers. The lower layer consists of laminated clay and is the aquiferous layer. The upper part consists of cobbles with gravel and sandy infillings.

The overall goal of the present study is to investigate the role of different parameters, such as grain size, moisture, temperature and the influences of different hydraulic conditions, contributing to bank erosion and mass failure. The secondary goal of the study is to evaluate in how far the one-dimensional (1D) numerical software CONCEPTS (CONservational Channel Evolution and Pollutant Transport System) (Langendoen, 2000) can be used for bank failures within such complex erosion processes. For typical and extreme combinations of discharges and water levels, the stream bank erosion rate was computed for scenarios with different stratigraphic compositions and vegetation covers, i.e. cropland or natural woodlands along the riverbank.

CONCEPTS was built in the National Sedimentation Laboratory at Agricultural Research Service of the US Department of Agriculture. The model assumes the flow in stream systems to be one-dimensional along the centerline of the channel. It computes the flow as a function of time simultaneously at a series of cross sections along the stream using the Saint Venant equations. Sediment-transport rates are a function of flow hydraulics, bed composition, and upstream sediment supply. The numerical model calculates total-load sediment-transport rates by size fraction from a mass conservation law, and taking into account the differing processes governing entrainment. For cohesive bed material, erosion rate is calculated following an excess shear-stress approach. The deposition rate is based on local shear stress and particle fall velocity.

The computed bank retreat rates were compared to bank retreat observations based on field observations, DEMs gained from laser scanning and air photos. The simulated results showed that bank failures due to gravity seem to play a significant role mainly for dedicated combinations of stratigraphic setups. However, CONCEPTS has limitations with freezing and thawing processes, which leads to an underestimation of bank failures.

1 INTRODUCTION

Areas which are used for agricultural use are rare in Norway and mainly limited to floodplains. In a natural river the riverbed meanders within a valley and riverbank failure is a common event throughout all natural riverbeds. The erosion and sedimentation processes are balanced. However the human interference usually destroys the balance by changing the river flow sealing the riverbank e. g. building bridges. In this case there might be an extraordinary amount of erosion, which leads to loss of fertile soil and if the erosion process continues in similar velocity the nearby road will also be spilled away within the next future. Processes which lead to bank failure are different. Thorne (1981) distinguishes between two basic processes of bank erosion. One is dominated by mass failure due to gravity and the other is mainly driven by fluvial erosion process. Most investigations have been conducted based on shear stress, which attacks the soil and sediment at the river bank. Exceeds the shear stress (τ) from the river the critical shear stress (τc) of the riverbank, fluvial erosion takes place. However, there are various factors influencing erosion and finally bank failure. There are freezing and thawing (Bertrand, 2009), groundwater pressure (Fox et al., 2007), texture and stratigraphy of the riverbank (Teixeira and Misra, 1997; Thorne, 1981; Wakindiki, 2002), and vegetation (Langendoen et al., 2005; Pollen-Bankhead, 2009; Simon et al., 2006).

This study presents preliminary results of an ongoing project which has recently started. This project is focused on bank erosion in meandering rivers and the overall goal is to quantify the amount of sediments eroded either by hydraulic processes or by the climate. CONCEPTS (CONservational Channel Evolution and Pollutant Transport System) has been developed to model bank retreat and bank failure in a channel. Its main application is in streams which have been anthropogenic altered. CONCEPTS is based on hydraulics and channel morphology. It calculates a 1D flow through a straight channel. In the literature this model is used for narrow stream channels were the height – width ratio > 0.04 (Fox et al., 2007). Further validation of the model have been done in climate zones were the mean temperature is always above 0° C and therefore no storage of the water and no freezing and thawing effect takes place. The focus in this study will be to model a stream channel with a height – width ratio < 0.02.

2 DESCRIPTION OF THE STUDY AREA

The research area is called Forraselva and is located about 40 km east of Trondheim, Norway (figure 1). Most parts of the riverbank are protected according to future use of waterpower. The water flow, however is not yet regulated and shows natural variations. The climate is a Dfc after Köppen-Geiger with a main precipitation from July until December. The yearly average is about 900 mm. During winter most of the precipitation occurs as snow and therefore water is held back until snowmelt around March to April. This leads to two water high stands; one in spring during snowmelt and one in autumn during the higher precipitation. While the discharge during spring flood is steadily high, the discharge oscillates during the autumn. The lowest discharge is in August with an average of .4 m^3s^{-1}.

The valley infilling is a typical Norwegian fjord valley infilling with changing layers of clay, silt and sediments of coarser compositions described by (Corner, 2006; Solberg et al., 2008). Along the research site the river cuts into marine-glaciomarine sediments which are covered by fluvial-deltaic sediments. The lower layer (marine-glaciomarine sediment) consists of clay layers interlaced by fine silt layers. The upper layer (fluvial-deltaic) consists of much coarser material ranging from fine sand up to cobbles. The amount of the clay and silt fraction is negligible. The covering soil layer is a 30 cm thick anthric horizon (Ap horizon) which is cultivated with crops. The riverbed consists of pebbles with a diameter of between 10 and 25 cm. Pebbles up to 50 cm occur sporadically. The riverbed shows no movement.

150 m upstream a geometrical contraction due to bridge piers narrows the river. Behind the bridge piers is farmland adjacent to the river. Along the upper half the farmland is protected by vegetation. The unprotected riverbank between vegetation and artificially placed blocks downstream the riverbank experiences severe erosion over a distance of about 150 m. The susceptible part of the riverbank is at the transition from a right turn of the river into a left turn. However, since the turn to the left of the studied riverbank is protected by rocks and therefore not naturally developed the water flow hits the riverbank with more energy as it would in a natural developed meandering river system.

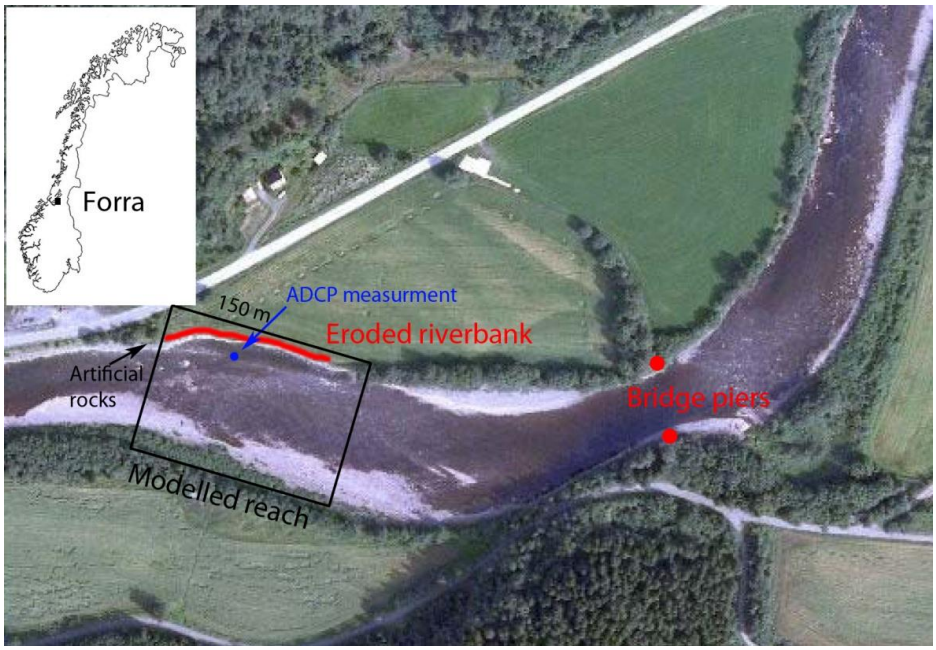

Figure 1 Study area in Nord-Trøndelag, Norway (source www.norgeibilder.no)

2 METHODS

2.1 *Sampling*

Discharge has been monitored by NVE (Norges vassdrags- og energidirektorat) about 10 km upstream. The water level has been measured at the bridge piers with a global water logger WL 16. Precipitation has been measured by a weather station (ID IUNDEFIN65) about 3 km west of Fornes. Shear stress measurements in the layers have been conducted with a vane shear stress meter H-60 with standard vane (20 x 40 mm).

Samples were taken at different places to insure that the layers are homogeneous along the site. The samples were sieved down to 2 mm grain size. Sieving showed that there were nearly no grains. Afterwards samples were air dried and then 10 g were taken for further processing. Each sample was wetted with H_2O and 35 % hydrogen peroxide solution (H_2O_2) was added. The samples were cleaned of organic matter by putting them into a water bath at 50° C. This treatment was necessary since fine roots in sample 1 and 11 were left after sieving and should be removed for better results. In preparation for grain size analysis samples were dissolved in H_2O and 50 ml of sodium hexametaphosphate $(NaPO_3)_6$. This solution was shaken for at least twelve hours at 160 rpm. For the texture analyses the laser diffractometry was chosen due to better reproducibility (Beuselinck, 1998). For the analyses a Coulter LS 230 was used with a particle size analysis range from 0.04 µm to 2000 µm. Three runs, each 120 sec for each sample were done using the Fraunhofer optical model.

The water velocities have been measured with an ADCP (StreamPro from Teledyn). It was stationary installed about 1 meter from the riverbank. The velocities during beginning of snowmelt were between 1.2 and 1.6 ms^{-1}. The moving bed test which can be performed with StreamPro ADCP is a measurement of the riverbed and its sediment movement. This has to be done to determine if it is possible to use the bottom track function to measure the distance the ADCP has moved during measurements. On the other hand is it possible to measure if actual erosion takes place under the present hydraulic conditions.

2.2 *Cross sections and terrestrial laser scanning*

The cross sections were recorded with a differential GPS. The riverbanks were scanned with a laser

scanner (GSL 1000 from Topcon). In 2010 the first scan was done with about 80,000 and in 2011 with more than 1,000,000 scan points. Three target points have been positioned. The target points were the same in each year to insure a perfect overlying of the two scans. The post processing has been done in the first step with ScanMaster software from Topcon. Afterwards data have been imported into ESRI ArcGIS. The slope inclination and the volumina difference (figure 4 and 5) were calculated with the 3D analyst of ArcGIS.

2.3 *Modeling with CONCEPTS*

The model CONCEPTS (CONservational Channel Evolution and Pollutant Transport System) was chosen due to a focus on soil texture, shear stress and erodibility within the soil layers. Additionally it allows different vertical soil layers within a riverbank. The intention was to model and evaluate stream-corridor restoration designs, especially to evaluate the long-term stability of stream corridors (Langendoen, 2000). It is made to compute one-dimensional channel flow simulations. The reach is relatively straight in comparison to other reaches modeled with CONCEPTS before. This is an advantage, since CONCEPTS is limited to straight channels. Further limitation is the morphology of the cross sections, which are not allowed to have a second descent away from the thalweg. That means, that hollows, pools, bars, and secondary channels within the riverbank and the floodplain cannot be calculated. The single points in the cross sections have been manually removed in order to receive cross sections of the river with increasing riverbanks away from the thalweg.

The discharge has been the hourly discharge measured by NVE. This data series was used during the same time interval of the laser scans. The manning value was chosen from Chow (1959). The shear strength was directly measured with a shear vane meter.

3 RESULTS AND DISCUSSIONS

3.1 *Riverbank and hydraulic*

All samples for grain size analyses showed the same texture within the same layer (figure 3). This result fits into the fjord fill stratigraphy (Corner, 2006). The lower layer represents the laminated glaciomarine/marine sedimentation and the upper layer the river delta foreset. Grain sizes between sand and medium gravel are missing and grain sizes bigger than medium gravel have been ignored. Grain sizes > 62 mm (coarse gravel) have been present. To insure, that these grain sizes are not influenced by the hydraulic the moving bed test has been conducted with the ADCP. This test makes sure, that the river bed is stable under the actual flow conditions. The velocity profile (figure 2) shows maximum velocities of about 1.6 ms^{-1} and 1.5 ms^{-1} close to the river bed. Taken into account, that the ADCP has a blanking zone of about 12-15 cm to the bottom, where no measurements are possible, the velocity at the gravel riverbed will be less than 1 ms^{-1}.The moving bed test has been positive for the river bed, which is armored by the same cobbles as in the upper layer abundant. However, these cobbles will not be influenced by flow velocities of less than 1 ms^{-1} as they will occur at the bank due to the bank movement test. The cobbles which built the skeleton of the coarse layer have a volume of 90 %. This outweighs the cohesion of the layer. For the estimation of the manning value the cobbles have been taken into account (Chow, 1959). The measured critical shear stress has been averaged for each layer. The difference between the upper and lower part in the clay layer has been about the double shear stress. The sand layer showed more homogeneous values.

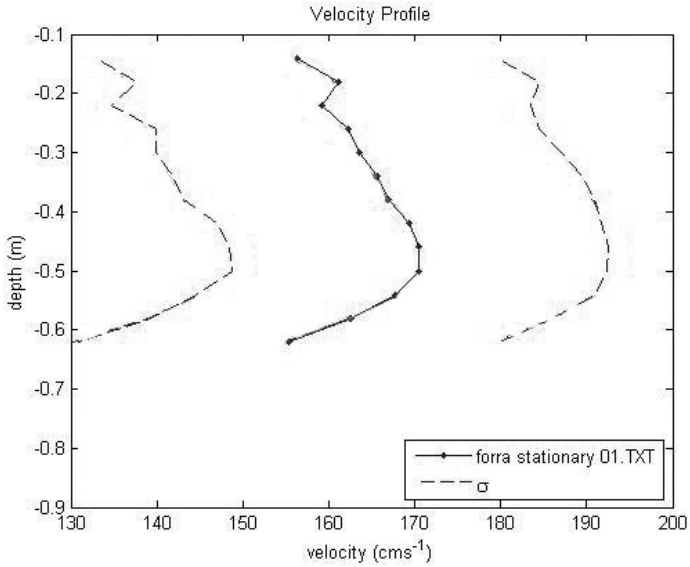

Figure 2 Velocity profile about 1 m from riverbank over gravel riverbed. Velocity is averaged over 10 min recording.

Table 1 Critical shear stress values measured in the field (averaged)

	Upper part averaged	Lower part averaged	Used
Lower layer	77 kPa	37 kPa	57 kPa
Upper layer	34 kPa	42 kPa	38 kPa

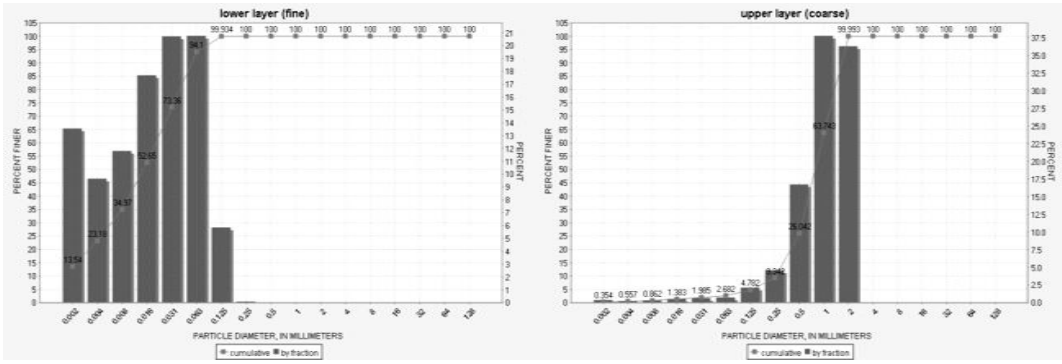

Figure 3 Grain size distributions in the upper and lower layer as used in CONCEPTS

3.2 *Laser scan*

Visual inspections at Forraselva gave a first idea, about erosion rates and processes. During wintertime soil and groundwater is frozen which keeps the riverbank stable. Spots exposed directly to the sun show also little gravitational erosion. After snowmelt near-vertical tension cracks about 30 cm deep and 2 to 10 cm wide appeared along the upper part of the riverbank. Similar observations have been made by Simon (2000). At Forraselva the tracks on the field are still very obvious. And if we assume that the distance from the field edge to the widest extent the farmer risks to drive with his tractor we can assume a bank retreat of nearly 1 meter within the last 6 month during winter. These observations are consistent with laser scan measurements.

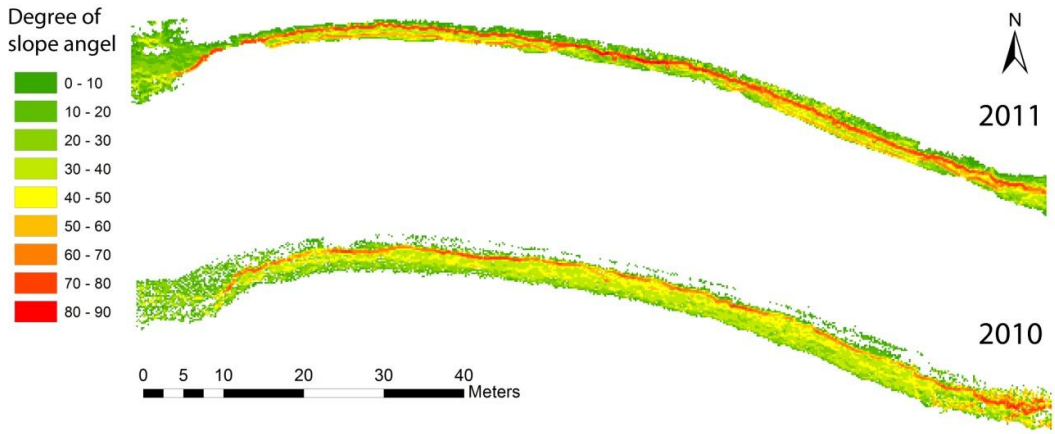

Figure 4 Comparison slope angel along the reach taken with terrestrial laser scanning

After snowmelt in spring 2011 the riverbank looked very different from autumn 2010. Most of the erosion took place during spring. This can be seen in figure 4 were the laser scan has been taken short after snowmelt in 2011. Along the site two steep steps are developed. These are consistent with the two sediment layers. At the west end of the riverbank is the lower layer not visible as a step. This is due to the development of a pool, where the lower layer is further eroded as the upper layer. The riverbank experiences an undercut at this position. The riverbank from 2010 does not show the second step. Lose material from the upper layer fell and accumulated on the lower layer. In between the gravel sand, smaller gravel accumulates and the nearly vertical river bank gets a lower angle. This covers the lower layer with another sediment layer. In the beginning the cobbles from the upper layer help to trap the sand fraction. Whenever the water level rises over the fresh deposited sediment, the finer material is washed away and the bigger cobbles stay at the lower part. These cobbles will be removed with the next retreat of the clay layer.

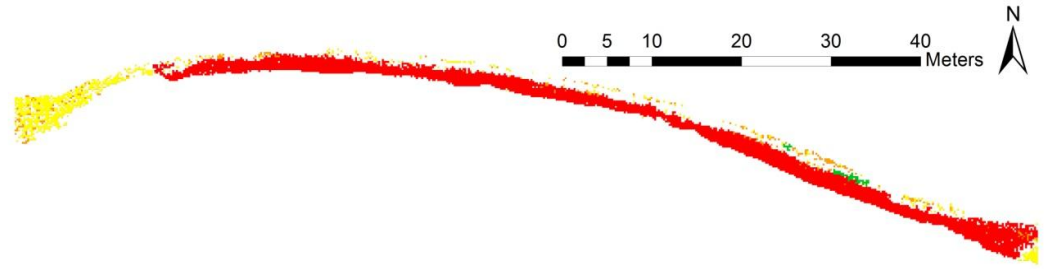

Figure 5 Erosion and sedimentation changes (Red: erosion, yellow: minimal erosion, green: accumulation/vegetation)

The scanned surface of the year 2011 was subtracted from the scanned surface of 2010 using the ESRI ArcGIS tool CutFill to define spots of erosion and sedimentation (figure 5). The red areas show erosion, while the green areas show accumulation which in this case is an error due to the vegetation that had not been removed from the point cloud. The developed pool at the west end is missing, due to the water, which does not allow collecting scan points. Yellow and orange parts show only minimal erosion. This might be a bias due to the accuracy of the laser scanner, since the blocks downstream should not experience any measurable erosion. The developed pool at the west end of the erosion site is not shown in this figure. Limitations during the scanning and post processing were missing data in the 2011 scan due to a higher water level. The result is the white area on the lower border between the red and the yellow part.

3.3 *Modeling with CONCEPTS*

The goal of using CONCEPTS was to model the bank retreat of a developed fjord valley river. Therefore some adaptations of the input data were necessary.

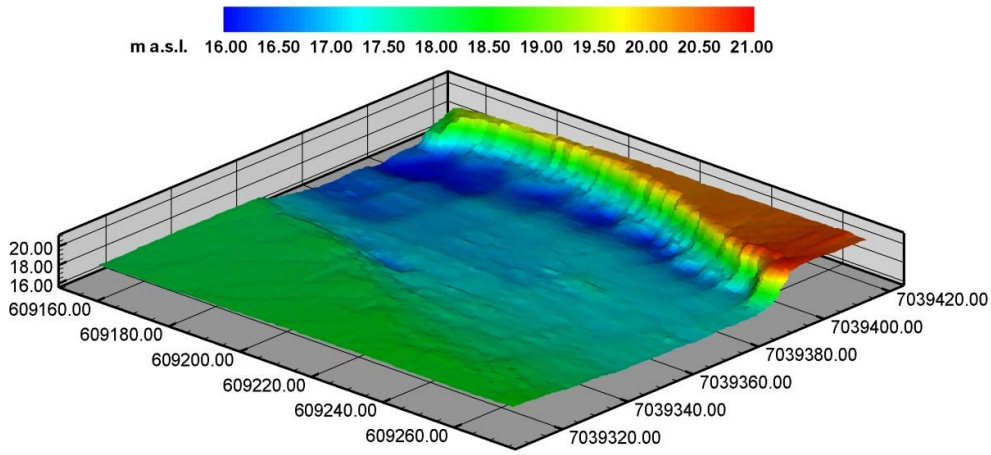

Figure 6 Bathymetry of Forraselva, channels are developed in the west part, bars are developed in the middle and east part of the reach, 4flow from east to west.

Soil texture was used as input data as described above. Hydraulic data have been taken as inflow from a time series from NVE. The cross sections were taken from the DGPS data and manually adapt to the requirements of CONCEPTS. Figure 6 shows that in this reach bars develop at the east end and in the middle part. Further a pool in the SW is part of the reach.

Other input data were set to standard, as they have been in the default setup from the model and used in other simulations by the author (LANGENDOEN, 2000). CONCEPTS did not give any sufficient results with these input data. The annual sediment output has been less than 1 m^3. Following reasons for this will be discussed.

1. Soil or sediment: The riverbank consists of two layers of sediment, disregarding the 30 cm of anthric horizon. CONCEPTS seems to calculate with properties of soil. Soil has a certain structure which is one property to distinguish between soil and sediment. Other regions where CONCEPTS is used are covered with huge layers of paleosols. Due to the inherent structure and often organic content of soil, the behavior should be different as in a sediment layer with theoretically the same texture. This cannot be a reason for the total underestimation of the erosion, but might be worth further tests and calibrations.
2. Cold climate and frozen rivers. During winter season in this climate precipitation is stored in form of snow and ice on the ground. Additionally even larger rivers freeze and this leads to a change from an open to a closed channel system. The water does not flow with a free surface during winter and still some weeks during snowmelt. The consequence is a change in hydraulic and therefore also a change of shear stress which interact with the riverbank. Since there are no measurements when exactly the huge retreat downstream happened it is not possible to give estimation whether this is possible to calculate with CONCEPTS. This would be possible if it happens after the river is totally ice free. Another possibility is that accumulating ice sheets scour into the riverbank. This explanation seems reasonable since direct above the artificial bank enforcement the erosion is biggest. Ice sheets would accumulate at this position and the friction along the riverbank would be biggest.
3. Loose material which accumulates on the lower layer is not taken into account. Material from the upper layer falls down during the year. The slope of the upper layer is normally very steep (figure 4). This

material will not be transported until the water level rises. If the water level over a longer period is low, it is possible that the accumulation of this material gains an amount that this protects the lower layer. This overlying sediment will be transported by the river with a delay. This is a problem which is partly known and described by Fox et al. (2007) and unlike in steeper river gauges, where lose material is directly washed away.

4. Available input parameter. CONCEPTS can be used with hundreds of input parameter. Most of them do not apply for this reach, such as tributaries and artificial structures. Others can be measured directly in the field such as critical shear stress, texture, discharge and others can be obtained from literature such as Manning values. Nevertheless there are more input data possible such as cohesion and suction angle. For the latter ones standard values were used, either default values of the program or taken from other examples.

5. Geometry. The geometry of the cross section does not allow bars and pools. Therefore it was necessary to remove these bathymetry features. This show, that CONCEPTS will have problems with further developed riverbeds where pools and bars are a common feature. Narrow channels as they occur in semi arid areas are more active in terms of erosion and have not developed a stable river bed (Foerst et al. 2008).

4 CONCLUSIONS AND OUTLOOK

In this study, the soil erosion rate has been measured for a riverbank consisting of two postglacial sediment layers. These layers show totally different properties. While the upper layer consists of very coarse and coarse material, the lower layer consists of clay with very thin layers of silt.

The laser scans show clear erosion. The main erosion took place at the downstream part of the reach. A pool has developed where the water flow divides into further downstream and backflow.

The use of CONCEPTS has some limits. First, the relatively wide river with pools and bars has a different geometry as it can be used in CONSEPTS. Second, the sediment accumulation on top of the clay layer, which is not directly influenced by the water flow, is not taken into account by CONCEPTS. Similar results have been gained by Simon et al. (2000) while investigating behavior of bank failure due to prolonged rainfall. Third, the accumulation of snow and the snowmelt is difficult to simulate. Though it is possible to adapt the amount of discharge, the problem of totally frozen rivers was not sufficiently solved. Taken into account, that CONCEPTS is not designed for cold climates, but at least for different layers, it is still limited to simulate fjord valley fills. This is due to the fact, that the layers change rapidly and often show very different textures (Corner, 2006).

Further work will be done during the next two seasons. The riverbank will be scanned in shorter intervals, especially before and after precipitation events, to get a better understanding of the impact of groundwater, rainfall, snow melt, ice sheets and water level on erosion.

REFERENCES

Bertrand, F., 2009, Effects of freezing and thawing processes on bank stability: Proceedings of World Environmental and Water Resources Congress 2009 - World Environmental and Water Resources Congress 2009: Great Rivers, v. 342, p. 6480-6488.

Corner, G.D., 2006, A transgressive-regressive model of fjord-valley fill: stratigraphy, facies and depositional controls: Society for Sedimentary Geology, v. 85, p. 161-178.

Chow, V. T., 1959, Open Channel Hydraulics. McGraw-Hill, New York, NY.

Foerst, M.; Terhorst, B.; Sedov, S. ; Solleiro-Rebolledo, E. ; Sycheva, S., 2008, Climate Change and Landscape Development in Central Mexico Based on the Investigation of Paleosols. Abstracts of the EGU-Conference in VIENNA, (CD-version).

Fox, G.A., Wilson, G.V., Simon, A., Langendoen, E.J., Akay, O., and Fuchs, J.W., 2007, Measuring streambank erosion due to ground water seepage: correlation to bank pore water pressure, precipitation and stream stage: Earth Surface Processes and Landforms, v. 32, p. 1558-1573.

Hanson, G.J.a.S., A., 2001, Erodibility of cohesive streambeds in the loess area of the midwestern USA: HYDROLOGICAL PROCESSES, v. 15, p. 23-28.

Julian, J.P., 2006, Hydraulic erosion of cohesive riverbanks: Geomorphology, v. 76, p. 193-206.

Langendoen, E.J., 2000, CONCEPTS – Conservational Channel Evolution and Pollutant Transport System, USDA, Oxford, USA.

Langendoen, E.J., and Simon, A., 2000, Stream channel evolution of Little Salt Creek and North Branch West

Papillion Creek, eastern Nebraska., Report, US Department of Agriculture, Agricultural Research Service, : Oxford, MS., National Sedimentation Laboratory, .
Langendoen, E.J., Lowrance, R.R., Williams, R.G., Pollen, N., and Simon, A., 2005, Modeling the impact of riparian buffer systems on bank stability of an incised stream, p. 591.
Langendoen, E.J., Simon, A., and Alonso, C.V., 2004, Modeling channel instabilities and mitigation strategies in eastern Nebraska, Volume 104.
Lawler, D.M., 2001, Application of a novel automatic erosion and deposition monitoring system at a channel bank site on the tidal River Trent, U.K: Estuarine, coastal and shelf science, v. 53, p. 237-247.
Lawler, D.M., 2005, Defining the moment of erosion: the principle of thermal consonance timing: Earth Surface Processes and Landforms, v. 30, p. 1597-1615.
Lawler, D.M., 2008, Advances in the continuous monitoring of erosion and deposition dynamics: Developments and applications of the new PEEP-3T system: Geomorphology, v. 93, p. 17-39.
NVE, Norges vassdrags- og energidirektorat. (www.nve.de, 2011)
Pollen-Bankhead, N., Simon, A., 2009, Hydrologic and hydraulic effects of riparian root networks on streambank stability: Is mechanical root-reinforcement the whole story?: Geomorphology.
Simon, A., 2000, Bank and near-bank processes in an incised channel: Geomorphology, v. 35, p. 193-217.
Simon, A., Pollen, N., and Langendoen, E., 2006, Influence of two woody riparian species on critical conditions for streambank stability: Upper Truckee River, California: Journal of the American Water Resources Association, v. 42, p. 99-113.
Solberg, I.L., Hansen, L., Rokoengen, K., Sveian, H., and Olsen, L., 2008, Deglaciation history and landscape development of fjord-valley deposits in Buvika, Mid-Norway: Boreas, v. 37, p. 297-315.
Teixeira, P.C., and Misra, R.K., 1997, Erosion and sediment characteristics of cultivated forest soils as affected by the mechanical stability of aggregates: Catena, v. 30, p. 119-134.
Thorne, C.R., 1981, Field measurements of rates of bank erosion and bank material strength, IAHS, Volume 133: Proceedings of the Florence Symposium, June 1981: Florence, p. 503-512.
Wakindiki, I.I.C.I.I.C., 2002, Soil mineralogy and texture effects on crust micromorphology, infiltration, and erosion: Soil Science Society of America Journal, v. 66, p. 897-905.

PAPER II

Post Processing Methods of Moving Boat ADCP Measurements Time Averaging vs. Distance Averaging

Markus Foerst, Nils Rüther
Department of Hydraulic and Environmental Engineering, Norwegian University of Science and Technology, Norway, S.P.Andersensvei 5, 7491 Trondheim
E-mail: markus.foerst@ntnu.no

Abstract

The development of ADCPs made it possible to extend their use from discharge and bathymetry measurements to measurements of water flow. This paper focuses on post processing methods: This paper compares three possible averaging methods for moving boat ADCP measurements: Time averaging, time averaging with moving window, and distance averaging. Time averaging with moving window, at the moment the most common method, shows rather smooth data, which are useful for model calibration. The distance averaging methods show more detail within the flow structure. In this way it was possible to detect and visualize secondary currents and the smaller outer bend circulation triggered by the secondary current.

Introduction and Aims

Acoustic Doppler Current Profilers (ADCP) have been used in first place to measure water discharge. Over the years of development the measurement method became effective and reliable, and therefore economical to use. In addition, when measuring the water flow with an ADCP, the bathymetry for each measurement is recorded. For basic understanding of ADCP measurements are described by Gunawan, Sterling, & Knight (2010), Muste et al. (2004), RDInstruments (2011), and Simpson (2001). Nowadays, scientists use the possibility to receive the raw data including the velocity vector for each cell. This makes the ADCPs a useful tool to analyse the velocity pattern and turbulence characteristics in rivers. Flow structure measurements usually are conducted by stationary ADCP measurements (Nystrom et al., 2007) or with Acoustic Doppler Velocimeters (ADV) (Abad et al., 2008). Latter one is more costly and more time consuming. ADCP measurements with a moving boat, however, make it easy to obtain a huge set of data along a cross section to measure velocities and flow directions. This method can also be used for measuring flow structures, such as main flow areas (Baranya et al., 2008). The disadvantage though is it was not possible to detect small flow structures by moving boat ADCP measurements. The purpose of this paper is to show, that it is possible to measure water flow with a much higher resolution using distance averaging post processing instead of time averaging post processing. Thus the data of 72 transects from a lowland river (Breivikseidet, W34 445098 7727911) in northern Norway have been analysed and post processed with a distance averaging method and a time averaging method. The reach is between20 and 30 m wide and its discharge between 9 and 20 m^3s^{-1}. In this study two transects from two consecutive meander bends will be compared. More detail about this case study is published in Foerst and Rüther (2012).

Post processing Methods for ADCP Data

Data collection

The ADCP sends an ultrasound ping with a frequency between 1 and 0.8 Hz while it is moving perpendicular to the thalweg. Each ping collects data about the depth, the water flow within a certain cell, and the movement of the vessel. While measuring, the velocity of the vessel must not exceed the velocity of the water; recommended is that the vessel moves with the speed of half the water velocity perpendicular to the main water direction (Muste et al., 2004; RDInstruments, 2011; Yorke and Oberg, 2002). This leads to different distances between single pings and therefore to different results depending on the post processing method. Further, it is necessary to record stationary at the beginning and end of the movement for 10 to 20 pings. This is necessary to get reliable interpolating for the discharge. In this study two transects from two consecutive meander bends will be compared. Figure 2 displays transect 23 and transect 64 on the left and right side, respectively. Transect 23 is from a right bend with the erosion bank on the left side and transect 64 shows a transect from the consecutive left bend with the erosion bank on the right side. The difference in velocity and geometry are due to different post processing methods.

Post processing – transects

The ADCP was mounted on a trimaran connected by a rope to a mobile cableway (Foerst and Rüther, 2012). In this way it was possible to collect data in different positions within a short time span. For each transect four measurements have been conducted. The direction and position of the moving boat were determined by bottom track and a digital compass inbuilt in the ADCP housing. The cableway made sure that the moving vessel measures along the same transect each time without any noteworthy divergence from the course.

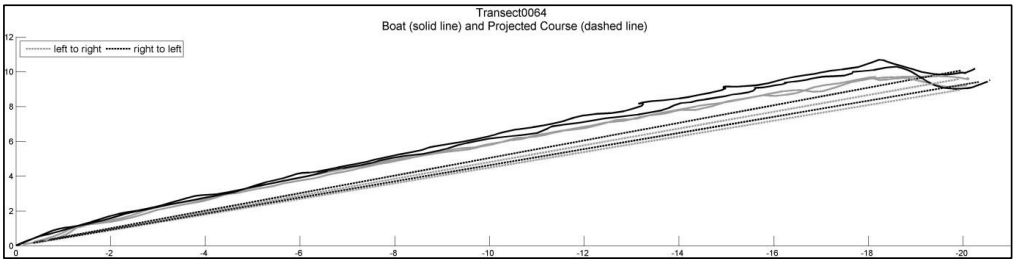

Figure 1: Boat course recorded (solid) and after projection (dashed); distance in m.

First the technical problem of slightly downstream bowed course had to be removed. This was done by projecting the course and the water velocity vector in each bin on an imaginary straight line between the two suspension points from the cable way (figure 01). In the same way each velocity vector has been projected onto this plane from the taken transect. The bend at the west bank (erosion bank) is a technical issue, which occurs since the suspention point needed to be mounted significant higher than the suspention point at the east bank.

Post processing velocities – distance averaging

Distance averaging is based on the thought that pings within a certain area have to be averaged. Since it can be assumed that all four movements are on the same course it is possible to average across all movements. In this case the distance has been determined by 0.75 m; a value, which gave

in the best overall results based on 72 transects. Criteria behind this evaluation have been a minimum of 4 pings within each 0.75 m and a minimum standard deviation (σ_{min}) for both, standard deviation for the north velocity component (σ_{Nvel}) and standard deviation for the east velocity component (σ_{Evel}) between 0.5 and 1.25 cm (equation 1) . Thereby it has been avoided that the averaging distance becomes too big, which would result in too few data to interpret. The vertical velocity component has not been taken into account.

$$\sigma_{min} = \sqrt{\sigma_{Nvel}^2 + \sigma_{Evel}^2}$$

Equation 1: Definition for optimized σ

The bathymetry shows a clear slip-off slope at the right bank (transect 23), and a distinguished erosion bank at the left side (transect 23); transect 64 the other way round. This is due to the geographical location in a right turn (transect 23) and left turn (transect 64).

The main velocity is in the middle of the river and decreases to the banks. The velocity is nearly 0 ms^{-1} at the erosion bank. Transect 23 shows one distinct high velocity cell, while in transect 64 the high velocity region is split into two. In transect 23 the high velocity cell is concentrated around one spot. Transect 64 has it more diffuse over a wider distance. The water flow shows a very well developed secondary current in transect 23, which goes along the bottom in point bar direction and moves from the point bar along the water surface. In transect 64, the secondary current exists, however, it is far weaker developed. In both transects the outer cell region (Blanckaert, 2004; Thorne and Hey, 1979) is visible and in the figure enlarged.

The velocity vectors give a homogenous picture. Exceptions are the flow structure vectors at the riverbed. These show velocities which are not realistic and are regarded as outliers.

Post processing velocities – time averaging

Time averaging is also known as ping averaging. This means that consecutive pings are averaged. This can be done by averaging a certain amount of pings together or by a moving window with a certain percentage overlap. The average of consecutive pings results in distinctive columns. Therefore it shows the average over this time span. An averaging across the movements is not sensible, since the amount of pings is usually different between the single movements. Therefore figure 2 B-D shows movement 3 from transect 23 and movement 2 from transect 64. These have been chosen, because they were most similar to the distance averaging plot.

Three different post processing and visualisation methods for time averaging are shown in figure 2. The chosen transects have been averaged over 6 pings (figure 2 B). This is similar to the average of the distance averaging method described above, except that only one movement is averaged rather than all four. There is no noteworthy difference in the bathymetry. Exceptional the left bank in transect 23. It looks like that there is the beginning of a horizontal ledge at the erosion bank, which does not exist. This phenomenon gets clearer in figure 2 D and is caused by the first and last stationary taken pings. In transect 23 the high velocity cell is overestimated. The contrast between low and high velocities is a bit higher than in the distance averaged transect. Transect 64 shows the opposite. The area of high velocity is smaller and the colour distribution looks smoother. The vectors for perpendicular flow show a less clear structure than before. Though in transect 23 the secondary flow is still recognizable, the outer region circulation is not detectable. In transect 64 have the

vectors a higher magnitude and show similar results as by distance averaging. Though the outer region circulation is hardly recognizable, it is still visible. The unrealistic vectors close to the riverbed are more abundant and not limited to the riverbed, but reach up to the water surface.

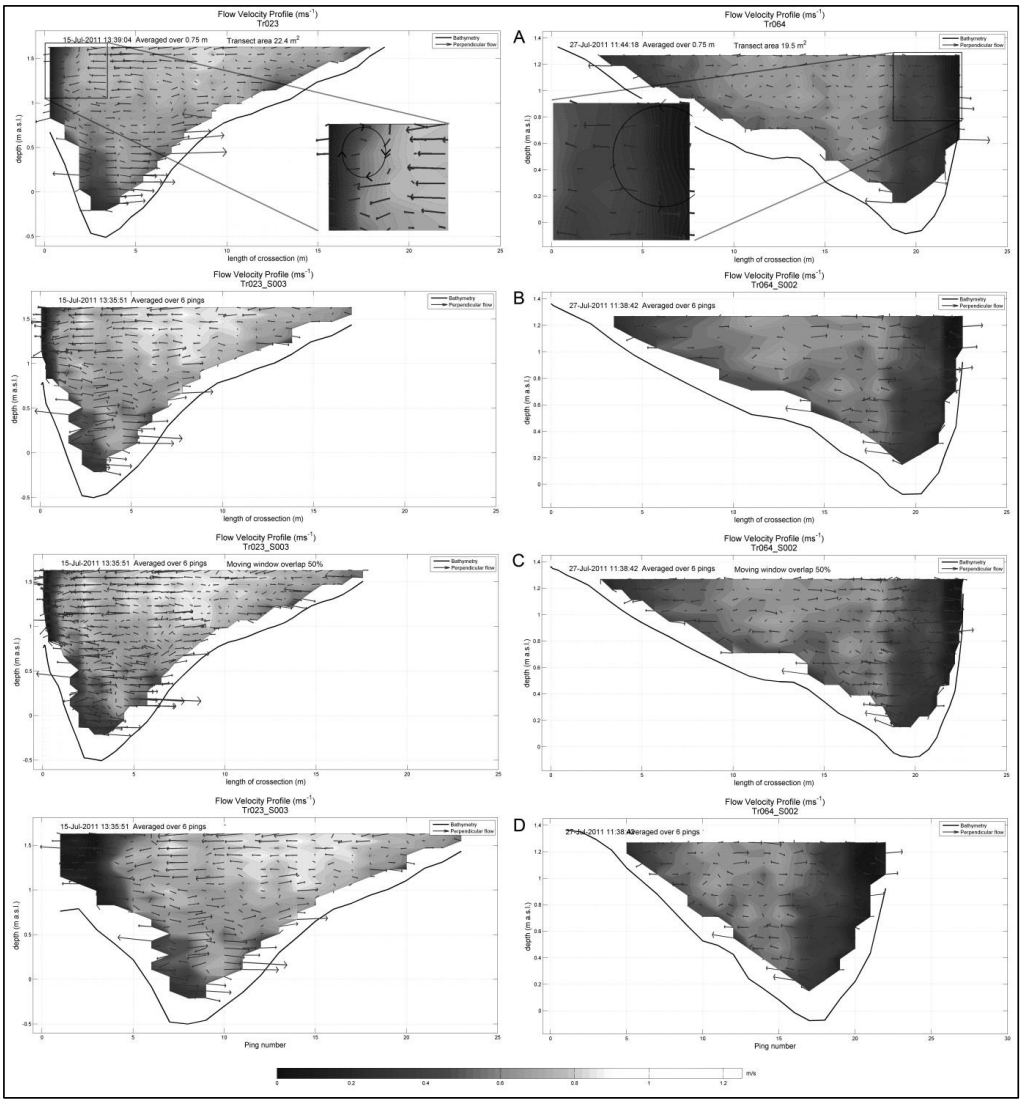

Figure 2: Flow structure by distance averaging (A), time averaging (B), time averaging with moving window 50 % overlap (C), and time averaging plotted against ping number (D). Vectors show a ratio z:h of 1:10

Figure 2 C shows the same data averaged with a moving window. The window size has been 6 pings as before, but with an additional overlap of 50 %. This results in seemingly more data. The difference to the averaging before is, that data get smoother. The bathymetry shows round edges where sharper edges were before. This smoothing leads also to a reduced contrast in the main velocity plot.

The vectors for the perpendicular flow are similar to figure 2 B. The smoothing effect is hardly influencing the vectors. It rather has the opposite effect. The vectors along the water surface in transect 64 are not as constant as they are in figure 2 B.

The transects in figure 2 D show the same method than figure 2 B. However, they have been plotted on a time scale (1 ping = 1.2 s). Plotted against time, the geometry will be compressed in the middle of the transect, where the vessel moved faster and stretched at the slower moving parts near the river banks. This is similar to the raw data which are visualized with the manufacturer software. At the left riverbank the indicated floodplain does not exist and is an artefact from the measurement method, where it is necessary to keep the vessel for 10 to 20 pings to get a reliable interpolation of the riverbank for the discharge.

Discussion

1. Transects: The divergence of the course at the right side of the river is caused by measurement errors and that the start and end position at the left side has been defined as fix position. This was to make calculations easier, since the ADCP was not equipped with a GPS system. The raw data show no indicator for bed movement, which would be an unusual bend along the course. Further the vessel was forced to stay on its course. Therefore it can be assumed, that all transects are on the same position within the cableway margins. This assumption is reinforced by the low divergence of 2 transect from the same direction. The average divergence is less than 30 cm, which lies within the movement tolerance of the cable way.

2. Bathymetry: It is not really apparent, that the smoother bathymetry with the moving window method gives better results. The bigger issue is the wrong geometry in areas where the vessel is moving back due to local turbulences or necessary low moving velocities.

3. Velocities: The mean velocities are overestimated in the first transect and underestimated in the second one by time averaging. The most likely reason is, that for the distance averaging more data has been available and for the time averaging only about 25 % of these data has been able to be considered. Therefore the over- and underestimation is based on lacking possibilities to average more data. Using a moving window smooth's data, this might be useful if data measured compared with data modelled.

4. Perpendicular flow: Time averaging shows worse data when it comes to flow structures. One reason that the moving window has little effect on the vectors might be that the weight has been on the direction rather than the actual magnitude. The fact that the outer cell region is recognizable in transect 64 through all 4 methods, is probably based on the lower overall velocity in this transect, which leads to less turbulent water flow. It is clear that the more turbulent the flow is, the more data are necessary at the same position to compensate fluctuations.

5. Plotting: Visualizing the data with a time plot results in a horizontal deformation. This can be useful when to many data would be plotted within a short distance. Otherwise, the deformation is difficult to evaluate, since the deformation can be different for each ping. This depends on the vessel movement during the measurement. The more homogenous the movement has been the more homogeneous is the time/distance ratio. This assumes first, that the water velocity is homogenous along the measured cross section and that it is possible to move the vessel in a homogenous speed.

Conclusion

The velocity of the vessel during the measurement is normally not constant. This is due to the adaption of the vessel speed on the water speed. Further the manual dragging of the vessel over the river leads normally to different velocities.

The practical limitation of similar moving speed across a transect is also given by the river size. In a river as big as the Danube (Baranya et al., 2008) it is not necessary to lower the vessel speed extremely when approaching the riverbank. Additionally, the error at the first and last meter may not count much for a wider cross section like e.g. 600 m. Time averaging seems acceptable with large rivers or to get an overview over the water velocities. The moving window method is an acceptable choice for comparison with model data. However, time averaging has its limitation in areas with low water velocity and rivers with a high velocity gradient along the cross section. The other limitation is that it is usually not possible that movements along the same cross section can combined together. When using time averaging it is highly important to improve the quality during measurements. First by moving the vessel in with a constant speed, second by moving as slow as possible to collect as many data within a short distance as possible. Further problems occur at places with low water velocity or mixing layers. In cases the vessel changes the direction (figure 1) the result of the post processing might lead to wrong interpretation of the data.

Using the distance averaging method the data on the one hand become more reliable, since all data from a transect can be averaged. On the other hand side single pings which are spatial adjacent are combined rather than chronological consecutive pings. This leads to possibilities that the flow structure can be visualized with a higher resolution as it is possible with time averaging. Regarding the comparison of transect 23 and transect 64 the distance averaging method gains on strength when the flow becomes more turbulent.

Literature

Abad, J.D., Rhoads, B.L., Guneralp, I., and Garcia, M.H., 2008, Flow structure at different stages in a meander-bend with bendway weirs: Journal of Hydraulic Engineering-Asce, v. 134, p. 1052-1063.

Baranya, S., Goda, L., Józsa, J., and Rákóczi, L., 2008, Complex hydro- and sediment dynamics survey of two critical reaches on the Hungarian part of river Danube: IOP Conference Series: Earth and Environmental Science, v. 4, p. 012038.

Blanckaert, K., 2004, Secondary flow in sharp open-channel bends: Journal of Fluid Mechanics, p. 353-380.

Foerst, M., and Rüther, N., 2012, Mean and Turbulent Flow Structures in two Consectutive Meander Bends, IAHR Europe, Proceeding 2012, Volume in press: Munich, Germany.

Gunawan, B., Sterling, M., and Knight, D.W., 2010, Using an acoustic Doppler current profiler in a small river: Water and Environment Journal, v. 24, p. 147-158.

Muste, M., Yu, K., and Spasojevic, M., 2004, Practical aspects of ADCP data use for quantification of mean river flow characteristics; Part I: moving-vessel measurements: Flow Measurement and Instrumentation, v. 15, p. 1-16.

Nystrom, E.A., Rehmann, C.R., and Oberg, K.A., 2007, Evaluation of Mean Velocity and Turbulence Measurements with ADCPs: Journal of Hydraulic Engineering, v. 133, p. 1310-1318.

RDInstruments, 2011, Acoustic Doppler Current Profiler Principles of Operation A Practical Primer: Poway, CA, USA.

Simpson, M.R., 2001, Discharge Measurements Using a Broad-Band Acoustic Doppler Current Profiler

Thorne, C.R., and Hey, R.D., 1979, Direct measurements of secondary currents at a river inflexion point [8]: Nature, v. 280, p. 226-228.

Yorke, T.H., and Oberg, K.A., 2002, Measuring river velocity and discharge with acoustic Doppler profilers: Flow Measurement and Instrumentation, v. 13, p. 191-195.

PAPER III

MEAN AND TURBULENT FLOW STRUCTURES IN TWO CONSECUTIVE MEANDER BENDS

Markus Foerst[1] & Nils Rüther[1]

[1]Department of Hydraulic and Environmental Engineering, Norwegian University of Science and Technology, Norway, S.P.Andersensvei 5, 7491 Trondheim

E-mail: markus.foerst@ntnu.no

Abstract

Soil erosion along riverbanks has been an important issue due to economic and ecological damage. One cause for erosion is natural river migration. A natural meandering river in northern Norway (Troms) has been subject for this investigation. The first bend is a 90 degrees turn after a straight reach. The following two bends turn each 180 degrees. Focus lies on the abundance of secondary currents and its influence on natural erosion processes within the first two bends. The river is non-regulated and is not exposed to scour protection on the river banks. It developed consecutive meander bends in Holocene fjord sediments. The meander bends are strong curved and show an upstream orientation. Climatic conditions cause an annual water high stand in spring. The hydraulic measurements have been conducted with a moving Acoustic Doppler Current Profiler (ADCP) along cross sections perpendicular to the main flow. The flow measurements were conducted in 72 cross sections with 8 crossing for each cross section. This density of measurements results in a detailed description of the mean flow in the meander bends. In addition, the secondary flow in the outer bank has been quantified with set of highly dense fixed position ADCP measurements.

The investigation shows that the flow is highly influenced by the macro roughness elements of the banks, i.e. trees, submerged trunks and relatively small coherent local scours in the bank. Different flow pattern were analyzed and grouped based on statistical similarity measurement. Results show that the flow pattern in the subsequent meander is more susceptible to changes in water level than the first one where the water has a rather straight inflow. The impact angle dips steeper into the second outer bank the higher the water level is. During snowmelt Breidvikelva shows a rather constant high water level which is 1.8 to 2.0 times above the water level during summer. A decrease of the occurrence and strength of secondary flow has been observed during lower water levels. Preliminary results show a stable pattern of the water flow though the water level alternates. Mayor changes occur in the water velocity.

Introduction

The use of Acoustic Doppler Current Profiler (ADCP) measurements in rivers has recently become more common in river surveying. Not only had the discharge measurement become easier and more comfortable (Muste, Yu, & Spasojevic, 2004), the ability to measure currents in different depths simultaneously without the bias of the instrument itself, makes it a valuable tool to get insight in flow regimes. Additionally, velocity and current measurements became possible due to the raw data output which most user software allows (Baranya, Goda, Józsa, & Rákóczi, 2008; Nystrom, Rehmann, & Oberg, 2007). Velocities and turbulence measurements have been conducted in artificial flumes (Nystrom, et al., 2007). Flow structure in a river, whether it is turbulent or laminar flow influences the sediment erosion, transport, and sedimentation. In river bends the secondary current is responsible for sediment transport from the erosion bank to the inner bank. The secondary current and the outer bend region have been investigated at the inflow of a river bend by Thorne & Hey (1979) and Thorne et al. (1985). Nanson (2010) investigated the flow structure in six separated meander bends. Blanckaert (2001, 2004) described the behavior of the secondary current and the outer bend region in a laboratory flume. Missing in the literature however, is the flow structure within connected river bends. The purpose of this paper is to investigate and compare the flow structures in two consecutive meander bends. The focus lies on the flow characteristics such as the mean velocities and secondary current (Thorne & Hey, 1979), outer bend region (Bathurst, 1977; Blanckaert, 2004) and the behavior of these characteristic in the changeover in between two meanders of a natural free meandering river.

Research Area

The river Breidvikelva is located in a glacial affected valley in northern Norway, Troms. The catchment covers an area of 163.7 km^2 with an altitude from 0 to 1400 m a. s. l. (NVE, 2012) and is sensitive to changes in the water input. The high latitude (69° 40” north) and the high mountains keep the snow until summer. This leads to a rhythmic

alteration of the water level during the end of snowmelt season. Long time radiation in a low angle melt snow even on the north exposed slopes of the surrounding mountains. This leads to a delayed slight rise in water level on a 24 h rhythm.

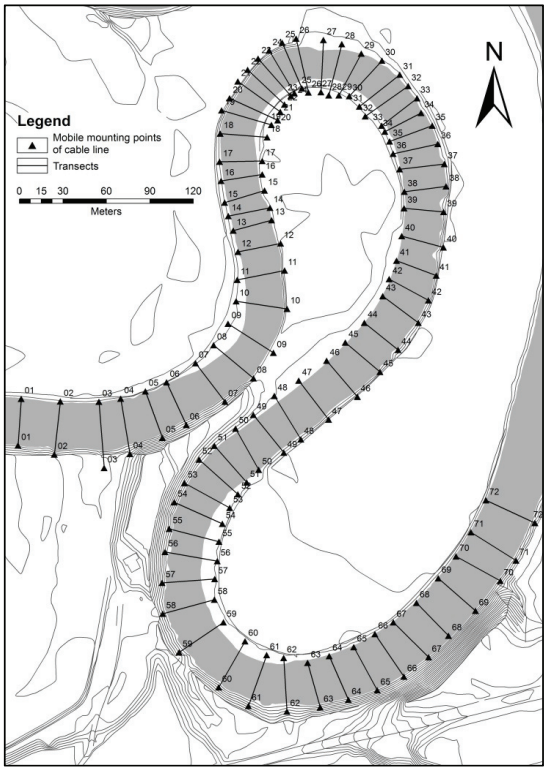

Figure 1: Map of investigated reach at Breivikselva. Flow is from W to E.

The reach consists of three consecutive meander bends with a straight inflow (figure 1). The investigated reach has a length of 1100 m and 0.40 m difference in altitude. The riverbed consists mainly of silt and sand. In lower layers cobbles appear and built the surface on some spots along the slip-off slope. The river cuts into former terraces of different heights. The river banks show therefore different altitudes from 2 m a. s. l. up to 25 m a. s. l. The lower banks, the left side and partly the right side of the river, are covered with vegetation: birches, scrubs and fern. The dead and living vegetation disrupt the water flow in these areas and might cause forming of pockets along the erosion slope. The higher banks are located at the right side in the beginning of the first bend and all along the third bend. They show loose material and are strongly affected by erosion. In these areas the water flow is disrupted only by very few trees, which fell into the water, neither did pockets develop.

Figure 2: a) View from transect 72 (right side) upstream: high bank with hardly vegetation disturbing the flow. b) view from transect 26 (right to left): low bank with dense vegetation, developed pocket, and dead wood.

Methods

Water level has been monitored with two water loggers. One located at the beginning and one at the end of the reach. The water loggers have been calibrated with a differential GPS. For calculating the water level at the measured transect, a linear slope has been assumed. All 72 transects have been taken by a four beam ADCP, *StreamPro* from RDI. Restrictions of ADCP measurement based on its technical limitations are blanking zones. These occur direct under the water surface because of ringing and flow disturbance caused by the submerged transducer (Nystrom, et al., 2007; RDInstruments, 2011). Further, the beams of *StreamPro* ADCP are directed in an angle of 20° from the vertically. Due to this type of construction occur blanking zones close to steep riverbanks. At the outer bank the accordant beam hits the wall while the other three get still data from the flow. This is known as sidelobe interference. The degree of interference along the geometry depends on beam and bin size setup. This effect is much less at a low transversal bed gradient. Measurements at the inner bank are more limited by the upper blanking zone beneath the vessel. These built in restrictions are described in various technical papers of which some of them are Gunawan, Sterling, & Knight (2010), Muste, et al. (2004), RDInstruments (2011), and Simpson (2001).

The ADCP was mounted on a trimaran connected by a rope to a mobile cableway. In this way it was possible to collect data in different positions within a short time span (figure 3). The direction and position of the moving boat

were determined by bottom track and a digital compass inbuilt in the ADCP housing.

Figure 3: Mounting of mobile cable way for *StreamPro* ADCP, transect 06, right bank.

The *StreamPro* is designed to measure the geometry of the riverbed and the water velocity and direction. These data are necessary for the usual use of discharge measurements. For the data collection water mode WM12 with long range feature has been used. WM12 uses a sequence of sub-pings, which are averaged to one ping. However, the data derived from the compass are sampled only for one ping, which consists of sub-pings. This bias can be neglected since the pings have been averaged further and the sizes of the flow structures which are to be identified are still larger as the measureable bin size and the boat movement. For each transect the ADCP was dragged two times in each direction over the river. Thus for each transect the data of four measurement have been available.

These profiles have been processed by averaging to get reliable data sets for further interpretation. Each ping has a timestamp and an ongoing number. The time interval between timestamps is equal about 0.7 Hz at WM 12. The position has been measured by bottom track, which gives for each ping a new position relative to the previous one. Thus, since the movement of the vessel is usually not steady and at positions with low water velocities and thus even lower vessel velocities, a time/ping based averaging will result in distortions. This might be negligible when the ADCP is mounted on a motor driven vessel and rivers with much higher discharge and the focus lies on water velocities (Baranya, et al., 2008). In this study the water velocities were below 1.5 ms^{-1} and even below 0.2 ms^{-1} along the riverbanks. To get reasonable results in the three-dimensional velocity field, which could be allocated to definite and equal sections along transects, the data have been averaged over distance rather than time.

The crux with this method is to find an appropriate averaging distance (AD). Small AD which would result in insufficient data in the deeper parts of the transects, due to faster movement of the vessel. Averaging over larger AD would smooth the data too much, so that sensible interpretation would be difficult or even impossible. In figure 4 four AD are applied to the data. The figure shows the bathymetry and the mean water velocity in ms^{-1}.The vectors show the direction of the water flow perpendicular to the transect plane with a 1:10 vertical:horizontal ratio. The main flow patterns become clearer with increasing the AD. At the same time the details in the flow pattern disappear.

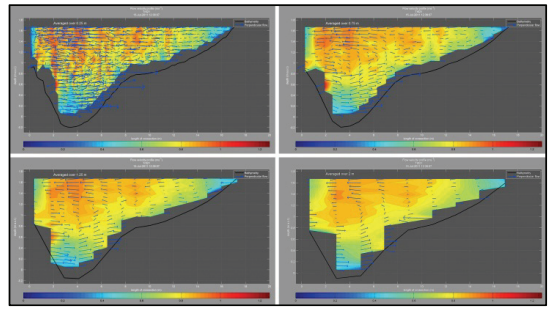

Figure 4: Transect 21 averaged with 25, 75, 125, and 200 cm columns over distance.

After carefully manually reviewing different AD from 25 up to 200 cm, the analysis and interpretation of the data is based on a 75 cm distance averaging. The averaged values are depth (bathymetry) and the velocity components in each direction (E, N, and U).

The perpendicular current is projected on the plane from the taken transect. This is not always exact perpendicular to the downstream direction as it is more detailed explained in Lane, Bradbrook, Richards, Biron, & Roy (2000), but it is in its accuracy more than sufficient for the goal of this paper.

The transects which have been chosen and compared are based on the relative water level change. Since the water level degreases downstream the water level needed to be compensated by the slope. Figure 5 shows the absolute water level (rhombuses) at time of measurement, the measured discharge (triangles), and the relative water level to first measurement (squares). The precipitation and snowmelt, which still occurs in the middle of the year from the valley slopes, has significant influence in the discharge. Therefore it is necessary to interpret transects at same water flow conditions. For this, consecutive transects, which have been measured during stable water level conditions, were chosen. A standard water gradient has been defined based on the water level data measured during the first transect. This was necessary to estimate the water level change within two transects by taking the river gradient into account (figure 5). The relative water level is the result of subtracting the actual water level during the measurement

from the defined standard gradient. In this way the data have been analyzed to identify groups of transects with similar hydraulic conditions. Transects 44-51 and 61-72 show stable conditions, while Transects 18-23 show a relative water level rise followed by a water level fall.

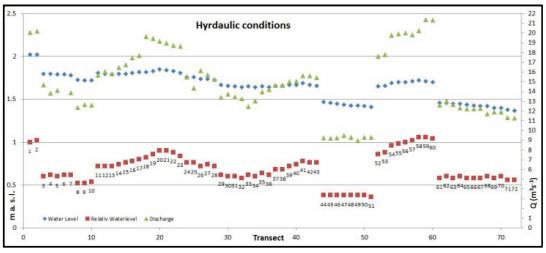

Figure 5: Hydraulic conditions during measurements. The discharge in m^3s^{-1}, water level in and relative water level in all 72 transects.

Transects 18 to 23 represent the inflow part into the second meander (Thorne, et al., 1985), while transects 44 to 51 represent the outflow of the second meander and the apex between the second and third meander. Transect 61 to 70 represent the outflow of the third meander. The locations of all transects are shown in figure 1.

Results

1. Bathymetry

The geometry of the cross section shows in the bends a steep slope along the erosional bank and a continuous low angle slope towards the point bar. Clear exceptions are transects 44-47, and 66-68, where a deeper channel has formed with a distinctive basal angle. In both cases this occurred at the outflow of the meander bend, a few meters before the bed transforms into a more rectangular shape (transect 49 and 70 respective). This bathymetry has been described by Kurvenkolk (1986). However, it is absent at the outflow of the first meander.

The transvers in the bathymetry from the right bend to the consecutive left bend happens at the end of the straight transvers part, immediately before the left bend begins. The developed channel of the right turning meander is still downstream (transect 48) of the inflection point (transect 46) present, long after the outflow of the meander bend (transect 43). This results in an abrupt change of the erosion bank within a short distance. A similar abrupt change occurs from the first (left) to the second (right) meander. Therefore, the bathymetry is not synchronous with the geometry of the meanders. Otherwise the change of the point bar would be symmetrical to the inflection point. A downstream distortion, however, confirms that the bathymetry is strongly influenced by the water flow.

2. Water mean velocity

The measured mean velocities within a transect show low velocities at the edges and an area of high velocities in the middle of the transect.

Given the deepest point in a transect as reference it happens that most of the high velocity cells occur shifted towards the point bar side. This coincides with the literature (Blanckaert, 2004; Nanson, 2010; Thorne & Hey, 1979). However, some transects show a shift of this cell to the outer bank and a bouncing back. This happens three times in transect 11, 21, and 56. Including the less intensive bouncing of the cell, which means that the high velocity cell does not cross the lowest point in the profile cross section, this happens four times in the second meander (transect 21-22, 24, 26-27, and 39-43) and two times in the last one (47-49 and 55-64) Similar behavior has been described in flume experiments (Blanckaert, 2001) and in natural rives (Kurvenkolk, 1986; Sukhodolov, 2012).

The high velocity cell in transects 18-20 and 47-51 appears much closer to the point bar than in other transects and moves with each transect towards the outer bank. This phenomenon is only observed during the inflow of the second and third meander. The transect 61-64 at the outflow of the last bend show two high velocity cells within the transect. These cells develop already in transect 59 and 60. A similar, but weaker pattern has been measured at the outflow of the first meander. Therefore, this seems not to be a local effect. The pattern persists even at significant different water levels, cp. transects 60 to 61 (figure 5).

3. Secondary current

The ADCP measurements show secondary flow in all meander bends. At the inflow into the second bend (transect 18-23) the successive development of the secondary cell is quite clearly. These currents disintegrate already at the outflow of this bend (transects 44-51) – thus long before the bathymetry or the mean velocity would indicate the transition to the next meander. Similar pattern can be observed at the outflow of the third meander (transects 61-70).

The outer cell (Bathurst, 1977; Blanckaert, 2004) was measured one time in transect 23 at the inflow, one around the apex (transect 61), and one at the outflow (transect 64). In these transects the outer cell region is enlarged in figure 6. In all three spots the outer cell region was measured at transects without or very little vegetation or dead wood in the water.

Conclusion

This study has been conducted to investigate the flow pattern in consecutive meander bends. Therefore 72 transects have been measured with an ADCP and analyzed.

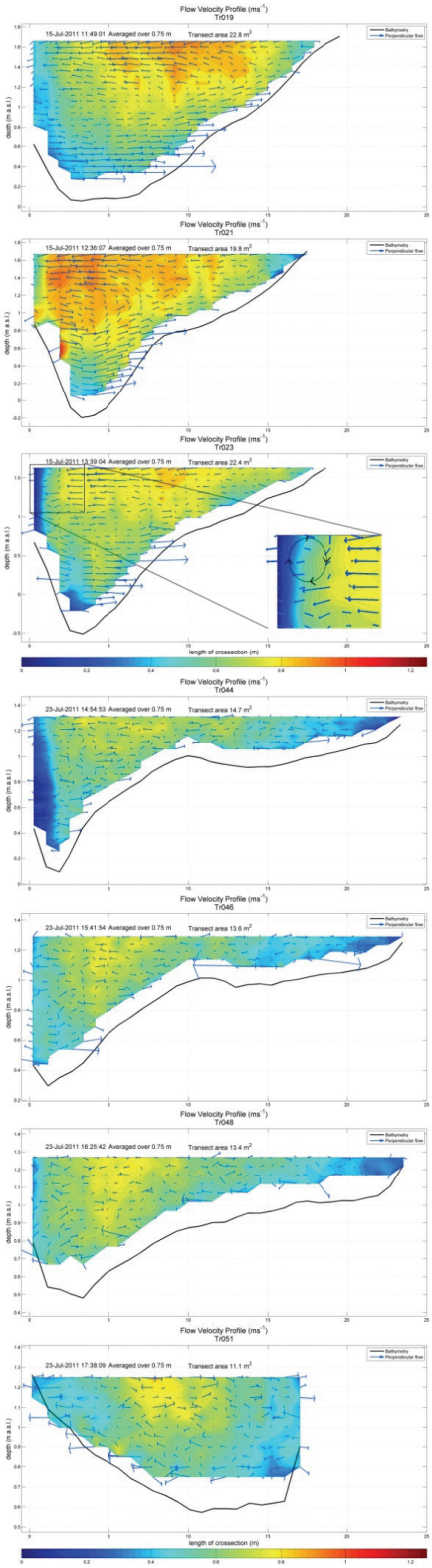

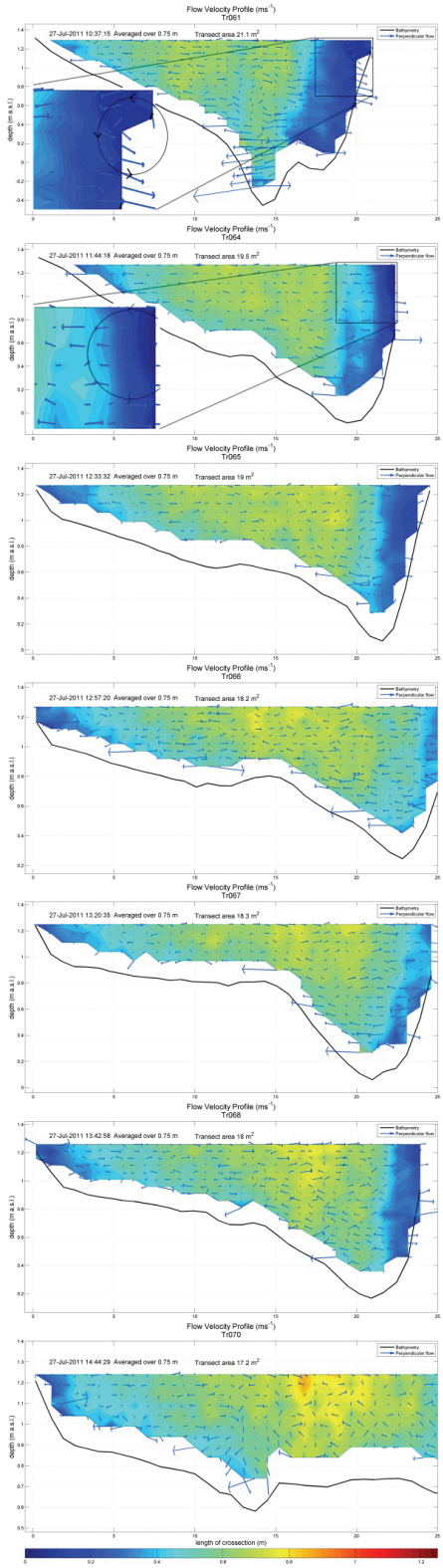

Figure 6: Left side: Transects 19, 21, 23, 44, 46, 48, and 51; Right side: Transects 61 and 64, 65, 66, 67, 68, and 70. Vectors show a ratio z:h of 1:10.

In the literature flow measurement with ADCPs have been described at very small rivers (Gunawan, et al., 2010; Nanson, 2010), in big rivers such as Danube (Baranya, et al., 2008) or in the laboratory flume (Blanckaert, 2004; Nystrom, et al., 2007). Further literature describes only single bends in natural rivers, or consecutive bends in laboratory flumes without the natural variation (Abad & Garcia, 2009). In this way this project will fill the two gaps in literature. A) by investigating a medium size low land river and B) by monitoring a natural reach along three meander bends.

The results show that in all meanders within this reach most patterns occur in a similar way: distortion of the bathymetry, movement of the high velocity cell, and secondary current.

Three features which typically occur in meander bends have been described in this paper:

1. Channel at the erosional bank.
2. High velocity cell above the channel.
3. Occurrence of a clear secondary current and its outer cell.

In case of the transition from one meander bend to the next these properties adapted not simultaneously. The disintegration of the secondary current begins already in the outflow of the bend (transect 44), the bathymetry changes after the inflection point (transect 51), and finally the high velocity cell crosses the side (transect 54).

These preliminary results also suggest that the change in water level does have a high influence on the strength of the water flow and the mean velocity, but only little influence on its pattern. The secondary current and the high velocity cell behaved similar in the in- and outflows of the meander and the flow pattern showed continuity in consecutive transects though the water level changed significantly. Further show the sequence of transects no significant interruptions of the flow structure though the discharge alternated significant between the measurements. Further suggest the data, that the outer cell region is sensitive to external disturbance such as vegetation. There was no evidence that the outer cell occurs where vegetation or dead wood was present.

The delay in the high water flow cell in respect to the geometry should cause higher shear stress and therefore erode the riverbed in these areas. The flow in this area is less influenced by the bathymetry rather than by the meander curvature. Therefore, further data have been taken by stationary measurements along the outflow of the first and the inflow of the second meander.

These data will be analyzed with respect to shear stress and its influence on bed load and erosion. A more detailed insight in the development of secondary current and the outer cell region will be yield by ADV measurements during the next field campaign. However, since the measurements have been just a snapshot of the flow. It will be necessary to monitor the change of water flow during different water levels.

Literature

Abad, J. D., & Garcia, M. H. (2009). Experiments in a high-amplitude Kinoshita meandering channel: 1. Implications of bend orientation on mean and turbulent flow structure. *Water Resources Research, 45*. doi: W02401
10.1029/2008wr007016

Baranya, S., Goda, L., Józsa, J., & Rákóczi, L. (2008). Complex hydro- and sediment dynamics survey of two critical reaches on the Hungarian part of river Danube. *IOP Conference Series: Earth and Environmental Science, 4*(1), 012038.

Bathurst, J. C. (1977). Direct measurements of secondary currents in river bends. *Nature, 269*(5628), 504-506.

Blanckaert, K. (2001). Mean flow and turbulence in open-channel bend. *Journal of Hydraulic Engineering, 127*(10), 835-847.

Blanckaert, K. (2004). Secondary flow in sharp open-channel bends. *Journal of Fluid Mechanics*(498), 353-380.

Gunawan, B., Sterling, M., & Knight, D. W. (2010). Using an acoustic Doppler current profiler in a small river. *Water and Environment Journal, 24*(2), 147-158. doi: 10.1111/j.1747-6593.2009.00170.x

Kurvenkolk, W. P. (1986). *Unteruschungen über die Sohlenausbildung in Flusskrümmungen*. PhD, Eidgenössische Technische Hochschule Zürich, Zürich. (85)

Lane, S. N., Bradbrook, K. F., Richards, K. S., Biron, P. M., & Roy, A. G. (2000). Secondary circulation cells in river channel confluences: Measurement artefacts or coherent flow structures? *Hydrological Processes, 14*(11-12), 2047-2071.

Muste, M., Yu, K., & Spasojevic, M. (2004). Practical aspects of ADCP data use for quantification of mean river flow characteristics; Part I: moving-vessel measurements. *Flow Measurement and Instrumentation, 15*(1), 1-16. doi: 10.1016/j.flowmeasinst.2003.09.001

Nanson, R. A. (2010). Flow fields in tightly curving meander bends of low width-depth ratio. *Earth Surface Processes and Landforms, 35*(2), 119-135. doi: 10.1002/esp.1878

NVE. (2012). NVE Atlas Retrieved 15.01.2012, 2012, from http://atlas.nve.no

Nystrom, E. A., Rehmann, C. R., & Oberg, K. A. (2007). Evaluation of Mean Velocity and Turbulence Measurements with ADCPs. *Journal of Hydraulic Engineering, 133*(12), 1310-1318. doi: 10.1061/(asce)0733-9429(2007)133:12(1310)

RDInstruments. (2011). Acoustic Doppler Current Profiler Principles of Operation A Practical Primer Retrieved from http://www.rdinstruments.com/mm_papers.aspx

Simpson, M. R. (2001). Discharge Measurements Using a Broad-Band Acoustic Doppler Current Profiler Retrieved from http://pubs.usgs.gov/of/2001/ofr0101/text.pdf

Sukhodolov, A. N. (2012). Structure of turbulent flow in a meander bend of a lowland river. *Water Resources Research, in press*.

Thorne, C. R., & Hey, R. D. (1979). Direct measurements of secondary currents at a river inflexion point [8]. *Nature, 280*(5719), 226-228.

Thorne, C. R., Zevenbergen, L. W., Pitlick, J. C., Rais, S., Bradley, J. B., & Julien, P. Y. (1985). Direct measurements of secondary currents in a meandering sand-bed river. *Nature, 315*(6022), 746-747.

PAPER IV

hydrology

MDPI

Article

Bank Retreat and Streambank Morphology of a Meandering River during Summer and Single Flood Events in Northern Norway

Markus Foerst * and Nils Rüther

Department of Hydraulic and Environmental Engineering, Norwegian University of Science and Technology, 7031 Trondheim, Norway; nils.ruther@ntnu.no

* Correspondence: markus.forst@sweco.no; Tel.: +47-46891194

Received: 11 November 2018; Accepted: 06 December 2018; Published: 11 December 2018

Abstract: In recent years, advanced methods for measuring riverbank migration have been used to understand the process of river planform evolution. However, the role of the so-called outer secondary cell in the hydraulic pattern in bank erosion remains unclear. For this purpose, a natural river meander with high curvature bends and steep riverbanks was chosen to quantify bank migration by high-resolution terrestrial laser scanning of three patches along two river bends in four time intervals. The first two time intervals were seasonal, from spring to autumn, and with relatively few water level changes, whereas the third and fourth time intervals were short, just before and after single flood peak events. The yielded point clouds were filtered and digital elevation models (DEMs) were created. These DEMs were used to analyze bank retreat, riverbank morphology, and slope gradient changes in order to understand the role of the outer secondary cell in these processes. In addition, it is shown that storm events causing short peaks in river discharge are less important for river migration than longer-lasting medium discharge.

Keywords: outer cell; river migration; meander; erosion; meandering; outer secondary cell; ADCP; terrestrial laser scanner

1. Introduction

Riverbank migration has been investigated for decades and many approaches have been used to understand the process. These approaches can be divided into studies, for example, by scale, spatial resolution, and temporal resolution. Studies on large meandering rivers have been conducted by, for example, Parker et al. [1–3]. On the other hand, Schnauder and Sukhodolov have been working on river migration in small meandering rivers in Germany [4]. At the lower end of the scale, investigations of fluvial morphological processes on small-scale models in the laboratory have been conducted [5–9]. Finally, more sophisticated numerical models have appeared [10–12] in recent years.

In the last decade, measurement methods have been developed to estimate the sediment balance over short time scales [13]. One of these methods is erosion pins, and Lawler developed the most sophisticated ones [14]. These are able to measure and log sediment changes. However, they are intrusive [14–19] and their spatial resolution is within square decimeters. The use of light detection and ranging (LiDAR) in airborne surveys over large areas has been applied recently [20]. However, its application is limited when surveying vertical or near-vertical structures. This limitation can be overcome by using terrestrial LiDAR (terrestrial laser scanning, TLS). As a nonintrusive method, it avoids the physical impact of the measurement device at the investigated ground. Additionally, it collects a large amount of measurement points. The horizontal setup direction of the laser beam makes it perfect for riverbank surveys with a slope gradient higher than 45°. This setup results in a

dataset with a much higher resolution compared to, for example, the abovementioned erosion pins [21–25], and hence more detailed insight into the sediment balance of a riverbank [26]. This high resolution is necessary to measure small changes in riverbank morphology between flood events that occur within a short time interval. The investigated patches are small and have a very high point cloud density with a resolution beyond photogrammetry [27]. In addition, the analysis of laser scan time intervals gives insight into the processes of river migration that occur at a riverbank [23,28]. The limitation of TLS, however, is the lack of ongoing monitoring and the small area it is able to cover with high resolution.

A further phenomenon, the outer secondary cell, which was discovered and described for the first time by Thorne and Hey and Thorne et al. [29,30] some decades ago, recently came into focus again. Blanckaert recreated the conditions for the outer secondary cell in a flume [6,31]. Blanckaert and Graf explained a change in the downstream momentum due to a change in curvature [32]. Further investigation followed to analyze the outer secondary cell changes under different curvatures and depth-to-width aspect ratios [6,33–35]. However, the influence of an active riverbank was not a subject of their study. Foerst and Rüther investigated the hydraulics in the same river as this study by measuring the secondary flow direction along 72 transects [36,37]. At transects, where the outer riverbank was nearly vertical, they measured the outer secondary cell in a natural river directly. Thorne and Hey assumed that the outer secondary cell is a trigger for erosion at the outer bank [29]. However, Blanckaert and Graf described the outer secondary cell as forming a protective zone between the main secondary cell and the riverbank [32].

Mainly two kinds of erosion are described in the literature for river migration. The first is so-called erosion by fluvial entrainment [38]. This can be from groundwater seeping into the river, so-called seepage erosion, or from shear between the river and its channel, so-called fluvial erosion [10]. The other kind is mass failure or cantilever failure due to gravity [39–42]. The first erosion type happens slowly and continuously, while the second one occurs suddenly after the riverbank has been destabilized.

For this study, a medium-size river in the northern part of Norway was chosen to fill the gap between large-scale and small-scale investigations. The investigated parts of the riverbank were chosen to avoid influence by riparian vegetation. This paper investigates erosion by fluvial erosion in microscale and analyzes bank retreat and the shape of the streambank on a long-term (summer) and short-term (single flood event) basis with a terrestrial laser scanner as the high-resolution measurement method. The special focus herein is the role of the so-called outer secondary cell and its effect on fluvial erosion. This paper contributes to a better understanding of the role of the outer secondary cell in the interaction of river hydraulics and riverbanks by looking into the processes of bank retreat at microscale.

2. Materials and Methods

2.1. Study Site

The surveyed river, Breivikelva, is a lowland river in the northern part of Norway (Figure 1). The area was strongly affected by the last ice age, and a fluvial terrace system has since developed [38]. The chosen riverbanks for this study belong to the lowest terrace level, which is about 1–2 m above water level. The catchment covers an area of 164 km^2 with an altitude from 0 to 1400 m a.s.l. [43]. The investigated reach ends about 4.5 km before it discharges into the fjord. It is not influenced by tidal water changes. The river has a width-to-depth (W/D) ratio of 17, an average bed slope just less than 2%, and a sinuosity of around 3. The investigated reach is about 1100 m long and has an average energy slope of 0.4‰. The discharges measured within the study period vary between 8.7 m^3s^{-1} in autumn and 24.3 m^3s^{-1} in spring. The catchment of the study reach, 164 km^2, is relatively small; 58% lies over the tree line, while 0.7% of the area is covered by lakes. Consequently, the water level changes are strongly sensitive to rainfall events and snow melt due to temperature changes.

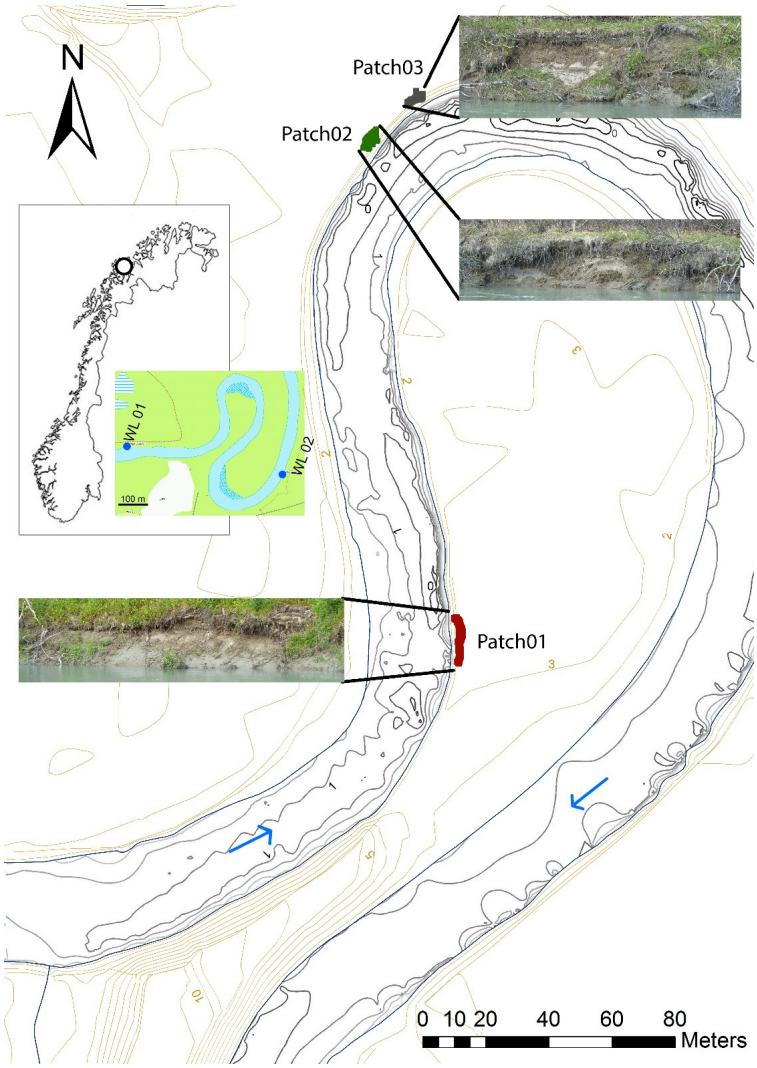

Figure 1. The investigated lowland river bend is located in the northern part of Norway. The flow is indicated by blue arrows. Investigated patches are shown at their locations. The locations of water level loggers are shown as WL01 upstream and WL02 downstream.

A meandering river can be divided into different sections along the bend: upstream of the bend apex, at the bend apex, and downstream of the bend apex [30]. Figure 1 shows the locations of the patches. They are all located at the outer side of the river bend. One is located downstream of the apex (patch 01) and two are located upstream of the apex (patches 02 and 03).

The river migrates through a valley filled with glaciofluvial sediments deposited since the end of the last ice age [39,40]. These deposits are thin undulating layers of sand and silt along the riverbank. A soil layer on top of the bank is thin and contributes little to stabilize the riverbank. The migration of the river through these deposits causes the formation of riverbanks up to 20 m high at the most downstream part of the investigated reach. The riverbed consists of both fine sand and coarse gravel. Throughout the study reach, downstream fining can be observed. In the upstream part

of the reach, the riverbed is armored so that gravels and cobbles dominate. Passing farther downstream, the armor layer disappears gradually and the riverbed consists of fine sand moving in ripples and dunes. The vegetation on the riverbanks consists of birch trees and vegetation patches (grass and moss), which fall and slide down the riverbank.

Following these parameters, the river can generally be classified after Rosgen to be an F-type river, which is described as an entrenched meandering riffle/pool channel on low gradients with a high width/depth ratio (study case: slope S_w = 0.36‰, W/D > 20). Specifically, it is an F4 river, since the bed material consists of sand and gravel [41]. According to Rosgen, an F4-type river has very high streambank erosion potential, but the influence of vegetation is only moderate. These criteria favor erosion by fluvial entrainment.

2.2. Data Acquisition

Several measurements were taken to investigate the bank erosion process at the study site. First, water level changes were recorded at the upstream and downstream ends of the reach (Figure 1). They were measured during May and August in 2011, June and October in 2012, and June and July in 2013. The fluctuation of water level showed a dependency on the amount of snow in the catchment. During spring and early summer, the water level rose with the course of the sun and the remaining snow in the mountains. This shows a certain influence of the amount of snow in the catchment on the hydraulics in the reach.

During 2011 and 2012, the measured water level fluctuated between 1.1 and 1.8 m a.s.l. downstream and 1.5 and 2.2 m a.s.l. upstream.

In spring 2013, the water level logger recorded one high-water event (2.3 m a.s.l.) after some days of rainfall from 23 to 27 June and a flood event at night from 3 to 4 July (Figure 2) at 2.55 m a.s.l. after heavy rain. The latter shows a rise in water level of about 60 cm within 4 h. The average discharge of the river during this three-season ongoing measurement campaign was about 9 m^3s^{-1} at a water level of 1.4 m a.s.l.

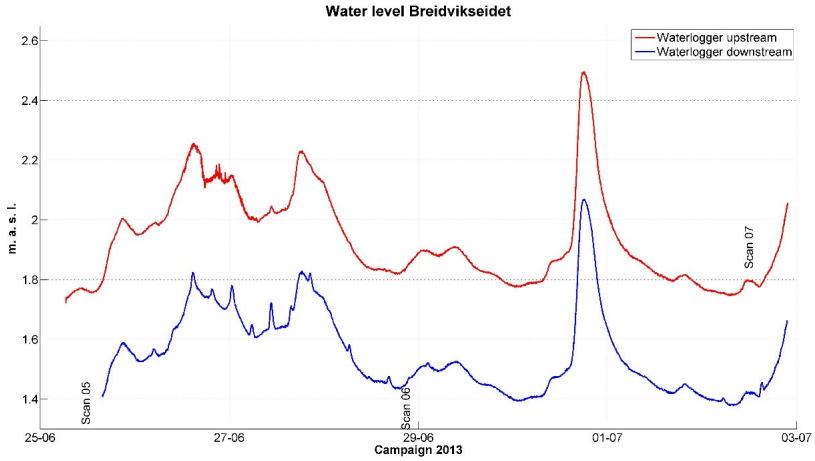

Figure 2. Water level during the third campaign as measured by the water loggers placed upstream and downstream.

Bathymetry was measured with a single beam echo sounder on an acoustic Doppler current profiler (ADCP) from Sontek (M9). The ADCP was directly coupled to a TopCon RTK-GPS (Real Time Kinetic GPS) system. Foerst and Rüther described the campaign and the results in detail [37]. The bathymetry of the two meanders shows the typical pattern of the riverbed for flow through strongly curved and steeply sloped channels. As displayed in Figure 1, a steep outer bank and a mild

gradient toward the inner bank characterize the profile of the cross section. Passing the end of the first meander bend, the riverbed flattens and becomes more symmetrical when the so-called crossover is passed. At the beginning of the second bend, a steep bank develops on the left side of the river. Analogous to the first river bend, a scour at the outer bank forms, causing a steep bank with a mild gradient toward the point bar.

In several field campaigns, the riverbank was scanned at six places along the outer banks to investigate longer-term and short-term processes. A TopCon GLS-1000 laser scanner with ScanMaster© software was used to conduct the scanning. The scanner was mounted on a tripod 1.5 m over the ground. The GLS-1000 operated with a Class 1 laser at 1535 nm. The accuracy of our measurement distance at <150 m was 4 mm under optimal conditions, which could be influenced by atmospheric conditions and the reflectivity of the scanned surface. The GLS-1000 was also equipped with a dual-axis compensator. Each outer bank was scanned from three scan positions in order to make sure that the parts lying in the shadow of one scan angle were covered by the other angles from the other positions. The scan distance was between 40 and 80 m. The three scan positions were combined by overlaying at least four georeferenced tie points. The target points were the same for each scan series and had to be removed between the scans. Therefore, a measurement error up to 0.010 m in the horizontal direction and 0.020 min the vertical direction had to be taken into account. This target-based registration is the standard procedure (Schürch et al., 2011). The mean error calculated by the ScanMaster© software was between 0.002 and 0.009 m, showing the high precision of the measurement method [42]. The georeferencing of the target point was done with a TopCon RTK-GPS system. The RTK correction came from a base station positioned on a known fixed point in the study area.

In 2011, these patches were scanned in May and June. Within this period, six rain events causing the water level to fluctuate strongly were recorded. In 2012, the same patches were scanned in June and October. During this period, the river discharge was strongly influenced by eight short rain events. During the field campaign in 2013, the periods between the three scans were shorter compared to the two previous ones. In total, three scans were taken with 10 days between the measurements. As can be seen in Figure 2, the hydrograph recorded in this period shows only one significant peak.

Additionally, in the investigated reach, a comprehensive dataset was taken, consisting of velocity and discharge measurements. Over 70 transects were measured with an ADCP under different hydraulic conditions. The analysis of the data gave valuable insight into the hydraulic conditions and the cross-sectional shapes prevailing at different flow stages and regimes (e.g., rather specific helical flow features in combination with steep riverbanks) [6]. These hydraulic features were observed independent of the prevailing flow stage. A detailed overview of these data is given in Foerst and Rüther [36].

2.3. Limitation of Method

The accuracy of the laser scan itself according to TopCon is a maximum at 4 mm from 1 to 150 m; this lies clearly within the measurement distance during this survey. The very low error during the overlay of the different scan angles confirms this assumption. Schürch et al. showed in their study that the uncertainty rises with the complexity of the scanned landscape [42]. In this study, the scanned area is a nearly vertical riverbank. Therefore, it can be assumed that the data within one scan of the described patches are highly reliable. However, the GPS accuracy is between 0.008 and 0.013 m in the horizontal and between 0.012 and 0.017 m in the vertical direction. Experience has shown that GPS data are very constant within a dataset. That means that the offset for one set of measured target points is the same as long as the GPS system has reception from the satellites without long interruptions. This was again confirmed by the low mean error calculated during the scan overlay. The GPS error might be avoided if it is possible to leave the targets at the same position. This was not possible due to the limited number of targets that were available. Another drawback is that the TLS scans were taken during different water levels (Table 1). The scans were therefore limited to the water surface and it was not possible to compare the total amount of sediment loss.

Table 1. Overview of scans and water level changes.

Scan	Date of Scan	Water Level m a.s.l.						
		Min	Max	Mean	σ	Scan	Flood Events	Comment
01	May 2011	1.67	2.38	2.02	0.28	1.84		Initial state
02	July 2011					1.64	8	After eight moderate high-water events
03	June 2012	1.35	2.16	1.95	0.16	1.58		Initial state
04	October 2012					1.26	6	After six moderate high-water events
05	19 June 2013	1.72	2.25	1.99	0.13	2.01		Initial state
06	28 June 2013					1.81	1	After one moderate high-water event over five days
07	6 July 2013	1.72	2.5	1.90	0.15	1.71	1	After one extreme high-water event

2.4. Data Postprocessing

2.4.1. Point Density Filtering and Digital Elevation Model (DEM)

This study focused on three positions along the first and second bends. These positions (patches 01–03) are shown in the plane view of Figure 1. The first patch was located at the end of the first river bend and the second and third patches were at the second river bend between inflow and apex. The patches were chosen because the heights of the riverbank have been the same and are located at the lowest level of the terrace system. Over the last three years, no considerable vegetation growth could be observed. The dimensions of the point clouds were defined by a vertical cut at 2.8 m a.s.l. as the upper limit. The lower limit was the water line at the moment when the scan was taken (Table 1). The point clouds showed single points, which have to be regarded as artifacts. These single points created during the scan were removed by a density filter. The basis of the filter was provided by the Point Cloud Library (PCL, 2013). The filter projected a sphere with radius R around each point and counted the number of points within this sphere. If there were a certain number of neighboring points N within this sphere, then it was defined as a good point; otherwise, it was regarded as an outlier [43,44]. The filter was applied with radius R from 0.01 to 0.15 m in steps of 0.015 m. The number of neighboring points was defined for N = (5, 10, 5, 20, 25). Points with fewer than N neighbor points were deleted. In this way, for each point cloud, 50 filtered point clouds were created, and these point clouds were plotted. Afterward, they were visually inspected for whether enough outliers were removed and whether the point cloud was still coherent. The result was very different and no special pattern concerning the settings was visible. The final parameters used for the filtering are displayed in Table 2. Vegetation and dead wood, which blocked the view in front of the riverbank during the laser scans, were removed manually, first in the 2D view of ArcGIS© and then in the 3D view of ArcScene©.

Table 2. Results of filtering of terrestrial laser scanning (TLS) point clouds.

	Scan	Date of Scan		Filter Parameter		Points Before Filtering	Points After Filtering	Points After Manual Cleaning	Water Level m a.s.l.		
				R	N				Min	Max	Scan
Patch 01	01	May 2011	2011	0.055	15	79,735	60,252	59,151	1.67	2.38	1.84
	02	July 2011		0.025	5	52,678	36,305	35,618			1.64
	03	June 2012	2012	0.040	5	124,040	113,854	113,415	1.35	2.16	1.58
	04	October 2012		0.055	10	180,588	168,735	1,164,403			1.26
	05	19 June 2013		0.040	5	286,670	270,056	269,707			2.01
	06	28 June 2013	2013	0.025	5	379,610	351,198	339,921	1.72	2.25	1.81
	07	6 July 13		0.040	5	566,067	549,132	523,337	1.72	2.5	1.71
Patch 02	01	May 2011	2011	0.040	15	94,658	91,164	91,145	1.67	2.38	1.76
	02	July 2011		0.040	5	26,579	23,992	23,949			1.72
	03	June 2012	2012	0.025	5	588,731	496,815	494,000	1.35	2.16	1.65
	04	October 2012		0.025	10	121,261	108,654	107,977			1.40

	05	19 June 2013		0.040	10	886,871	824,974	818,160			1.60
	06	28 June 2013	2013	0.040	10	147,365	130,180	129,223	1.72	2.25	1.77
	07	6 July 2013		0.025	10	445,743	430,526	425,447	1.72	2.5	1.76
Patch 03	01	May 2011	2011	0.040	5	41,569	26,706	26,665	1.67	2.38	2.03
	02	July 2011		0.040	10	27,570	20,741	20,741			1.73
	03	June 2012	2012	0.025	5	621,165	609,966	607,381	1.35	2.16	1.67
	04	October 2012		0.025	10	164,582	124,335	124,335			1.25
	05	19 June 2013		0.040	10	907,733	887,744	887,409			1.60
	06	28 June 2013	2013	0.040	15	109,946	99,567	98,975	1.72	2.25	1.80
	07	6 July 2013		0.040	20	297,441	242,797	239,662	1.72	2.5	1.71

2.4.2. Statistical Methods

For analysis of the DEM, patches 02 and 03 were virtually rotated so that the orientation was the same as patch 01, north-south. In this way, each row from the DEM displays the vertical extension and each column the horizontal extension. The vertical mean slope gradient and horizontal mean gradient were calculated by calculating the mean for each row and each column of the grid. In order to investigate the significance of slope change within a measurement period, the data were statistically verified. The slope gradient for each patch within a measurement period was compared, with the aim of verifying that the gradient between the scans was significantly different. To decide which statistical method was appropriate, the data needed to be tested for normal distribution. Therefore, the slope gradient for each patch was tested for normality with the Kolmogorov–Smirnov test. Since the slope gradient data were not normally distributed, the Kruskal–Wallis test was used to verify the significant difference between the slope gradients (Table 3).

2.4.3. Bank Retreat

The bank retreat was converted to a mass balance of sediments at the riverbank and was defined as the horizontal difference perpendicular to the shore line between successive scans. For this purpose, a DEM with a grid size of 0.05 m was created for each scan. The bank retreat was defined as the smallest distance between one point in the first scan and the surface to the consecutive scan; otherwise, there would be an overestimation of the retreat [17]. To estimate the bank retreat, for each grid cell, the horizontal distance to each grid cell was calculated at the same elevation a.s.l. of the successive scan. Then, the smallest value was used to define the retreat at each point. To avoid false data at positions where gaps in the point cloud existed, the maximum horizontal distance was set at 0.5 m. These grid cells, which had no corresponding grid cells within this distance in the second cell, were discarded. Finally, the total mass balance was calculated, and the volume change is given in m^3 per horizontal square meter.

2.4.4. Slope Angle

From the filtered point cloud, a mesh was created with a cell size of 0.005 m. On this mesh, the point clouds were projected and a DEM was created. From this DEM, the slope gradient in degrees was calculated. The slope gradient ∇F is defined by

$$\nabla F = \frac{\partial F}{\partial x} \hat{i} + \frac{\partial F}{\partial y} \hat{j}$$

where i^ and j^ are standard unit vectors for the horizontal x and y coordinates.

Thus, the gradient in degrees (G_{deg}) was calculated with

$$G_{deg} = atan\left(\sqrt{(\nabla F_x)^2 + (\nabla F_y)^2}\right) \times \frac{180}{\pi} \ .$$

For the change in slope angle along the width of each patch, a mean vertical slope gradient (MVSG) was calculated. The MVSG is the average slope angle for each column in the grid of the DEM

and the average slope at a given position along the riverbank. For the average slope angle, the mean value of all slope angles within the DEM was calculated.

3. Results

Riverbank Changes

Figure 3 shows the horizontal bank retreat at patch 02 between the scans over three years from a bird's-eye perspective in meters. The blue arrow indicates the direction of water flow. Positive numbers (red shades) mean retreat/erosion and negative numbers (blue shades) mean advance/sedimentation.

Scans 01 and 02 in Figure 3 showed changes from May to July 2011. Between these scans, the water level alternated between 1.67 and 2.38 m, with eight peaks during that period. The mean water level was at 2.02 m a.s.l. Erosion took place nearly the whole way along the riverbank. The bank was stable or experienced a little sedimentation only during the first meter upstream. The erosion increased downstream. The average erosion was 0.31 m^3/m^2 (Table 3) and the slope angle changed from 52° to 40°.

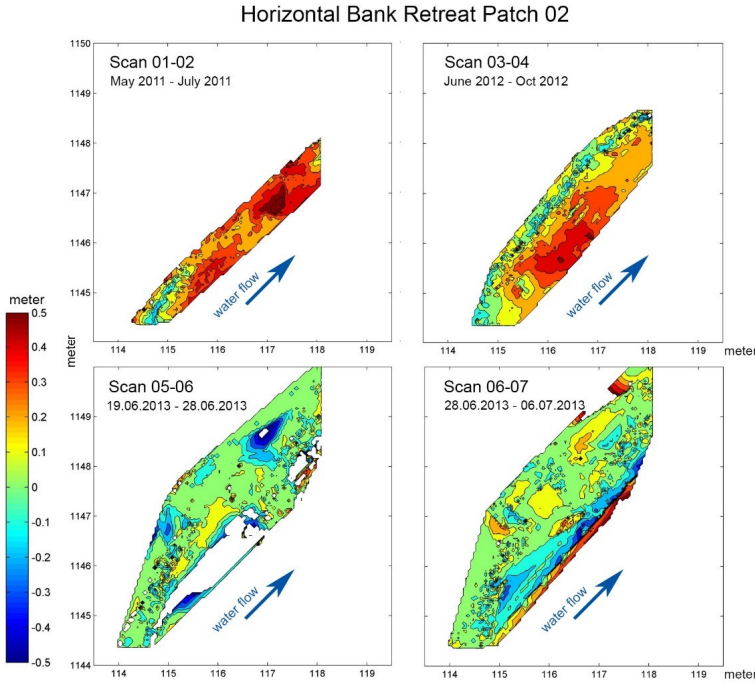

Figure 3. Horizontal bank retreat for patch 02 between scans.

Table 3. Change of riverbank. MVSG, mean vertical slope gradient, and significance of change with * $p < 0.05$ significant, ** $p < 0.01$ highly significant and *** $p < 0.001$ highly significant.

	Scan	Date of Scan	Average Slope Angle	Volume Change		Significance of Change
				Net	m^3/m^2 = Meter Retreat	MVSG
Patch 01	01	May 2011	31.3°			***
	02	July 2011	32.7°	4.24	0.17	
	03	June 2012	32.5°	8.70	0.34	$p = 0.098$
	04	October 2012	34.2°	5.26	0.19	

	05	19 June 2013	39.9°	8.86	0.42	***	
	06	28 June 2013	38.5°	3.99	0.11		$p = 0.446$
	07	6 July 2013	39.3°	2.97	0.09		
Patch 02	01	May 2011	52.0°			***	
	02	July 2011	40.0°	1.14	0.31		
	03	June 2012	43.9°	1.60	0.28	***	
	04	October 2012	38.2°	1.33	0.21		
	05	19 June 2013	51.5°	1.49	0.18	***	
	06	28 June 2013	47.9°	0.11	0.01		***
	07	6 July 2013	49.2°	0.55	0.05		
Patch 03	01	May 2011	56.4°			***	
	02	July 2011	44.6°	1.53	0.28		
	03	June 2012	47.4°	3.27	0.40	***	
	04	October 2012	42.8°	0.82	0.11		
	05	19 June 2013	50.4°	−1.07	−0.17	***	
	06	28 June 2013	47.3°	0.48	0.08		***
	07	6 July 2013	48.2°	0.81	0.10		

Scans 03 and 04 showed changes from June to October 2012. The water level alternated between 1.35 and 2.16 m with six peaks during that period. The mean water level was 1.95 m a.s.l. The highest erosion rates were in the middle part. The upper part along the patch did not experience erosion. The average slope angle changed from 43.9° to 38.2° and the average erosion was 0.21 m^3/m^2.

Scans 05 and 06 showed changes between 19 and 28 June 2013. During this period, there was only one high-water event with a duration of five days and two distinctive peaks (Figure 2). The water level alternated between 1.72 and 2.25 m a.s.l., with a mean water level at 1.99 m a.s.l. The patch showed little erosion. The average erosion was 0.01 m^3/m^2 and the average slope angle changed from 51.5° to 47.9°.

Scans 06 and 07 showed changes between 28 June and 6 July 2013. During this period, the highest flood event during the three-year field study occurred. The water level alternated between 1.4 and 1.5 m a.s.l. before and after the high peak and reached its maximum at 2.5 m a.s.l., while the mean water level was 1.9 m a.s.l. The patch showed hardly any erosion, except a narrow strip just above the water line. The color distribution shows increased erosion downstream. The average erosion was 0.05 m^3/m^2 and the average slope angle changed from 47.9° to 49.2°.

Table 3 compares all patches. The volume change showed similar patterns at all three patches. As seen in patch 02, the main erosion happened during lower water levels over a long time, three months in 2011 and four months in 2012. Little erosion happened during high-water events, as these happened twice in 2013. Patch 01 experienced 0.17 and 0.19 m^3/m^2 during the summer in 2011 and 2012, while in 2013, only 0.11 m^3/m^2 of erosion happened during one high-water event over five days and as little as 0.9 m^3/m^2 during a short, severe high-water event at the end of the campaign. Patch 03 showed similar erosion behavior, with 0.28 and 0.11 m^3/m^2 retreat during summer 2011 and 2012, and only 0.08 and 0.10 m^3/m^2. However, the difference between the long-term and short-term events is not as clear as with patches 01 and 02; it shows less erosion after the short-term high-water event.

Thus, the retreat for each patch was not dependent on the size of the patch and was therefore comparable to each other.

Figure 4a–f shows the riverbank evolution from the side by showing a transect at the center part of each patch. Red lines show the riverbank in the beginning of the season and blue lines show the riverbank at the end of the season. As described previously, there were no changes during the flood events in 2013. Therefore, the cross sections for 2013 are not considered at this point. Table 3 shows the corresponding average slope angles.

Patch 01 showed an irregular slope in 2011 (Figure 4a). The upper part was slightly convex, and in the middle part, a step appeared. At the lower part, it had a 45° slope. Looking at the changes over time, it seems that the center of this patch advanced.

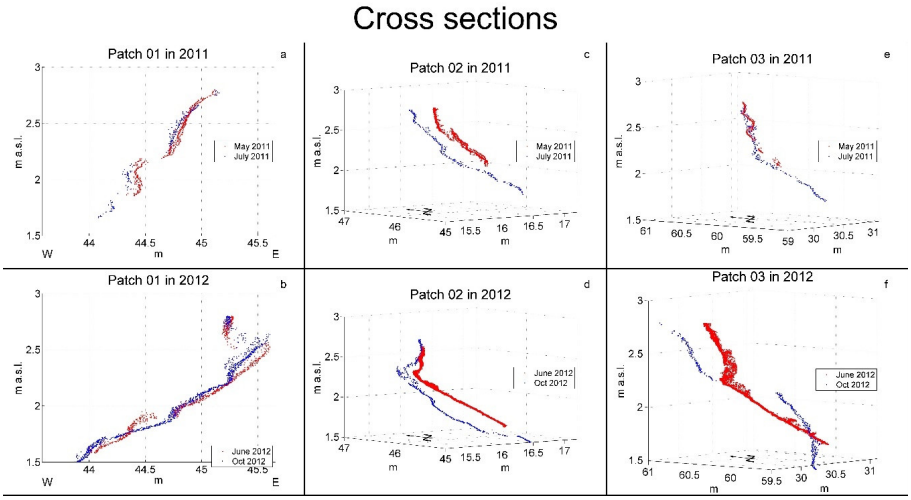

Figure 4. Cross sections of all three patches for the first and second measurement campaigns. Red lines show cross sections in the beginning of a campaign and blue lines show cross sections at the end. Changes for patch 01 are shown in **a** and **b**, changes in patch 02 are shown in **c** and **d**, and changes in patch 03 are shown in **e** and **f**. The first letters (**a**, **c**, and **e**) represent 2011 and the letters **b**, **d**, and **f** represent 2012.

The year after (Figure 4b), patch 01 was characterized by an overhanging block and a mild downward slope. Looking at the changes over time, one can observe two major changes. One is that the overhang eroded partly and deposited just below. The other one is that in the lower third of the slope, material eroded and moved farther down the slope, while no changes were recorded in the middle part of the slope.

Patch 02 (Figure 4c) showed two different slope lines. The slope line from May was nearly vertical in the upper part, and after a breakpoint, the slope flattened. The slope line from July 2011 was not as steep in the upper part and flattened even more in the lower half. It had two distinctive steps, one just below the upper edge, and the second one at 2.1 m a.s.l. marking the change to the lower half. Patch 02 showed a clear bank retreat between May and July 2011.

In June 2012 (Figure 4d), the slope line changed. The upper part was nearly vertical at the top and had a straight slope with an angle below 45° at the beginning of the measurement in June. The scan in October the same year showed a retreat below the top and had a concave slope toward the water line. The patch had no erosion at the top part, but showed clear bank retreat just below.

Patch 03 had a nearly vertical upper part and a less steep part farther down. The slope from May 2011 flattened downward, though the point where the flattening started was not clearly visible. On the other hand, the slope line from July showed a distinct break point at 2.1 m a.s.l. and flattened to an angle smaller than 45°. Patch 03 showed a stable steep part, while bank retreat occurred in the part below the break point.

In June 2012 (Figure 4f), the upper part had a convex, nearly vertical slope at the top and a straight slope with an angle below 45° at the beginning of the measurement in June. The scan from October in the same year showed a retreat at the upper part, where the convex slope changed to a straight slope. In the lower part, the straight slope changed to a convex slope. The transition points from convex to straight in June and from straight to convex in October were the same. Near the water surface, the slope from October became vertical. This patch showed in the upper part of the bank as retreat, in the middle part as sedimentation, and in the lowest part as retreat again.

For a better understanding of the mass distribution, the slope gradient was averaged in the vertical direction (Figure 5). The MVSG (Figure 5), plotted for each season and patch, describes the change of slope angle along the patch.

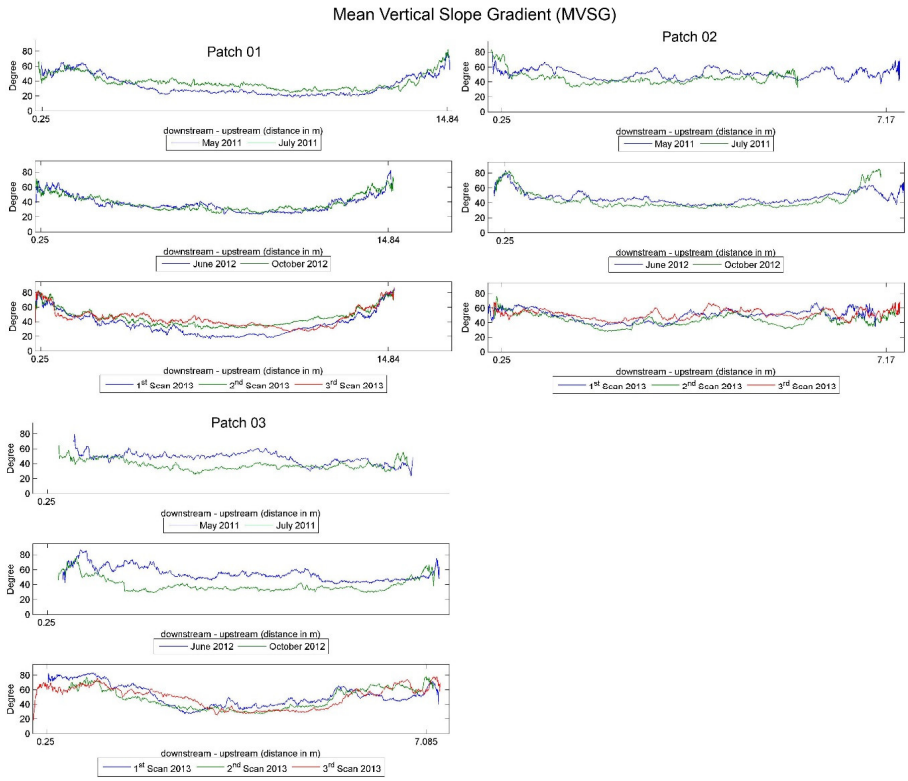

Figure 5. Change of mean vertical slope gradient for all patches during the study.

Patch 01 showed a steepening of the slope in the middle part from May to July 2011, while the edges did not change. In 2012, the June and October scans showed similar MVSGs along the patch. The analysis of the short-term scanning in 2013 showed an increase of MVSG at the middle part from the first to the second scan. The change from the second scan to the third scan after the main flood event showed an increase of the slope angle downstream and a decrease upstream. The edges kept stable and did not show any change in slope angle during 2013.

The change of MVSG at patch 02 was not homogeneous over the width of the patch. It showed a general flattening between May and July 2011. In some small sections, around 1-m wide, no change of MVSG occurred at all, and in other sections, the change was more than 20°. The downstream edge showed a much steeper angle in July than in May. The following year, the slope became flatter equally over the length of the patch. However, the change of MVSG was much smaller, with a maximum around 10°. An exception was the upstream edge, where the slope got much steeper, from 45° to nearly vertical, while the downstream edge was stable. The short-term monitoring of patch 02 in 2013 showed a rather stable slope at the first quarter along the patch. The second middle part showed a flattening of the slope after the first flood event and a steepening after the main flood event. The slope after the main flood event was similar to the slope in the beginning of 2013.

Patch 03 for the first scan in 2011 showed a steep slope downstream (~60°). This changed upstream when the slope was below ~40°. During the second scan, the slope was unchanged

downstream but flattened over the whole length until it had about the same angle at the upstream part as in the beginning. The following season showed a similar pattern. In June, the slope angle was much steeper downstream (~80° to 70°) and decreased upstream. The second scan showed steeper angles just in the beginning on the downstream side. After that, the slope was stable around 30°. The changes in 2013 were smaller. Between the first and second scans in 2013, patch 03 flattened in the downstream and middle sections, while it got steeper upstream. The change from the second scan to the third scan after the flood event showed steeper sections up- and downstream but hardly any changes in the middle part.

4. Discussion

This study focused on three patches located along the outside of two consecutive river bends. A retreat of the riverbank toward the outer side of the upper edge was measured at all three patches. The results show that the erosion rate was different at the three patches. Kleinhans discusses many interacting factors, such as vegetation, sediment, and climate, among others, that influence erodibility and, thereby, river channel formation. In the following, the results from this study are discussed in order to understand the reasons for the erosion and deposition patterns from the hydraulic point of view[44] .

The following discussion is divided into two parts. The first part discusses the results of the first two observation intervals and the three locations, and the second part discusses the changes during the third and fourth intervals, which were significantly shorter.

Considering Figure 4 and Table 3, it can be seen that all three patches behaved according to the general understanding of bank erosion or retreat in meander bends. Looking at the details, one can see different erosional behavior for the different patches. Patches 02 and 03 behaved similarly but in a significantly different way compared to patch 01.

Patch 01 was located downstream of the apex in the most upstream bend. As can be seen in Figure 1, this bend had the lowest curvature compared to the other bends in this reach. Following Table 3, one can see that the average horizontal retreat of patch 01 was 0.17 m. This fell within the range of the measured values of the whole dataset. However, looking at Figure 4, this number seems contradictory to the obvious advance. One possible explanation for this behavior is that a block at this location started to rotate and had not yet failed.

Figure 4b illustrates the results of the measurement at the same patch the following year, during the period from June to October. The data from June show a significant overhang at the crest of the riverbank and accumulated material at the bottom of the slope. The data from October, represented by the blue line in Figure 4b, indicate that the crest partly collapsed and the material deposited in the upper half of the slope. In addition, one can see that the accumulated material shown in the data of June was eroded.

The observed changes at the upper part of the slope during the campaign in 2011 as well as those during the campaign of 2012 can be classified as failure due to gravity, which is described in detail by Langendoen [8,25,28].

Following Figure 1, patches 02 and 03 were located in the second bend, which had significantly higher curvature compared to the first bend, where patch 01 was located. Patches 02 and 03 were situated just upstream of the apex of the second bend, with approximately 10 m in between.

The observed erosion process over time is characterized by three steps. First, one can observe a steepening of the riverbank (step I). At the second step (II), bank material falls from the top and accumulates in front of the bank toe. During the third step (III), this accumulated material is eroded, returning the riverbank back to its vertical shape, restarting the cycle in step I. Looking at Figure 4, it is now possible to identify when the measured changes occurred during the three steps. The changes in Figure 4c–e happened right after step II, where accumulated material starts to erode, while Figure 4f shows step II, where eroded bank material accumulates at the bank toe. In this context, the discussion is continued as to whether or not the outer secondary cell had a stabilizing effect on the riverbank. Experiments in the laboratory and field measurements have shown that as long as the riverbank is steep, outer secondary cells form [6,32,36,37]. Steep riverbanks are observed in step I of

the described process, which leads to the assumption that the outer secondary cell, which dampens the boundary shear stress, prevents the riverbank from further erosion. The dampening of the boundary shear stress will then also lead to material originating from the riverbank accumulating at the bank toe, as described in step II of the process. At the end of step II, the deposited material has flattened the riverbank, and the outer secondary cell will disappear, so that the increased boundary shear stress will initialize erosion (step III). This is schematically illustrated in Figure 6.

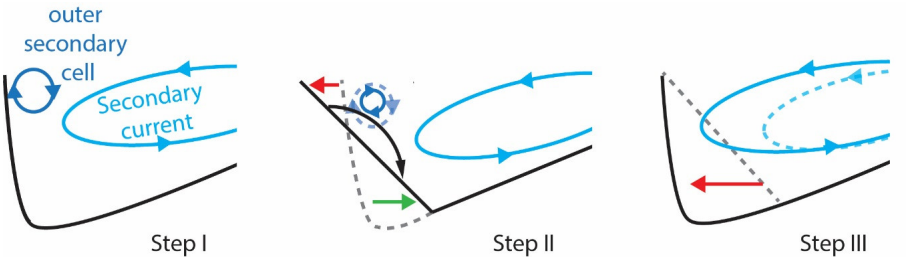

Figure 6. Schematic drawing of the three steps of the erosion process.

As can be seen from Figure 4, patches 02 and 03 behaved differently in the second time interval. This seems to be a contradiction, since they followed the same steps of the erosion process. A possible explanation can be that the location of the erosion process is dependent on the water level. Different discharge leads to a different water level and different hydraulic conditions. It is known from the literature that different hydraulic conditions lead to a relocation of the high-velocity cell as well as the strength level of the secondary current [45–47]. Therefore, the different behavior of patches 02 and 03 at the same measurement time interval was observed.

As a second part of the discussion, the analysis of changes during the third and fourth intervals is as follows. Compared to the first two observation intervals discussed above, the third and fourth are relatively short. As described in the previous section, the measured riverbank changes during these short observation intervals were not significant. However, the measured water levels recorded the maximum value within the total study time. The stable riverbank can be explained by the fact that the above-described process of the three steps was interrupted by the falling water level so that neither erosion nor deposition occurred. According to the hypothesis above, the outer secondary cell dampened the boundary shear stress so that no material could be eroded (step I), and the short period of high water level prevented new material from depositing (step II).

5. Conclusions

This study focused on the erosional process and changes in the geomorphology of a riverbank triggered by river hydraulics. Herein, the riverbank of a lowland medium-size river was scanned with a terrestrial laser scanner in order to analyze the changes of bank geometry over time. The yielded point clouds were postprocessed by filtering for outliers, both automatically and manually. Based on these filtered data, the bank retreat and slope gradient were calculated. The Kruskal–Wallis test statistically tested the changes of the mean vertical slope gradient. It was possible to show which changes were highly statistically significant. This test proved to be a valuable tool to analyze point clouds for its difference in horizontal and vertical shapes. These results give insight into riverbank migration processes within an alternating water level over two summer seasons as well as migration processes within two short peak events. Hence, the sediment transport became clear.

The results lead to the following conclusions:

1. In the laboratory-observed phenomenon, the formation and existence of an outer secondary cell dampened the shear stress close to the riverbanks, and a possible consequence was observed and documented in a natural meandering river at bends with high curvature and relatively steep

riverbanks. The dampening of the erosive behavior was documented by subsequent terrestrial laser scans of three patches along the riverbank.
2. This phenomenon could explain the stable riverbanks in short-peak events.
3. The location of the erosion process was dependent on the water level. Therefore, different erosional behaviors along one riverbank were observed simultaneously.

Author Contributions: M.F. and N.R. planned the fieldwork. The final research site was chosen by M.F. The laser scans were done by master's students under supervision by M.F. Point clouds were filtered with a script written by Aljoscha Sander. M.F. analyzed the data and verified them statistically. M.F. wrote the manuscript and N.R. reviewed it before submitting.

Funding: This research received no external funding.

Acknowledgments: We would like to thank Felix Hahn and Christian Mörtl, who carried out their master's and bachelor's studies, respectively, in the framework of this study. They contributed significantly to the success of this study. Their help during data acquisition and in handling the challenging logistics of the fieldwork is highly appreciated. A huge thank you also to Aljoscha Sander, who wrote a script for filtering of point clouds, which we were allowed to use.

Conflicts of Interest: The authors declare no conflict of interest.

References

1. Parker, G. Stability of the channel of the Minnesota River near State Bridge No. 93, Minnesota.; University of Minnesota: Minneapolis, MN, USA, 1982.
2. Parker, G.; Diplas, P.; Akiyama, J. Meander bends of high amplitude. *J. Hydraul. Eng.* **1983**, *109*, 1323–1337.
3. Parker, G.; Shimizu, Y.; Wilkerson, G.V.; Eke, E.C.; Abad, J.D.; Lauer, J.W.; Paola, C.; Dietrich, W.E.; Voller, V.R. A new framework for modeling the migration of meandering rivers. *Earth Surf. Proc. Land* **2011**, *36*, 70–86, doi:10.1002/esp.2113.
4. Schnauder, I.; Sukhodolov, A.N. Flow in a tightly curving meander bend: Effects of seasonal changes in aquatic macrophyte cover. *Earth Surf. Proc. Land* **2012**, *37*, 1142–1157.
5. Abad, J.D.; Garcia, M.H. Bed Morphology in Kinoshita Meandering Channels: Experiments and Numerical Simulations. In Proceedings of the 5th IAHR-Symposium on River, Coastal and Estuarine Morphodynamics, Enschede, The Netherlands, 17–21 September 2007; pp. 869–875.
6. Blanckaert, K. Secondary flow in sharp open-channel bends. *J. Fluid Mech.* **2004**, *498*, 353–380.
7. Daly, E.R.; Miller, R.B.; Fox, G.A. Modeling streambank erosion and failure along protected and unprotected composite streambanks. *Adv. Water Resour.* **2015**, *81*, 114–127, doi:10.1016/j.advwatres.2015.01.004.
8. Langendoen, E.J.; Simon, A.; Alonso, C.V. Modeling channel instabilities and mitigation strategies in eastern Nebraska. *Build. Partnersh.* **2000**, doi:10.1061/40517(2000)337
9. Farhadi, A.; Sindelar, C.; Tritthart, M.; Glas, M.; Blanckaert, K.; Habersack, H. An investigation on the outer bank cell of secondary flow in channel bends. *J. Hydro-Environ. Res.* **2018**, *18*, 1–11, doi:10.1016/j.jher.2017.10.004.
10. Klavon, K.; Fox, G.; Guertault, L.; Langendoen, E.; Enlow, H.; Miller, R.; Khanal, A. Evaluating a process-based model for use in streambank stabilization: Insights on the Bank Stability and Toe Erosion Model (BSTEM). *Earth Surf. Proc. Land* **2017**, *42*, 191–213, doi:doi:10.1002/esp.4073.
11. Gu, L.; Zhang, S.; He, L.; Chen, D.; Blanckaert, K.; Ottevanger, W.; Zhang, Y. Modeling Flow Pattern and Evolution of Meandering Channels with a Nonlinear Model. *Water* **2016**, *8*, 418.
12. Bosa, S.; Petti, M.; Pascolo, S. Numerical Modelling of Cohesive Bank Migration. *Water* **2018**, *10*, 961.
13. Thomas, S. Review of methods to measure short time scale sediment accumulation. *Mar. Geol.* **2004**, *207*, 95–114.
14. Lawler, D.M. Application of a novel automatic erosion and deposition monitoring system at a channel bank site on the tidal River Trent, U.K. *Estuar. Coast. Shelf Sci.* **2001**, *53*, 237–247.
15. Couper, P.; Stott, T.; Maddock, I. Insights into river bank erosion processes derived from analysis of negative erosion-pin recordings: Observations from three recent UK studies. *Earth Surf. Proc. Land* **2002**, *27*, 59–79, doi:10.1002/esp.285.
16. Erlingsson, U. A sensor for measuring erosion and deposition. *J. Sediment. Petrol.* **1991**, *61*, 620–623.

17. Haigh, M.J. The use of erosion pins in the study of slope evolution. *Br. Geomorphol. Res. Group Tech. Bull.* **1977**, *18*, 31–49.
18. Lawler, D.M. Advances in the continuous monitoring of erosion and deposition dynamics: Developments and applications of the new PEEP-3T system. *Geomorphology* **2008**, *93*, 17–39, doi:10.1016/j.geomorph.2006.12.016.
19. Thorne, C.R. Field measurements of rates of bank erosion and bank material strength. In Proceedings of the IAHS Florence, Florence, Italy, 22–26 June 1981; pp. 503–512.
20. Milan, D.J.; Heritage, G.L.; Large, A.R.G.; Entwistle, N.S. Mapping hydraulic biotopes using terrestrial laser scan data of water surface properties. *Earth Surf. Proc. Land* **2010**, *35*, 918–931, doi:10.1002/esp.1948.
21. Day, S.S.; Gran, K.B.; Belmont, P.; Wawrzyniec, T. Measuring bluff erosion part 1: Terrestrial laser scanning methods for change detection. *Earth Surf. Proc. Land* **2013**, *38*, 1055–1067.
22. Day, S.S.; Gran, K.B.; Belmont, P.; Wawrzyniec, T. Measuring bluff erosion part 2: Pairing aerial photographs and terrestrial laser scanning to create a watershed scale sediment budget. *Earth Surf. Proc. Land* **2013**, *38*, 1068–1082.
23. O'Neal, M.A.; Pizzuto, J.E. The rates and spatial patterns of annual riverbank erosion revealed through terrestrial laser-scanner surveys of the South River, Virginia. *Earth Surf. Proc. Land* **2011**, *36*, 695–701, doi:10.1002/esp.2098.
24. Resop, J.P.; Hession, W.C. Terrestrial laser scanning for monitoring streambank retreat: Comparison with traditional surveying techniques. *J. Hydraul. Eng.* **2010**, *136*, 794–798, doi:10.1061/(asce)hy.1943-7900.0000233.
25. Wheaton, J.M.; Brasington, J.; Darby, S.E.; Sear, D.A. Accounting for uncertainty in DEMs from repeat topographic surveys: Improved sediment budgets. *Earth Surf. Proc. Land* **2010**, *35*, 136–156, doi:10.1002/esp.1886.
26. Nasermoaddeli, M.H.; Pasche, E. Application of terrestrial 3D laser scanner in quantification of the riverbank erosion and deposition. In Proceedings of the International Conference on fluvial Hydraulics, Cesme-Ismir,Turkey, 3–5 September 2008; p. 10.
27. Brasington, J.; Vericat, D.; Rychkov, I. Modeling river bed morphology, roughness, and surface sedimentology using high resolution terrestrial laser scanning. *Water Resour. Res.* **2012**, *48*, 11.
28. Jaboyedoff, M.; Demers, D.; Locat, J.; Locat, A.; Locat, P.; Oppikofer, T.; Robitaille, D.; Turmel, D. Use of terrestrial laser scanning for the characterization of retrogressive landslides in sensitive clay and rotational landslides in river banks. *Can. Geotech. J.* **2009**, *46*, 1379–1390.
29. Thorne, C.R.; Hey, R.D. Direct measurements of secondary currents at a river inflexion point. *Nature* **1979**, *280*, 226–228.
30. Thorne, C.R.; Zevenbergen, L.W.; Pitlick, J.C.; Rais, S.; Bradley, J.B.; Julien, P.Y. Direct measurements of secondary currents in a meandering sand-bed river. *Nature* **1985**, *315*, 746–747.
31. Blanckaert, K. Mean flow and turbulence in open-channel bend. *J. Hydraul. Eng.* **2001**, *127*, 835–847.
32. Blanckaert, K.; and Graf, W.H. Momentum transport in sharp open-channel bends. *J. Hydraul. Eng.* **2004**, *130*, 186–198.
33. Blanckaert, K. Hydrodynamic processes in sharp meander bends and their morphological implications. *J. Geophys. Res. Earth Surf.* **2011**, *116*, doi:10.1029/2010JF001806.
34. Ottewanger, W.; Blanckaert, K.; Uijttewaal, W.S.J. A parameter study on bank shear stresses in curved open channel flow by means of large-eddy simulation. *RCEM Proc.* **2011**, 1917–1927.
35. Van Balen, W.; Uijttewaal, W.S.J.; Blanckaert, K. Large-eddy simulation of a mildly curved open-channel flow. *J. Fluid Mech.* **2009**, *630*, 413–442, doi:10.1017/S0022112009007277.
36. Foerst, M.; Rüther, N. Post Processing Methods of Moving Boat ADCP Measurements: Time Averaging vs. Distance Averaging. In 14. Treffen junger WissenschaftlerInnen an Wasserbauinstituten. Beiträge zum JuWi-Treffen am 25. und 26. Juni 2012 an der Technischen Universität München; TU Munich: Munich, Germany, 2012; p. 216.
37. Foerst, M.; Rüther, N. Mean and Turbulent Flow Structures in two Consectutive Meander Bends. In Proceedings of the IAHR Europe 2012, Munich, Germany, 27–29 June 2012.
38. Langendoen, E.J.; Simon, A. Stream Channel Evolution of Little Salt Creek and North Branch West Papillion Creek, Eastern Nebraska; National Sedimentation Laboratory: Oxford, MS, USA, 2000.

39. Istanbulluoglu, E.; Bras, R.L.; Flores-Cervantes, H.; Tucker, G.E. Implications of bank failures and fluvial erosion for gully development: Field observations and modeling. *J. Geophys. Res. Earth Surf.* **2005**, *110*, doi:10.1029/2004JF000145.
40. Langendoen, E.J. CONCEPTS-Conservational Channel Evolution and Pollutant Transport System. In *Guidline NSL Technical Report*, Laboratory, U.-A.N.S.: Oxford, MS, USA, 2000; p. 180.
41. Langendoen, E.J. Modeling the Evolution of Incised Streams. II: Streambank Erosion. *J. Hydraul. Eng.* **2008**, *134*, 905.
42. Patsinghasanee, S.; Kimura, I.; Shimizu, Y.; Nabi, M. Experiments and modelling of cantilever failures for cohesive riverbanks. *J. Hydraul. Res.* **2018**, *56*, 76–95, doi:10.1080/00221686.2017.1300194.
43. NVE. NEVINA. Availabe online: nevina.nve.no (accessed on 1 July 2012).
44. Kleinhans, M.G. Sorting out river channel patterns. *Prog. Phys. Geogr.* **2010**, *34*, 287–326.
45. Abad, J.D.; Rhoads, B.L.; Guneralp, I.; Garcia, M.H. Flow structure at different stages in a meander-bend with bendway weirs. *J. Hydraul. Eng.* **2008**, *134*, 1052–1063, doi:10.1061/(asce)0733-9429(2008)134:8(1052).
46. Kasvi, E.; Alho, P.; Lotsari, E.; Wang, Y.; Kukko, A.; Hyyppä, H.; Hyyppä, J. Two-dimensional and three-dimensional computational models in hydrodynamic and morphodynamic reconstructions of a river bend: Sensitivity and functionality. *Hydrol. Process* **2015**, *29*, 1604–1629, doi:10.1002/hyp.10277.
47. Nanson, R.A. Flow fields in tightly curving meander bends of low width-depth ratio. *Earth Surf. Proc. Land* **2010**, *35*, 119–135, doi:10.1002/esp.1878.

© 2018 by the authors. Licensee MDPI, Basel, Switzerland. This article is an open access article distributed under the terms and conditions of the Creative Commons Attribution (CC BY) license (http://creativecommons.org/licenses/by/4.0/).

7.2. Appendix B: Transects

Map over transects along the reach

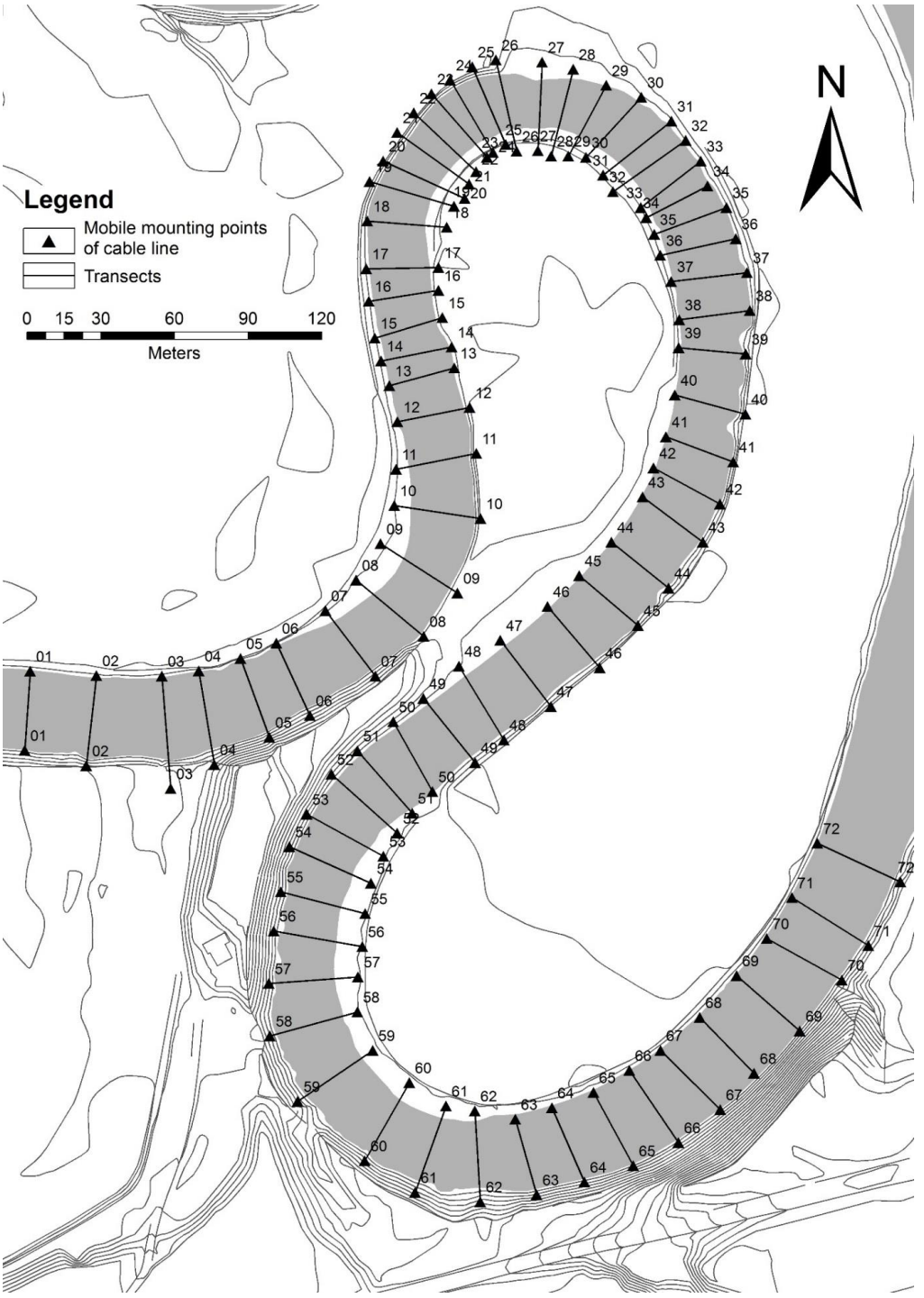

Hydraulic conditions during measurment of each transect

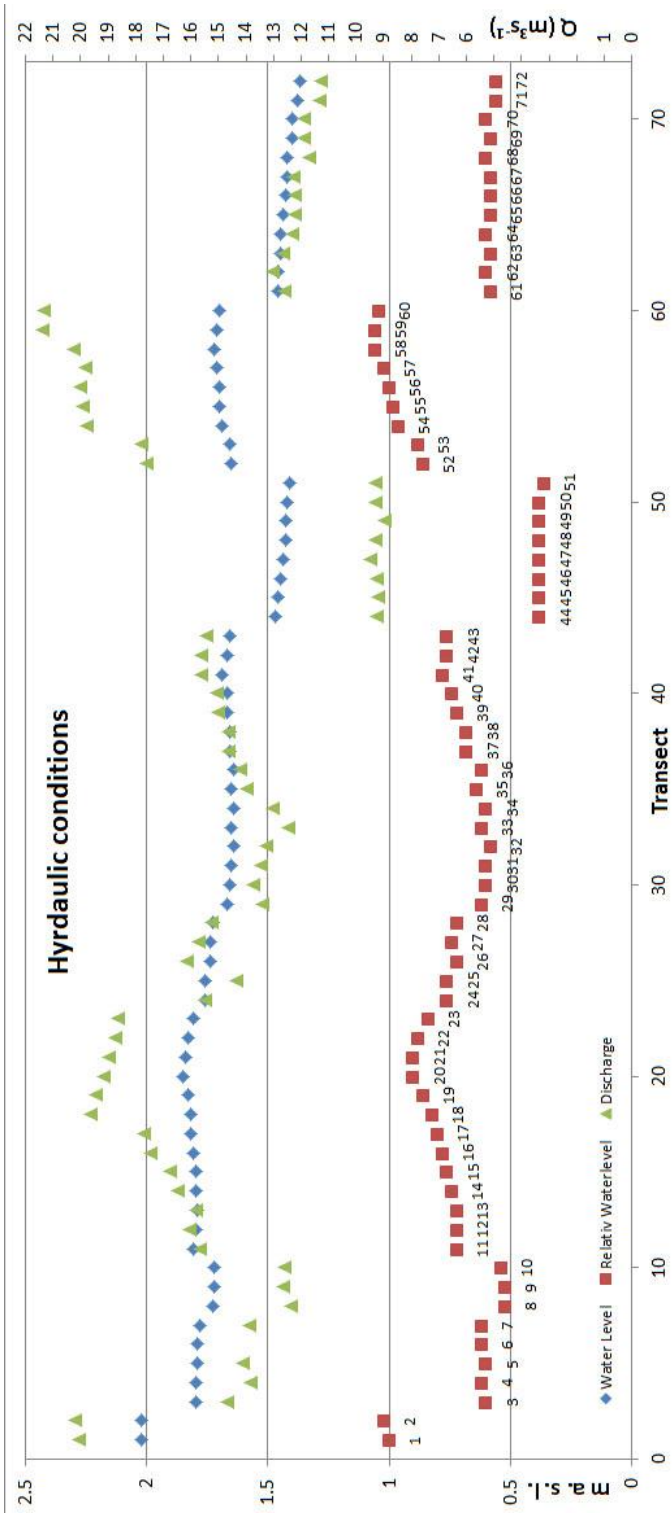

Following the flow structure for each transect.

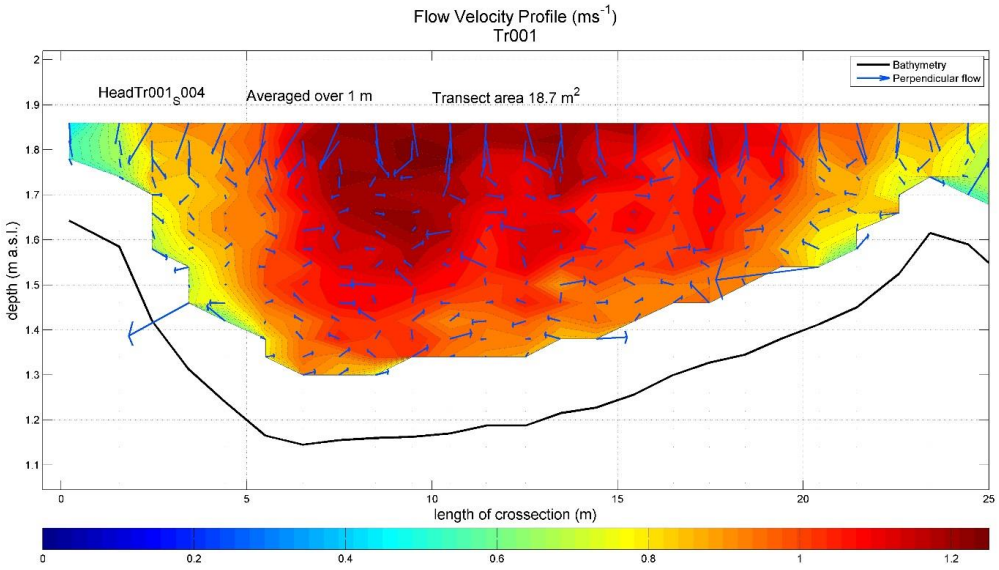
Flow Velocity Profile (ms-1)
Tr001
HeadTr001s004
Averaged over 1 m
Transect area 18.7 m2
Bathymetry
Perpendicular flow
depth (m a.s.l.)
length of crossection (m)

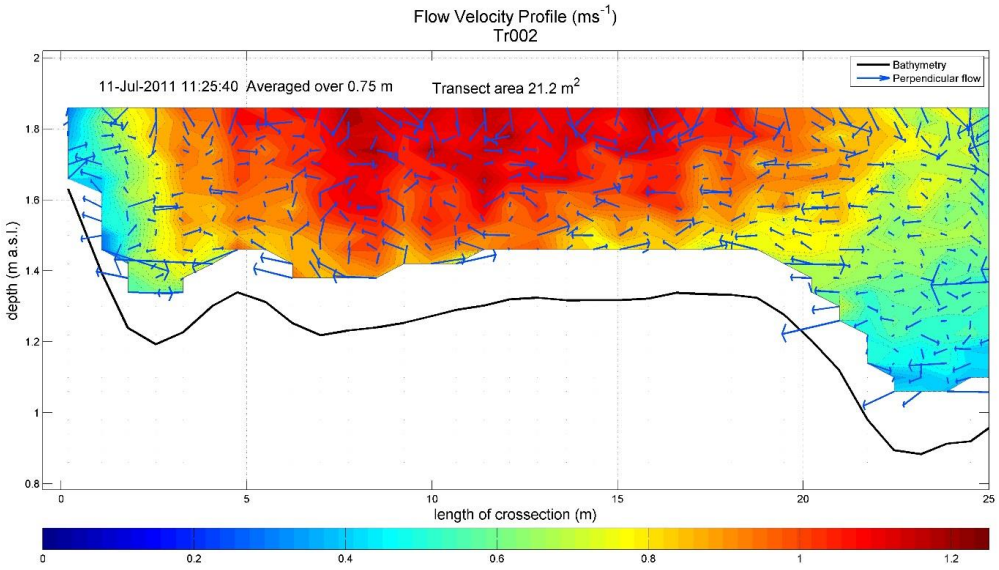
Flow Velocity Profile (ms-1)
Tr002
11-Jul-2011 11:25:40
Averaged over 0.75 m
Transect area 21.2 m2
Bathymetry
Perpendicular flow
depth (m a.s.l.)
length of crossection (m)

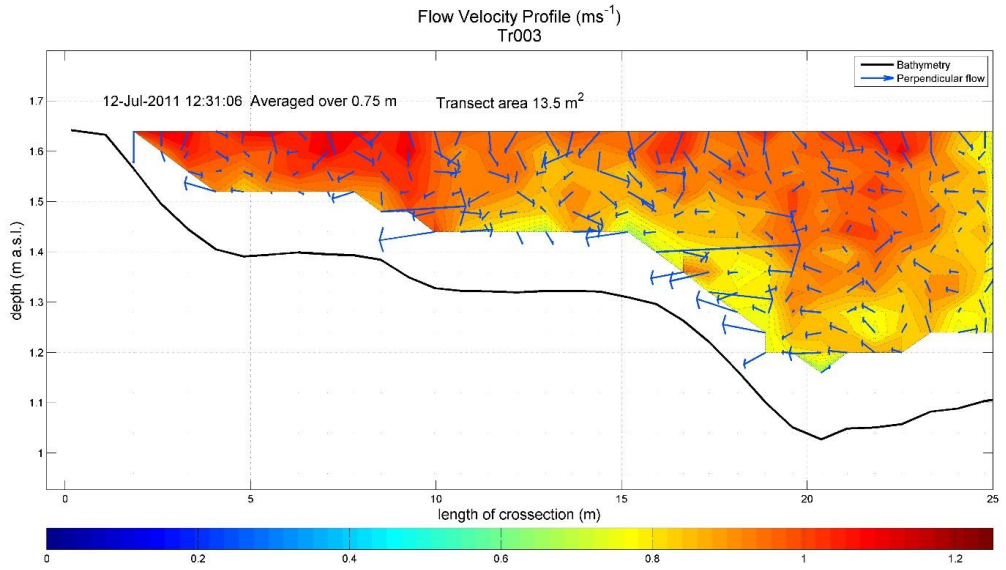
Flow Velocity Profile (ms-1)
Tr003
12-Jul-2011 12:31:06 Averaged over 0.75 m
Transect area 13.5 m2
Bathymetry
Perpendicular flow
depth (m a.s.l.)
length of crossection (m)

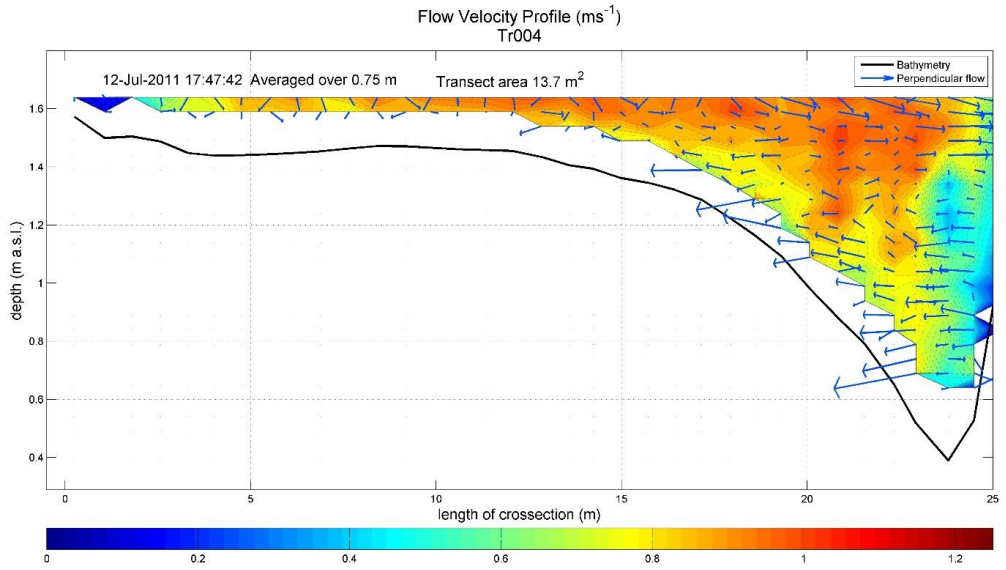
Flow Velocity Profile (ms-1)
Tr004
12-Jul-2011 17:47:42 Averaged over 0.75 m
Transect area 13.7 m2
Bathymetry
Perpendicular flow
depth (m a.s.l.)
length of crossection (m)

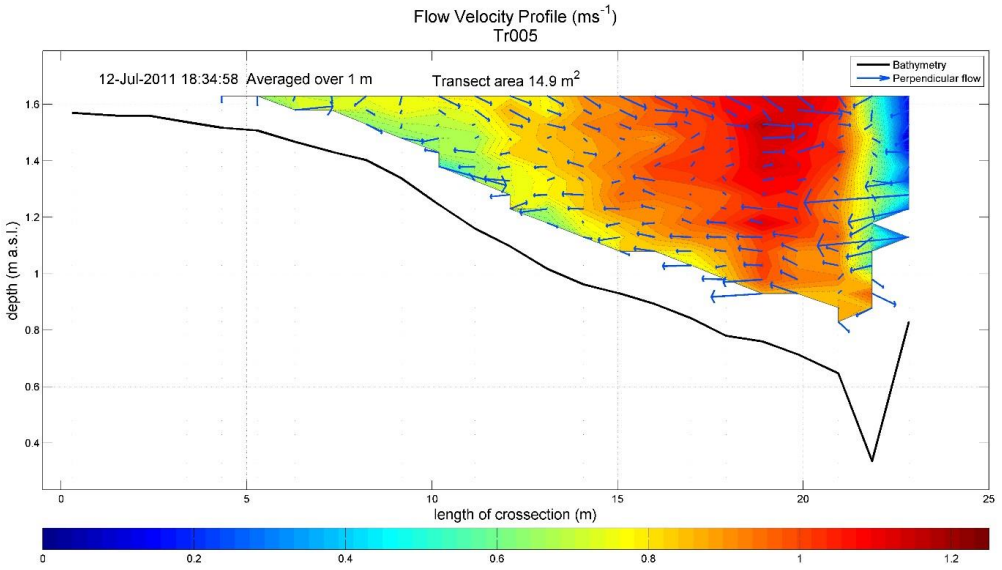
Flow Velocity Profile (ms-1)
Tr005
12-Jul-2011 18:34:58 Averaged over 1 m
Transect area 14.9 m2
Bathymetry
Perpendicular flow
depth (m a.s.l.)
length of crossection (m)

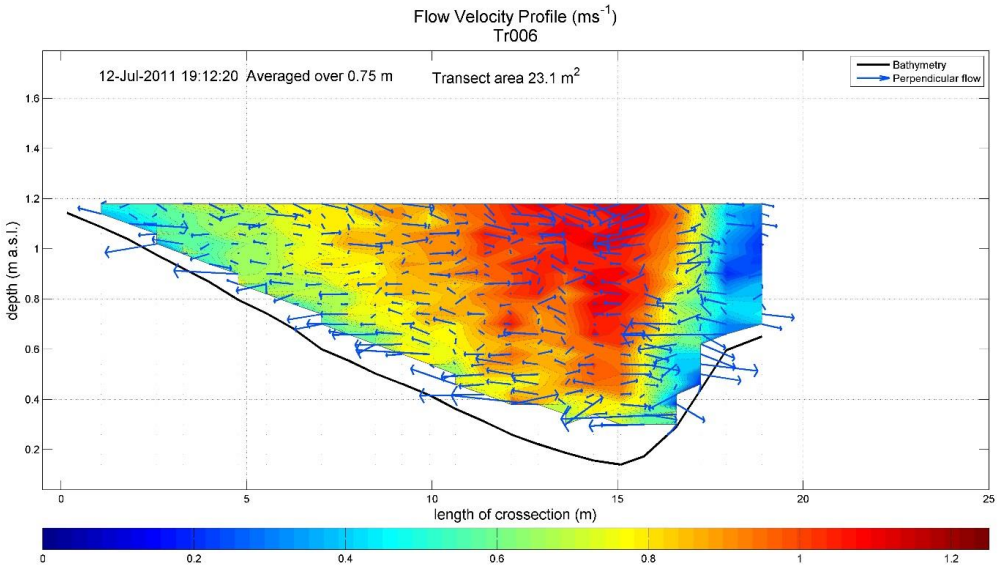
Flow Velocity Profile (ms-1)
Tr006
12-Jul-2011 19:12:20 Averaged over 0.75 m
Transect area 23.1 m2
Bathymetry
Perpendicular flow
depth (m a.s.l.)
length of crossection (m)

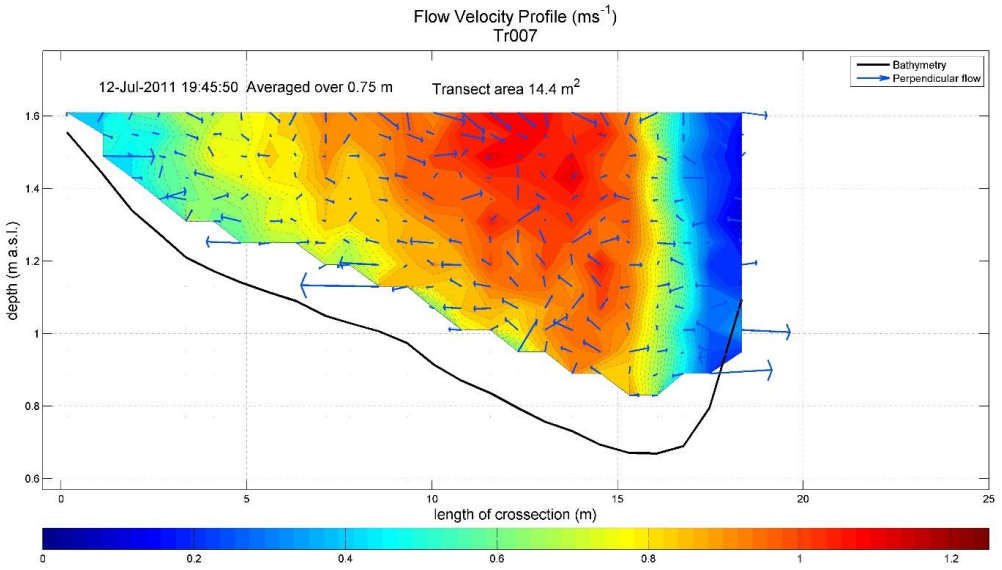
Flow Velocity Profile (ms-1)
Tr007
12-Jul-2011 19:45:50 Averaged over 0.75 m
Transect area 14.4 m2
Bathymetry
Perpendicular flow
depth (m a.s.l.)
length of crossection (m)

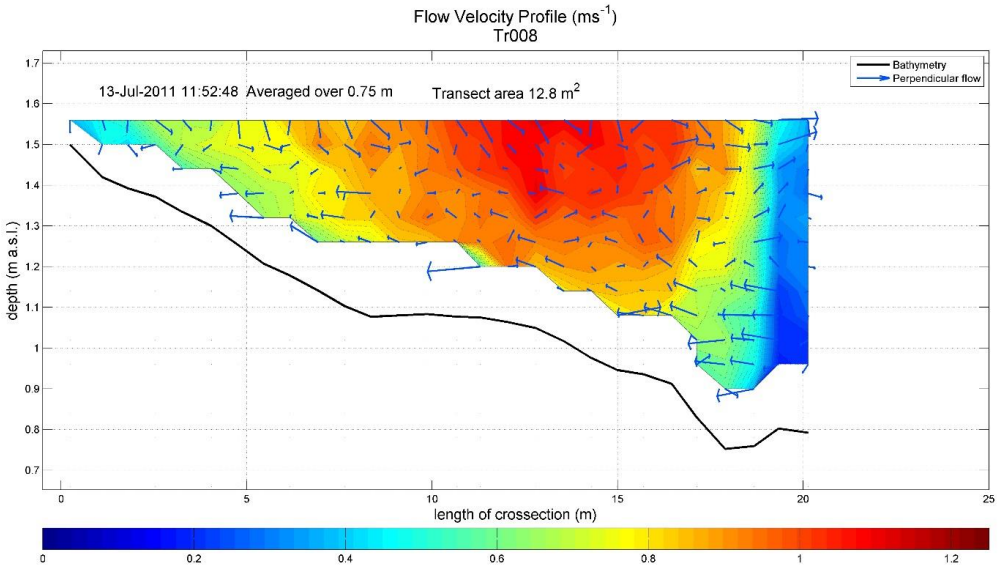
Flow Velocity Profile (ms-1)
Tr008
13-Jul-2011 11:52:48 Averaged over 0.75 m
Transect area 12.8 m2
Bathymetry
Perpendicular flow
depth (m a.s.l.)
length of crossection (m)

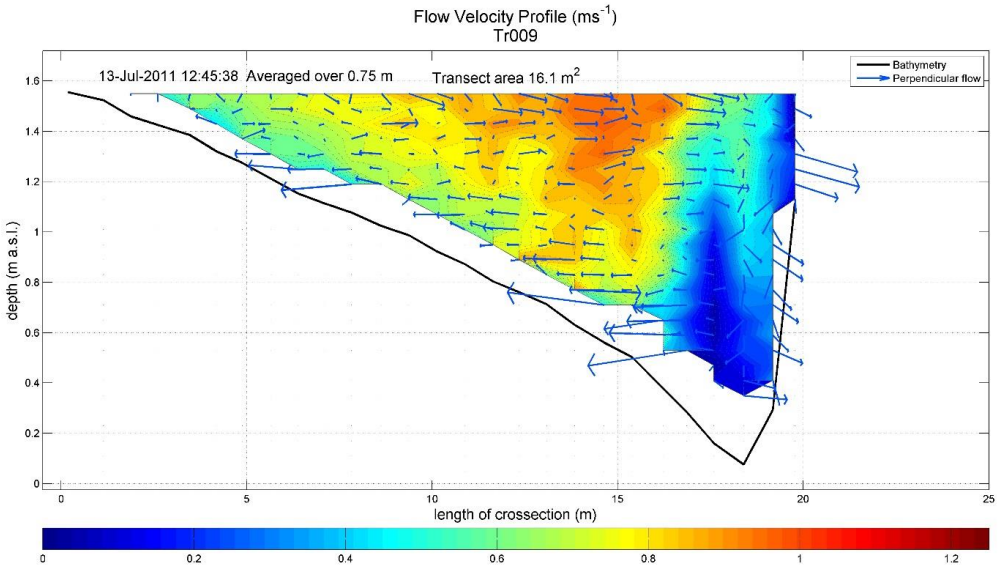
Flow Velocity Profile (ms-1)
Tr009
13-Jul-2011 12:45:38 Averaged over 0.75 m
Transect area 16.1 m2
Bathymetry
Perpendicular flow
depth (m a.s.l.)
length of crossection (m)

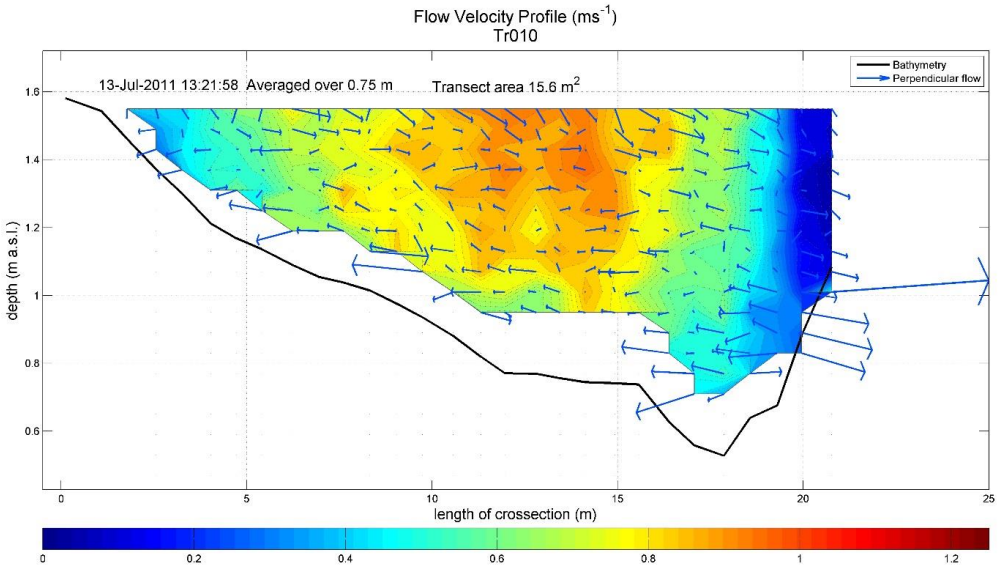
Flow Velocity Profile (ms-1)
Tr010
13-Jul-2011 13:21:58 Averaged over 0.75 m
Transect area 15.6 m2
Bathymetry
Perpendicular flow
depth (m a.s.l.)
length of crossection (m)

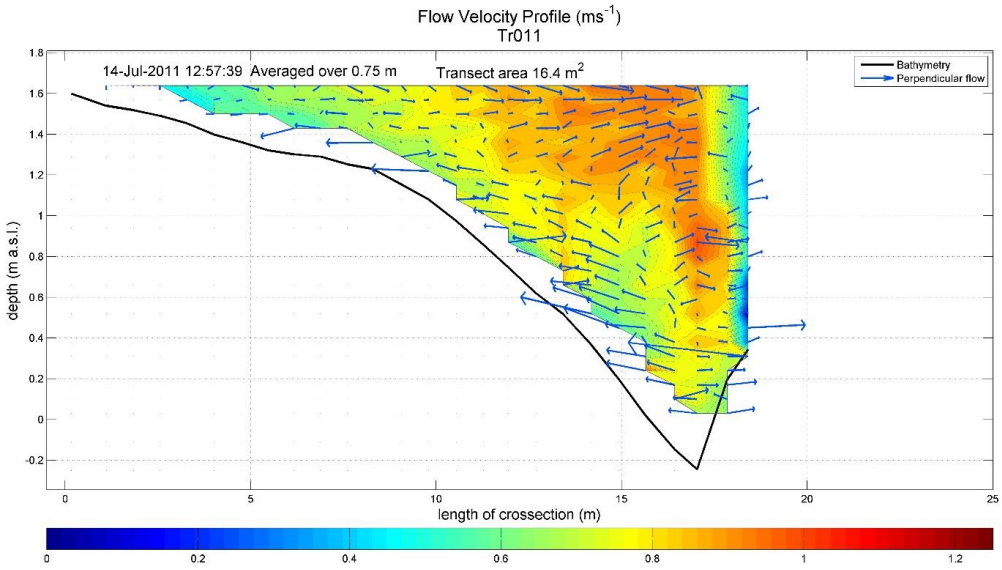
Flow Velocity Profile (ms-1)
Tr011
14-Jul-2011 12:57:39 Averaged over 0.75 m
Transect area 16.4 m2
Bathymetry
Perpendicular flow
depth (m a.s.l.)
length of crossection (m)

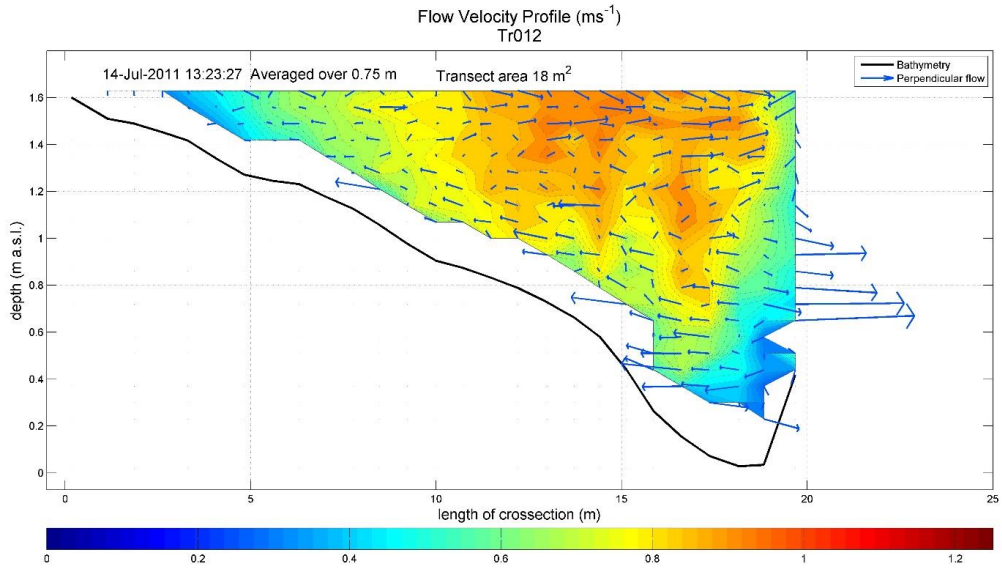
Flow Velocity Profile (ms-1)
Tr012
14-Jul-2011 13:23:27 Averaged over 0.75 m
Transect area 18 m2
Bathymetry
Perpendicular flow
depth (m a.s.l.)
length of crossection (m)

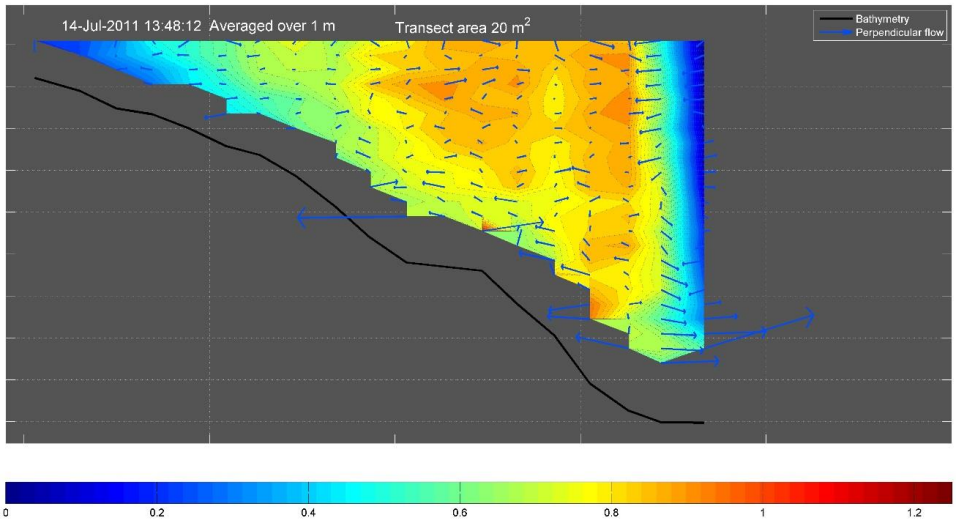
14-Jul-2011 13:48:12 Averaged over 1 m
Transect area 20 m2
Bathymetry
Perpendicular flow
0
0.2
0.4
0.6
0.8
1
1.2

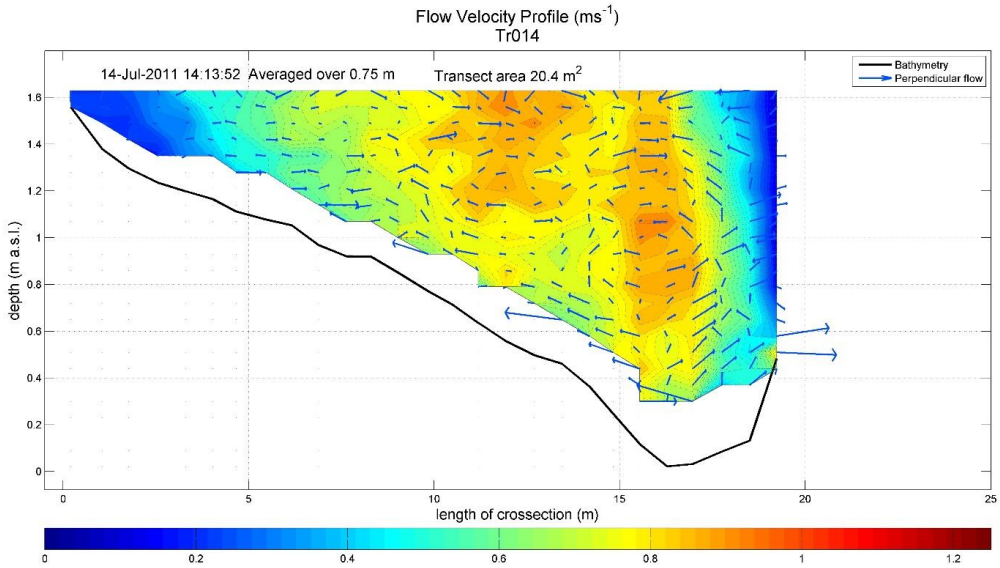
Flow Velocity Profile (ms-1)
Tr014
14-Jul-2011 14:13:52 Averaged over 0.75 m
Transect area 20.4 m2
Bathymetry
Perpendicular flow
depth (m a.s.l.)
length of crossection (m)
0
0.2
0.4
0.6
0.8
1
1.2
1.4
1.6
0
5
10
15
20
25

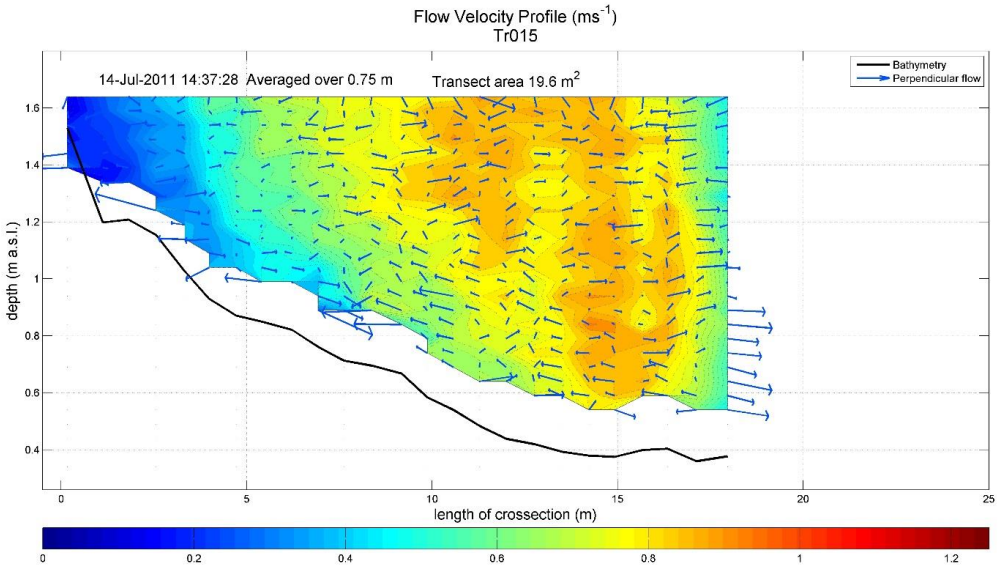
Flow Velocity Profile (ms-1)
Tr015
14-Jul-2011 14:37:28 Averaged over 0.75 m
Transect area 19.6 m2
Bathymetry
Perpendicular flow
depth (m a.s.l.)
length of crossection (m)

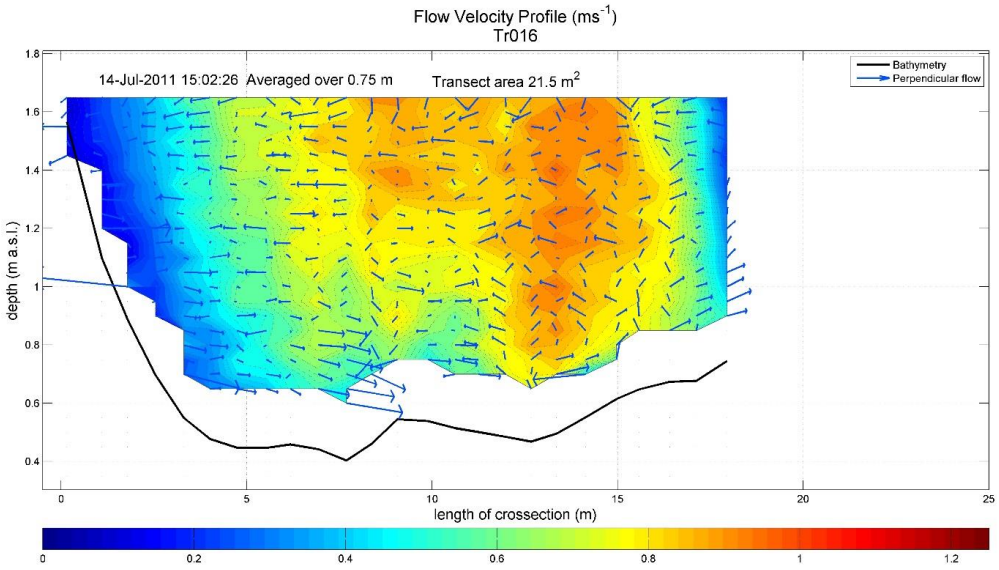
Flow Velocity Profile (ms-1)
Tr016
14-Jul-2011 15:02:26 Averaged over 0.75 m
Transect area 21.5 m2
Bathymetry
Perpendicular flow
depth (m a.s.l.)
length of crossection (m)

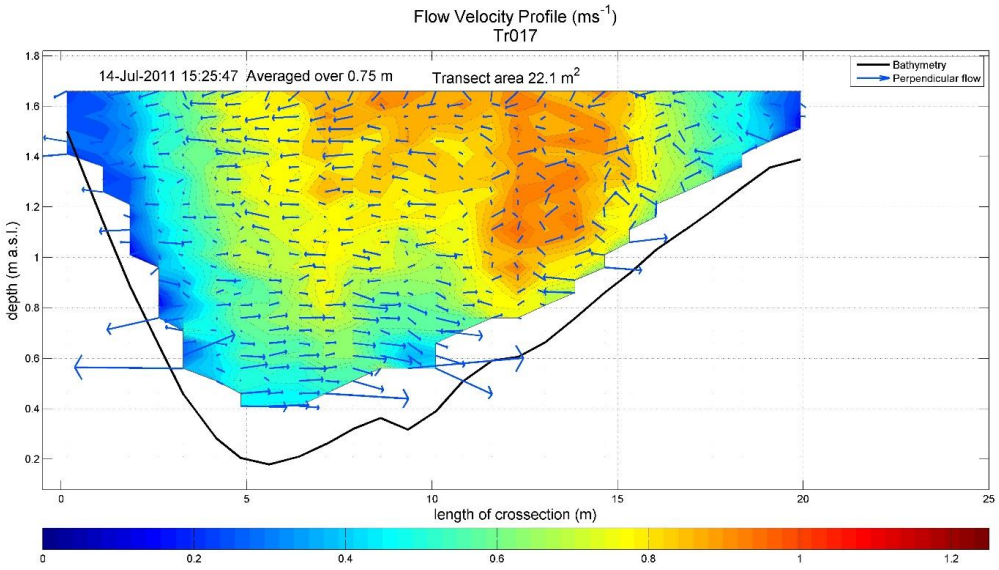
Flow Velocity Profile (ms-1)
Tr017
14-Jul-2011 15:25:47 Averaged over 0.75 m
Transect area 22.1 m2
Bathymetry
Perpendicular flow
depth (m a.s.l.)
length of crossection (m)

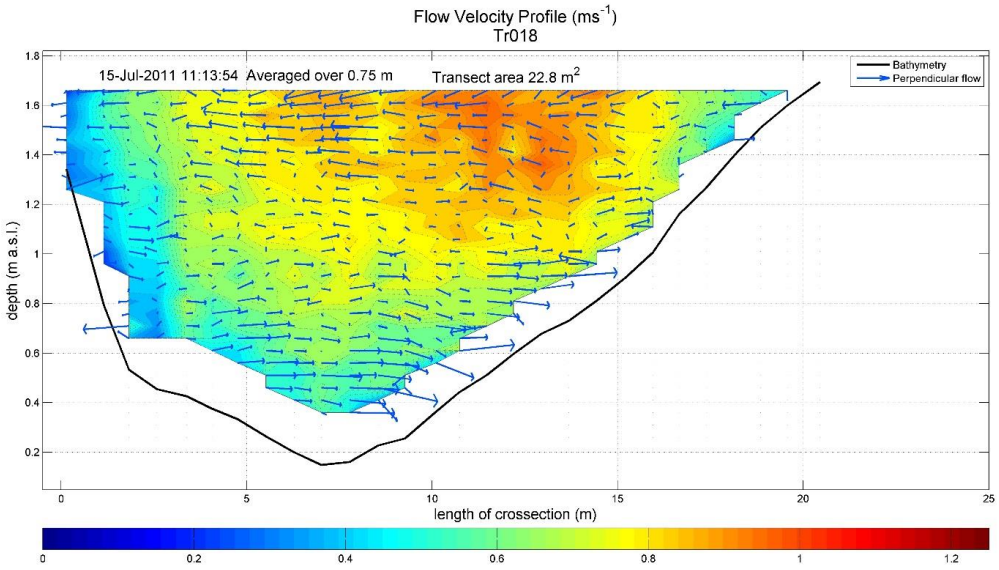
Flow Velocity Profile (ms-1)
Tr018
15-Jul-2011 11:13:54 Averaged over 0.75 m
Transect area 22.8 m2
Bathymetry
Perpendicular flow
depth (m a.s.l.)
length of crossection (m)

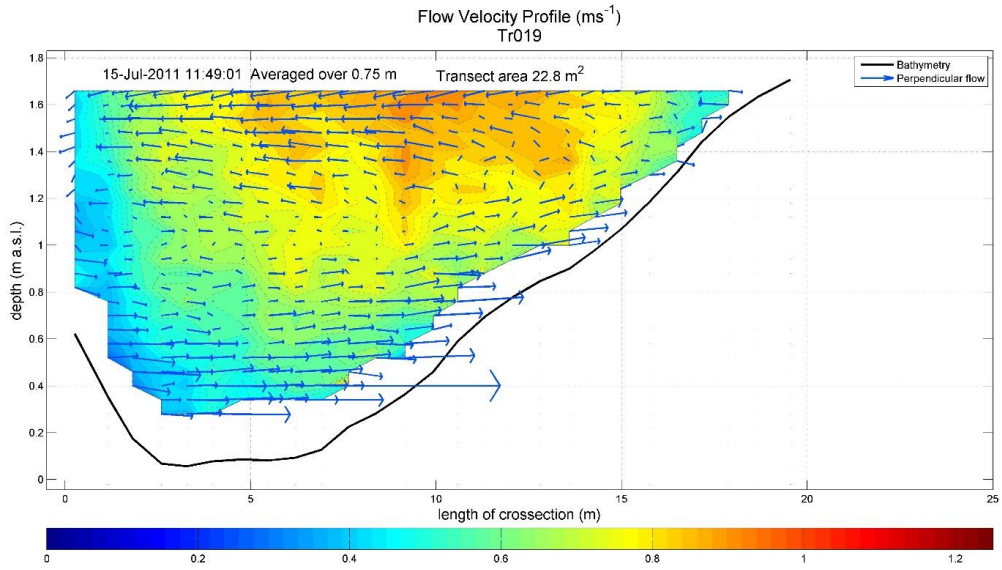
Flow Velocity Profile (ms-1)
Tr019
15-Jul-2011 11:49:01 Averaged over 0.75 m
Transect area 22.8 m2
Bathymetry
Perpendicular flow
depth (m a.s.l.)
length of crossection (m)

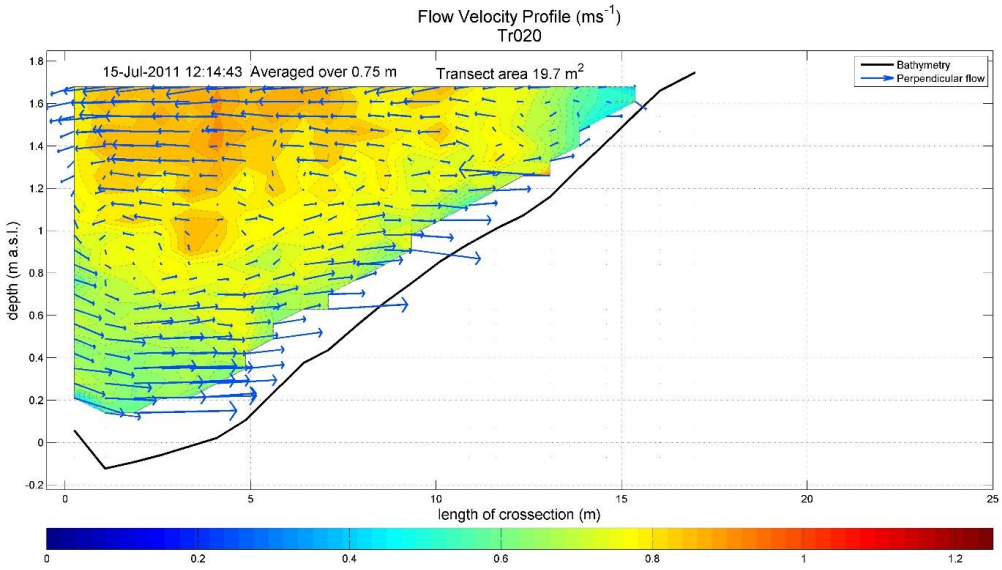
Flow Velocity Profile (ms-1)
Tr020
15-Jul-2011 12:14:43 Averaged over 0.75 m
Transect area 19.7 m2
Bathymetry
Perpendicular flow
depth (m a.s.l.)
length of crossection (m)

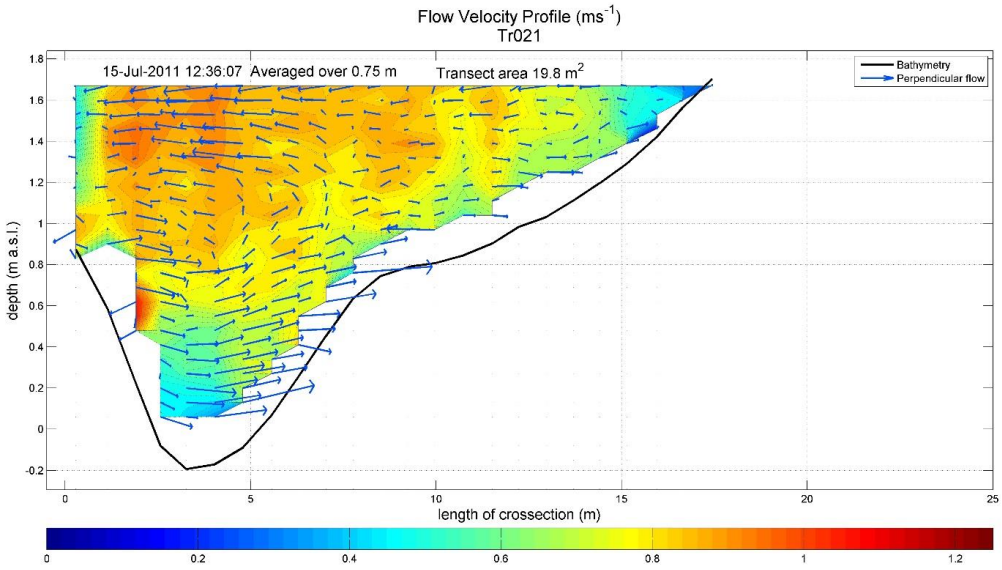
Flow Velocity Profile (ms-1)
Tr021
15-Jul-2011 12:36:07 Averaged over 0.75 m
Transect area 19.8 m2
Bathymetry
Perpendicular flow
depth (m a.s.l.)
length of crossection (m)

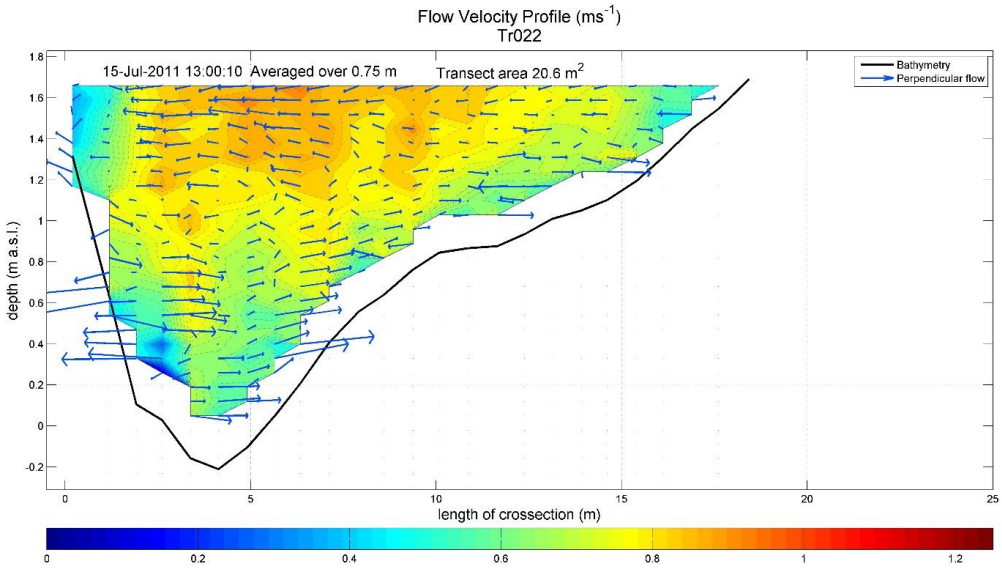
Flow Velocity Profile (ms-1)
Tr022
15-Jul-2011 13:00:10 Averaged over 0.75 m
Transect area 20.6 m2
Bathymetry
Perpendicular flow
depth (m a.s.l.)
length of crossection (m)

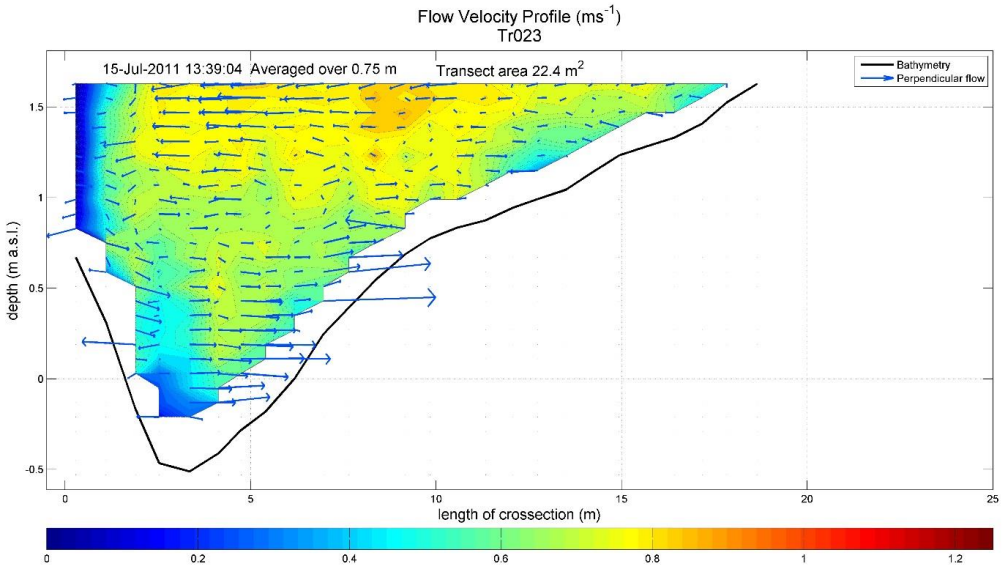
Flow Velocity Profile (ms-1)
Tr023
15-Jul-2011 13:39:04 Averaged over 0.75 m
Transect area 22.4 m2
Bathymetry
Perpendicular flow
depth (m a.s.l.)
length of crossection (m)

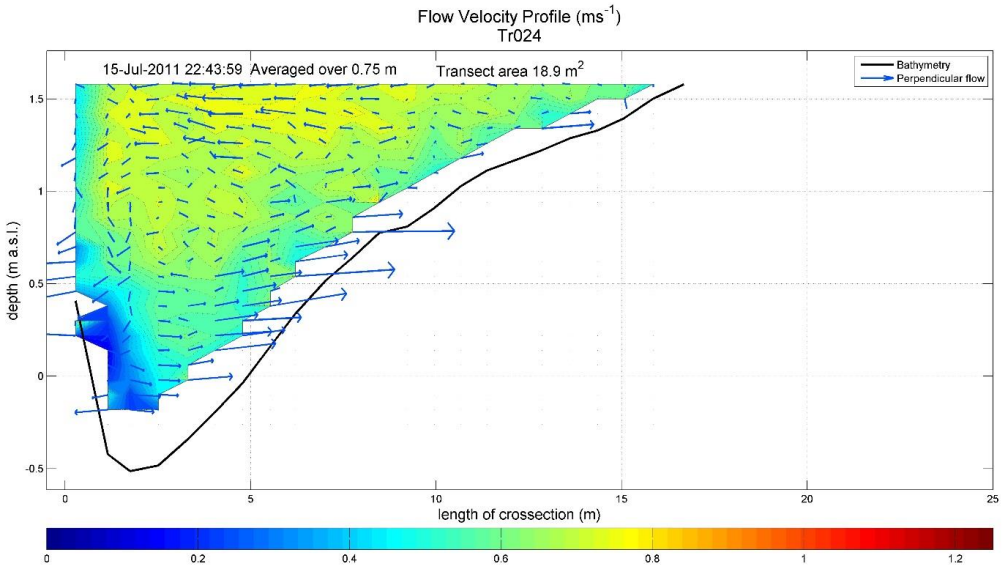
Flow Velocity Profile (ms-1)
Tr024
15-Jul-2011 22:43:59 Averaged over 0.75 m
Transect area 18.9 m2
Bathymetry
Perpendicular flow
depth (m a.s.l.)
length of crossection (m)

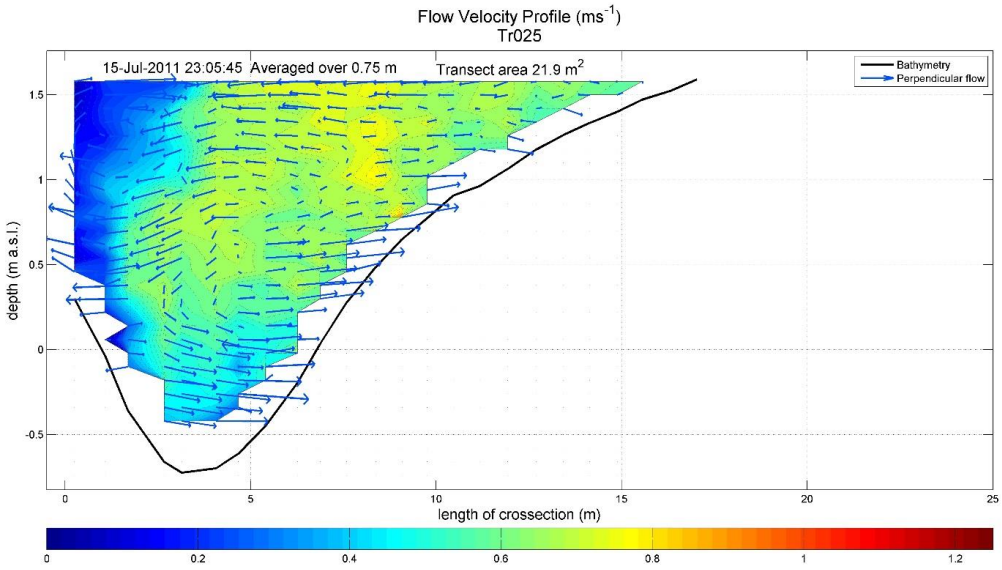
Flow Velocity Profile (ms-1)
Tr025
15-Jul-2011 23:05:45 Averaged over 0.75 m
Transect area 21.9 m2
Bathymetry
Perpendicular flow
depth (m a.s.l.)
length of crossection (m)

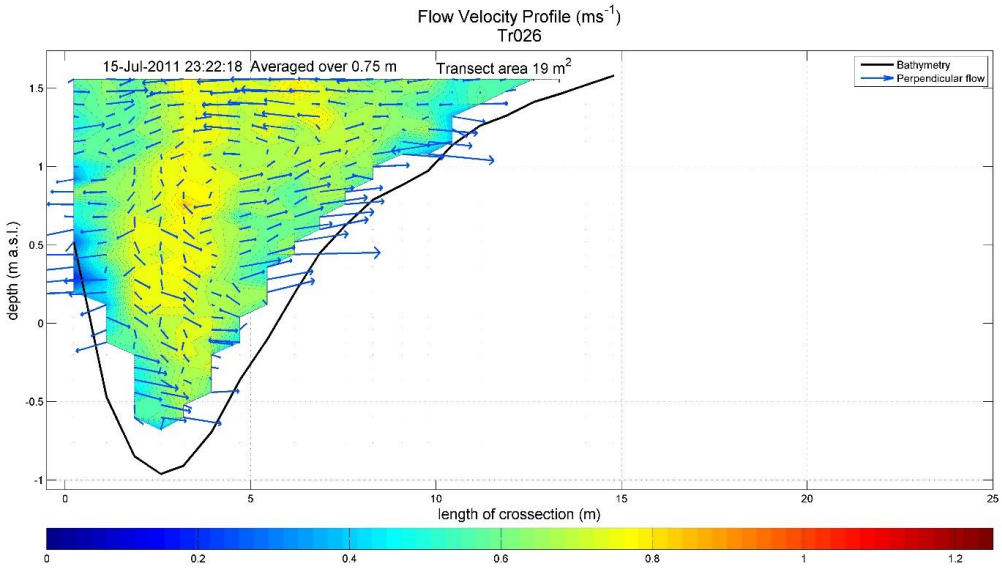
Flow Velocity Profile (ms-1)
Tr026
15-Jul-2011 23:22:18 Averaged over 0.75 m
Transect area 19 m2
Bathymetry
Perpendicular flow
depth (m a.s.l.)
length of crossection (m)

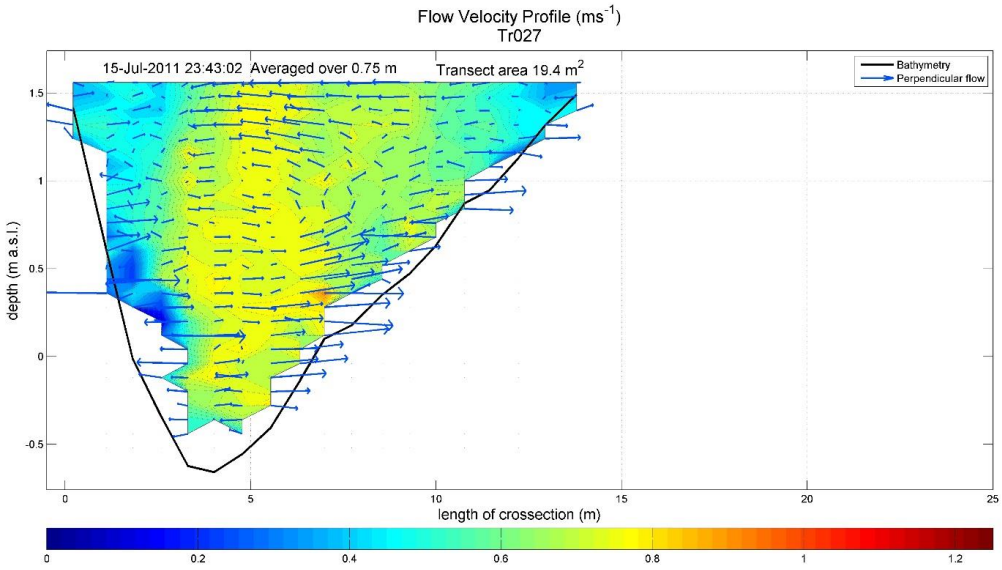
Flow Velocity Profile (ms-1)
Tr027
15-Jul-2011 23:43:02 Averaged over 0.75 m
Transect area 19.4 m2
Bathymetry
Perpendicular flow
depth (m a.s.l.)
length of crossection (m)

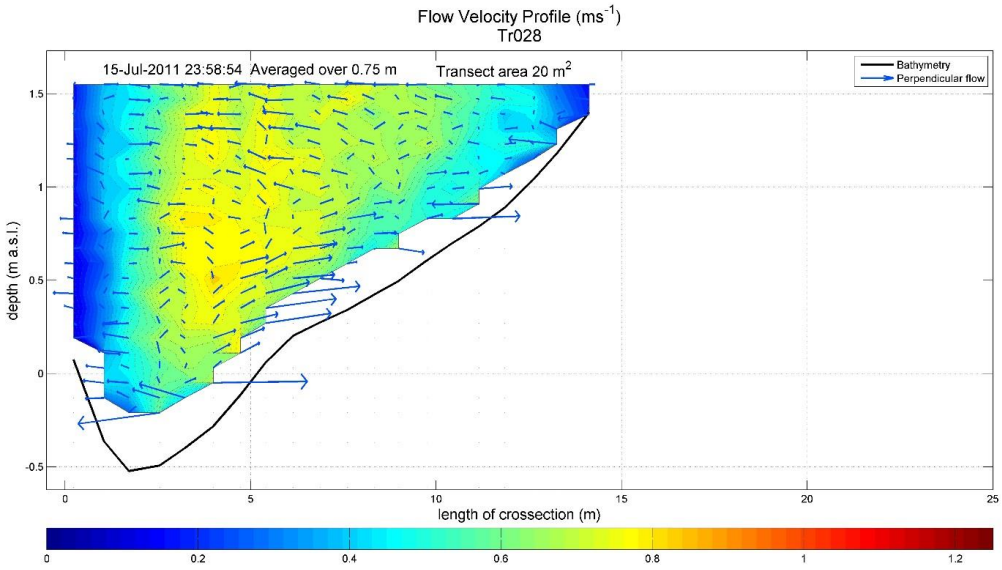
Flow Velocity Profile (ms-1)
Tr028
15-Jul-2011 23:58:54 Averaged over 0.75 m
Transect area 20 m2
Bathymetry
Perpendicular flow
depth (m a.s.l.)
length of crossection (m)

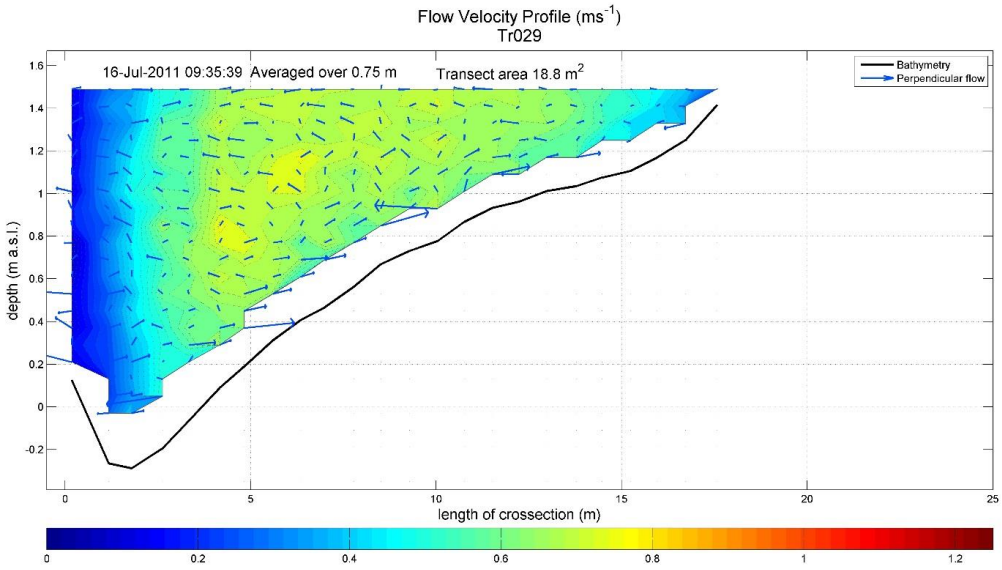
Flow Velocity Profile (ms-1)
Tr029
16-Jul-2011 09:35:39 Averaged over 0.75 m
Transect area 18.8 m2
Bathymetry
Perpendicular flow
depth (m a.s.l.)
length of crossection (m)

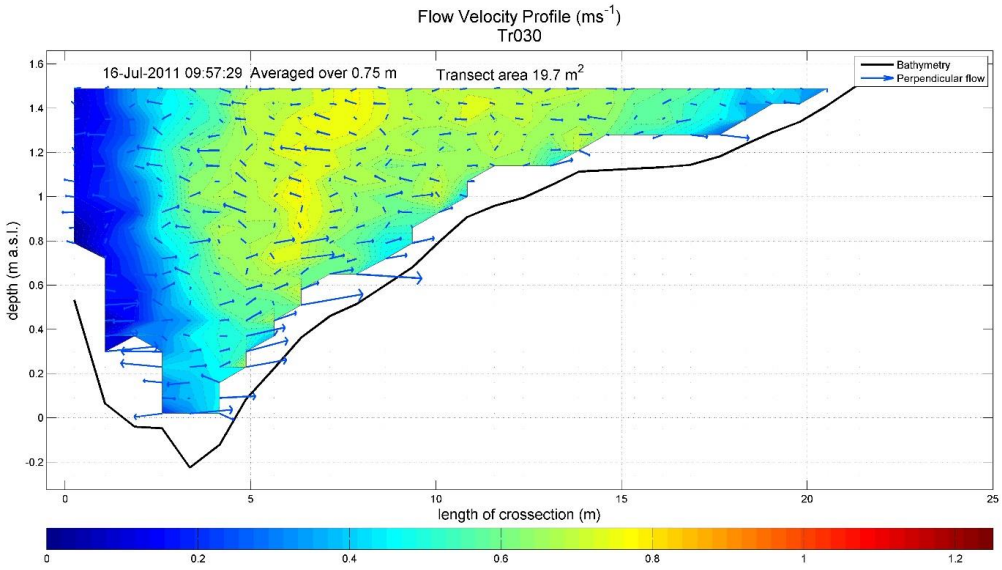
Flow Velocity Profile (ms-1)
Tr030
16-Jul-2011 09:57:29 Averaged over 0.75 m
Transect area 19.7 m2
Bathymetry
Perpendicular flow
depth (m a.s.l.)
length of crossection (m)

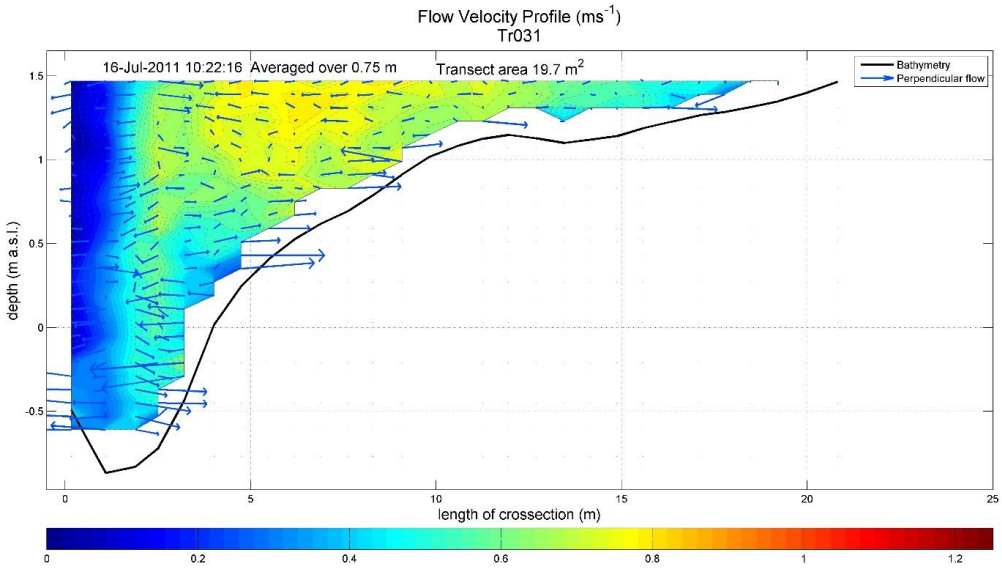
Flow Velocity Profile (ms-1)
Tr031
16-Jul-2011 10:22:16 Averaged over 0.75 m
Transect area 19.7 m2
Bathymetry
Perpendicular flow
depth (m a.s.l.)
length of crossection (m)

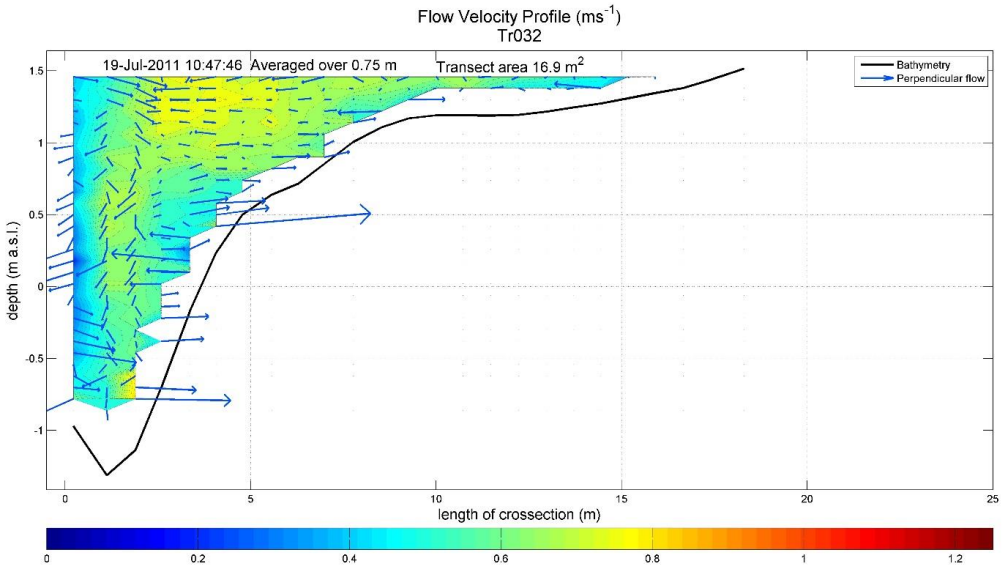
Flow Velocity Profile (ms-1)
Tr032
19-Jul-2011 10:47:46 Averaged over 0.75 m
Transect area 16.9 m2
Bathymetry
Perpendicular flow
depth (m a.s.l.)
length of crossection (m)

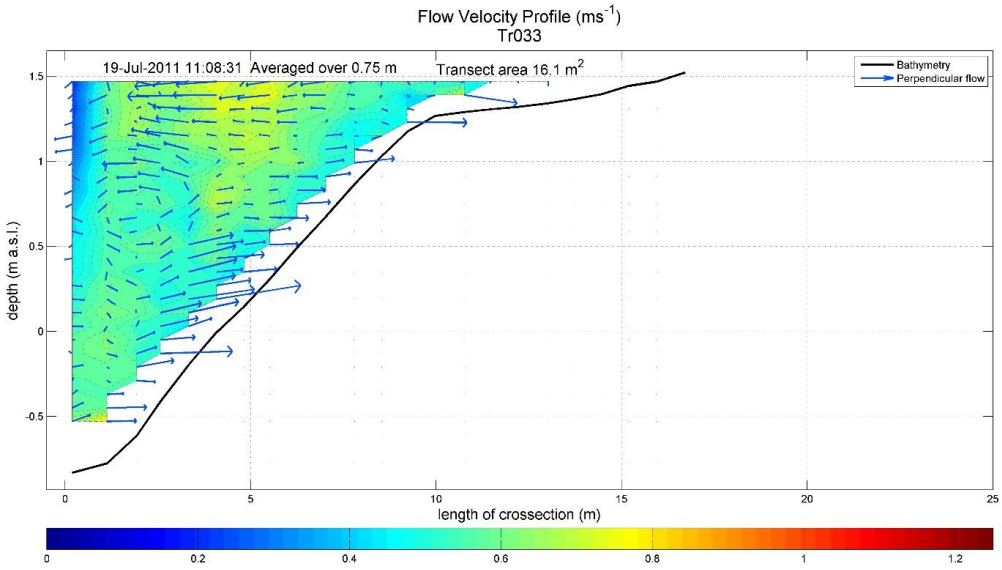
Flow Velocity Profile (ms-1)
Tr033
19-Jul-2011 11:08:31 Averaged over 0.75 m
Transect area 16.1 m2
Bathymetry
Perpendicular flow
depth (m a.s.l.)
length of crossection (m)

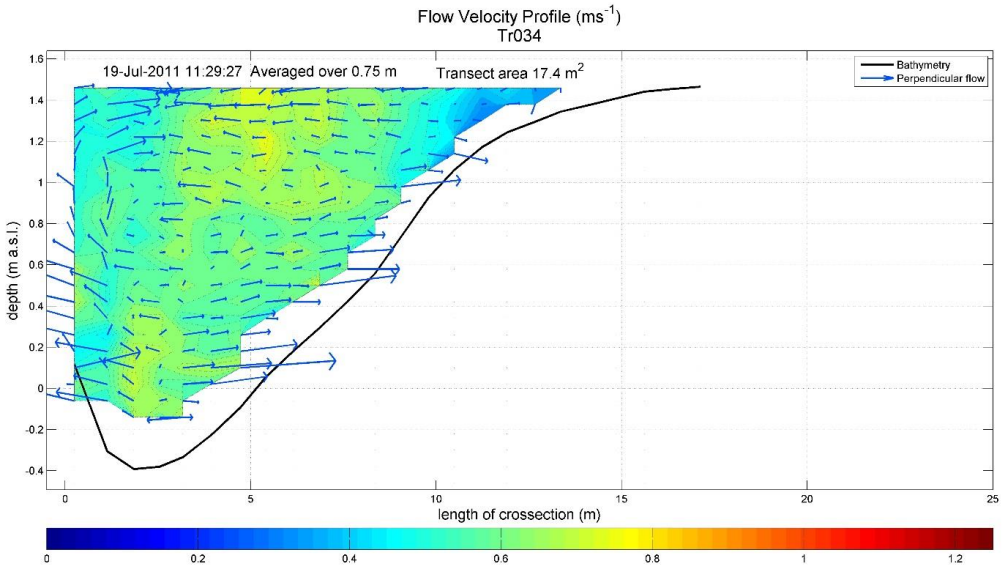
Flow Velocity Profile (ms-1)
Tr034
19-Jul-2011 11:29:27 Averaged over 0.75 m
Transect area 17.4 m2
Bathymetry
Perpendicular flow
depth (m a.s.l.)
length of crossection (m)

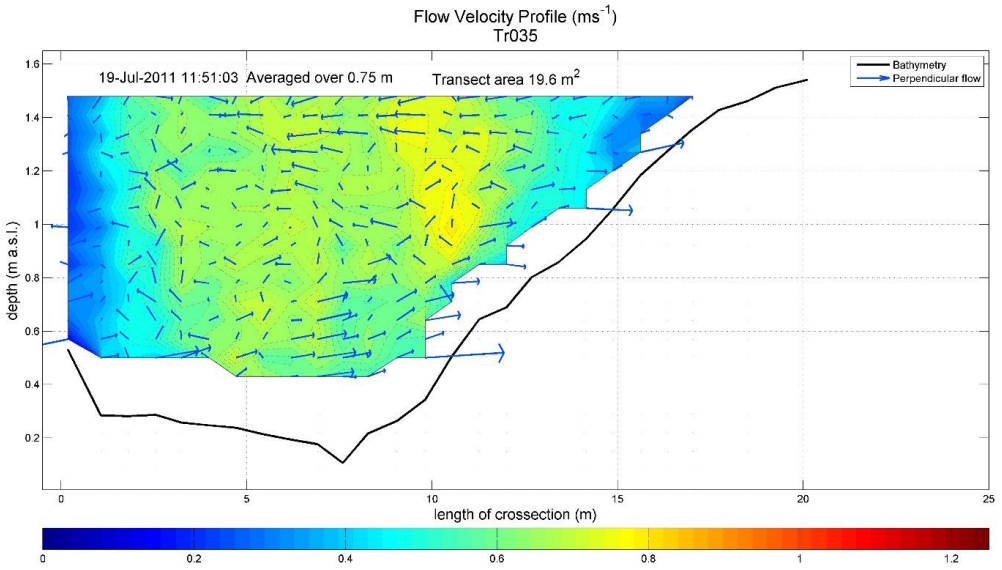
Flow Velocity Profile (ms-1)
Tr035
19-Jul-2011 11:51:03 Averaged over 0.75 m
Transect area 19.6 m2
Bathymetry
Perpendicular flow
depth (m a.s.l.)
length of crossection (m)

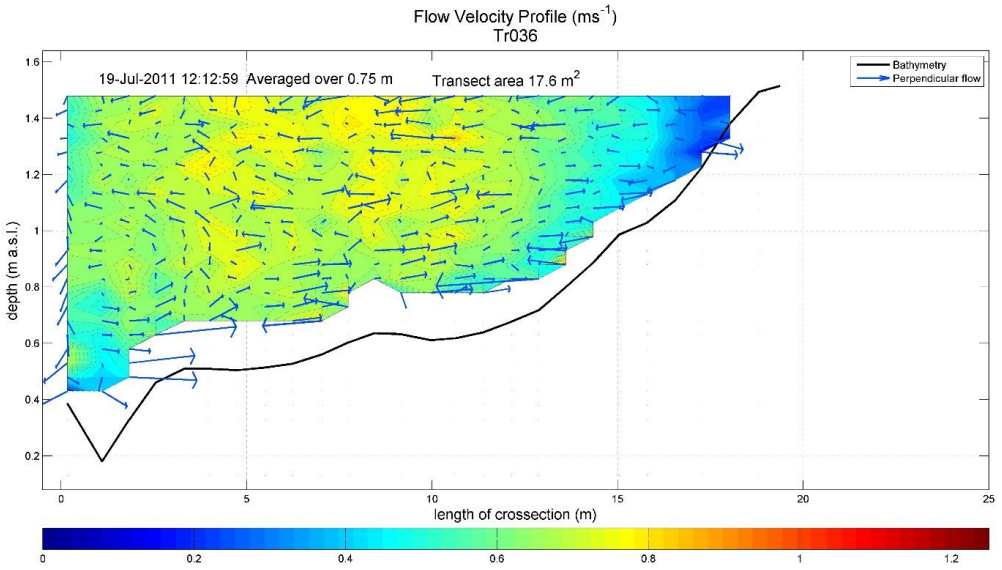
Flow Velocity Profile (ms-1)
Tr036
19-Jul-2011 12:12:59 Averaged over 0.75 m
Transect area 17.6 m2
Bathymetry
Perpendicular flow
depth (m a.s.l.)
length of crossection (m)

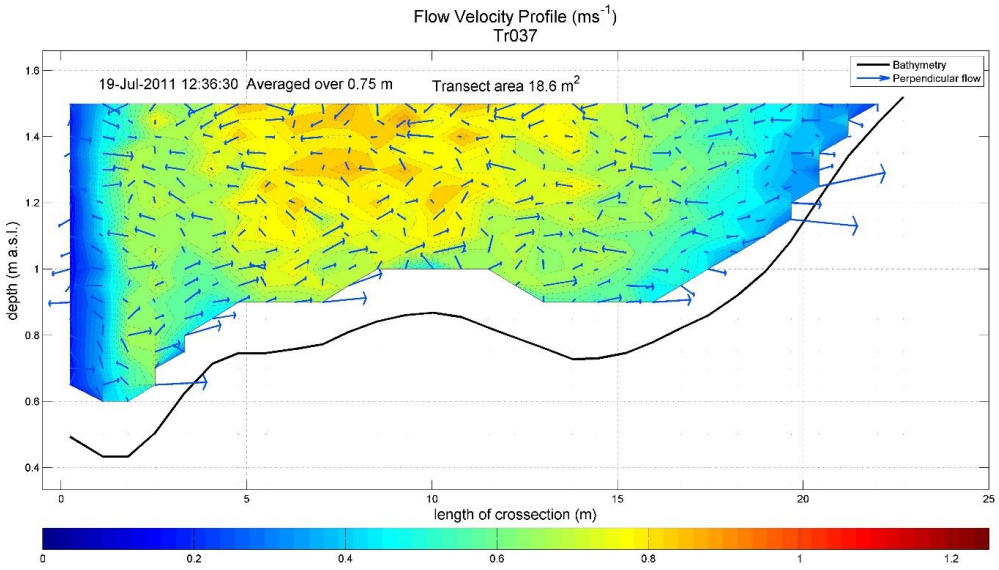
Flow Velocity Profile (ms-1)
Tr037
19-Jul-2011 12:36:30 Averaged over 0.75 m
Transect area 18.6 m2
Bathymetry
Perpendicular flow
depth (m a.s.l.)
length of crossection (m)

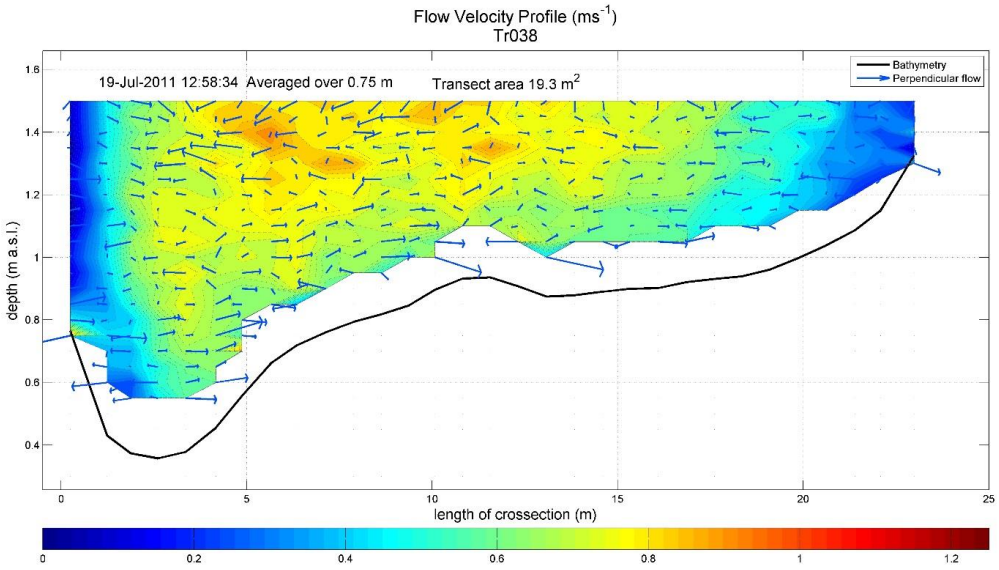
Flow Velocity Profile (ms-1)
Tr038
19-Jul-2011 12:58:34 Averaged over 0.75 m
Transect area 19.3 m2
Bathymetry
Perpendicular flow
depth (m a.s.l.)
length of crossection (m)

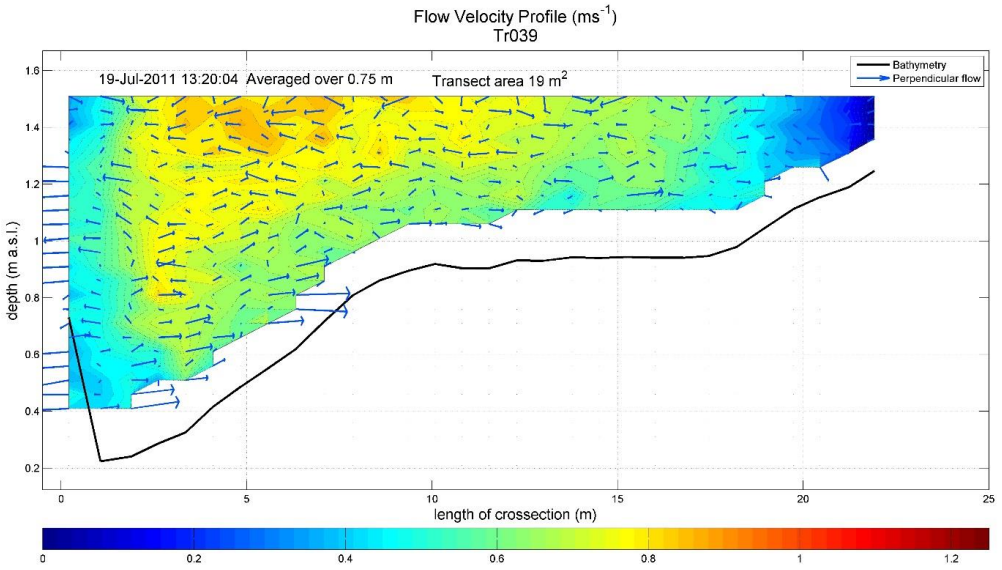
Flow Velocity Profile (ms-1)
Tr039
19-Jul-2011 13:20:04 Averaged over 0.75 m
Transect area 19 m2
Bathymetry
Perpendicular flow
depth (m a.s.l.)
length of crossection (m)

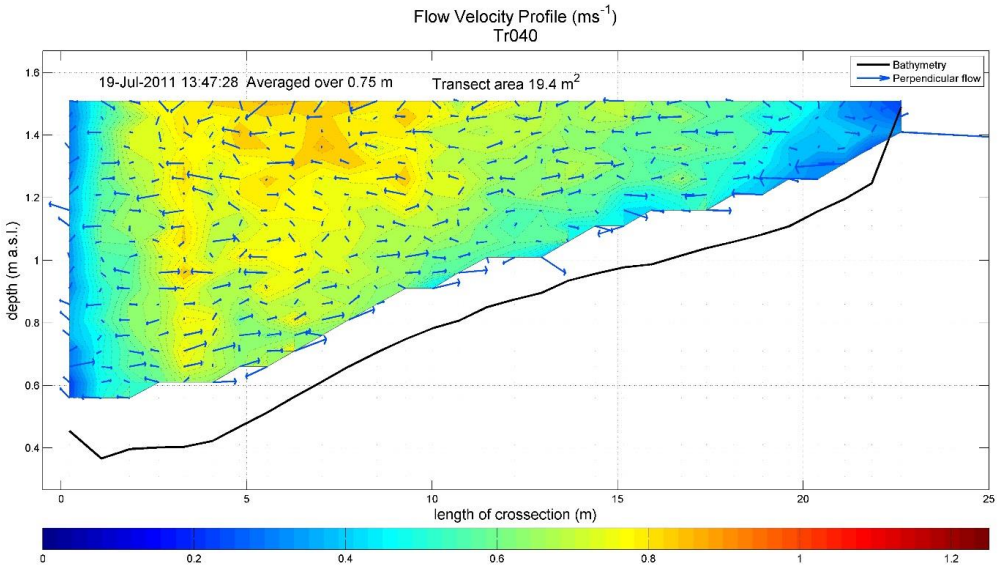
Flow Velocity Profile (ms-1)
Tr040
19-Jul-2011 13:47:28 Averaged over 0.75 m
Transect area 19.4 m2
Bathymetry
Perpendicular flow
depth (m a.s.l.)
length of crossection (m)

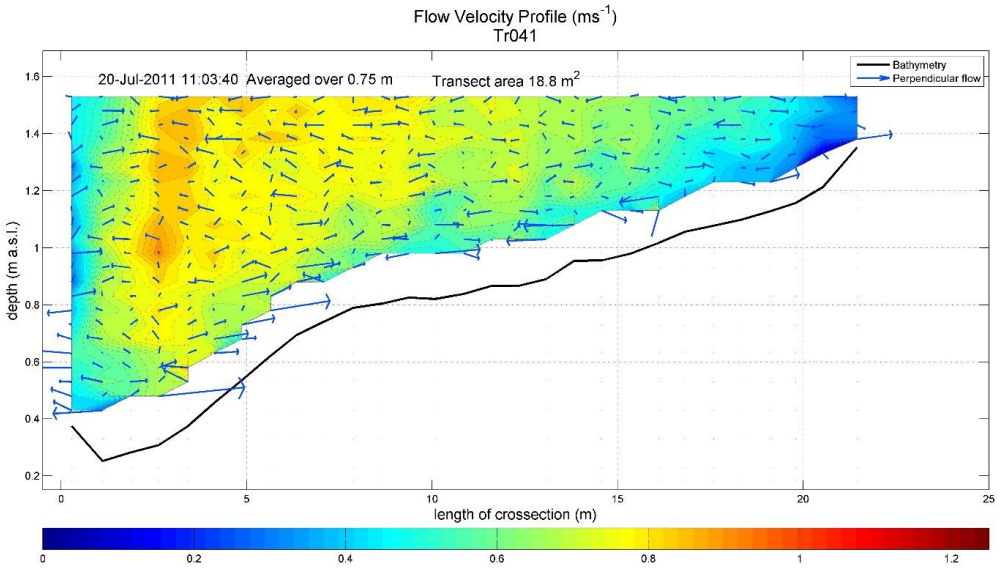
Flow Velocity Profile (ms-1)
Tr041
20-Jul-2011 11:03:40 Averaged over 0.75 m
Transect area 18.8 m2
Bathymetry
Perpendicular flow
depth (m a.s.l.)
length of crossection (m)

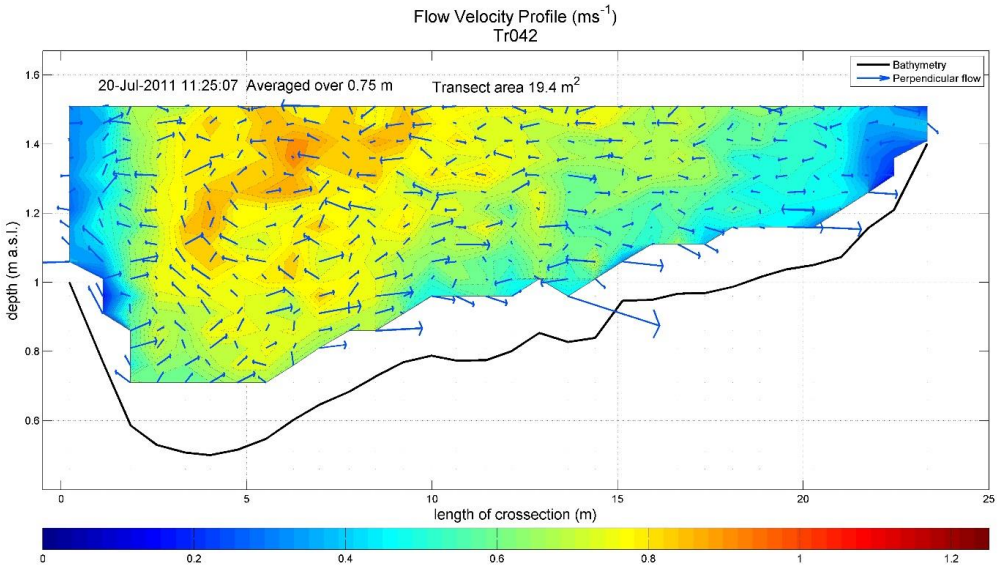
Flow Velocity Profile (ms-1)
Tr042
20-Jul-2011 11:25:07 Averaged over 0.75 m
Transect area 19.4 m2
Bathymetry
Perpendicular flow
depth (m a.s.l.)
length of crossection (m)

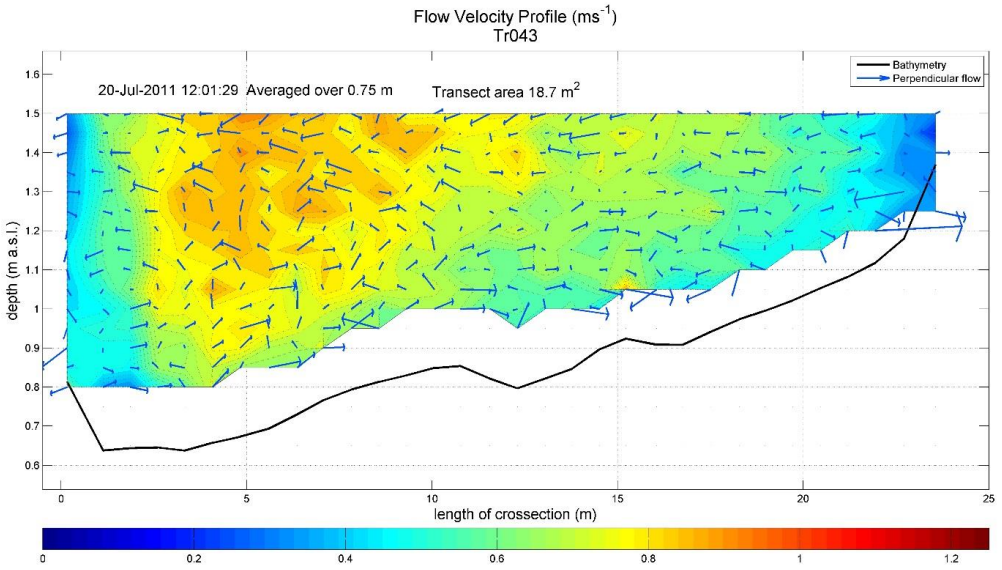
Flow Velocity Profile (ms-1)
Tr043
20-Jul-2011 12:01:29 Averaged over 0.75 m
Transect area 18.7 m2
Bathymetry
Perpendicular flow
depth (m a.s.l.)
length of crossection (m)

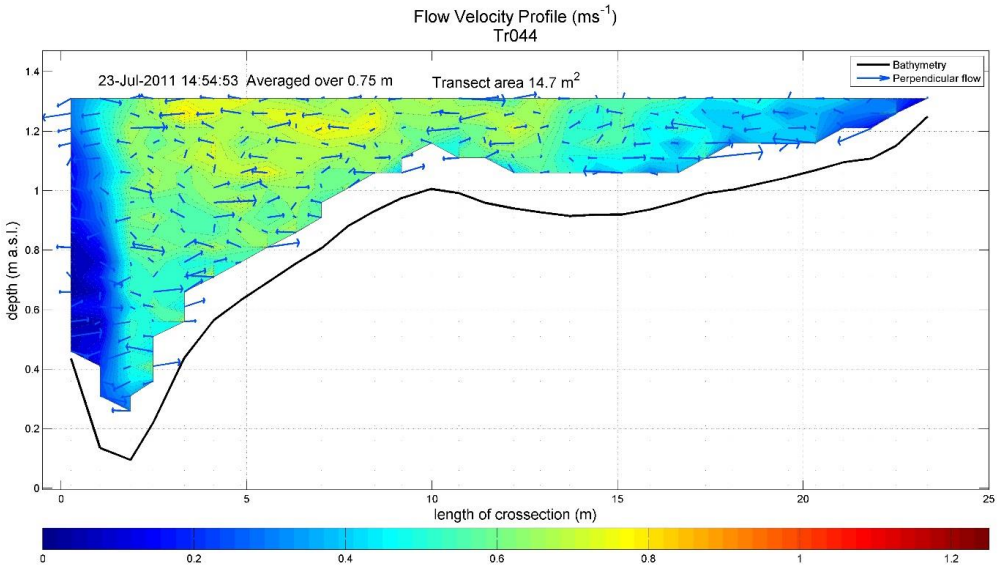
Flow Velocity Profile (ms-1)
Tr044
23-Jul-2011 14:54:53 Averaged over 0.75 m
Transect area 14.7 m2
Bathymetry
Perpendicular flow
depth (m a.s.l.)
length of crossection (m)

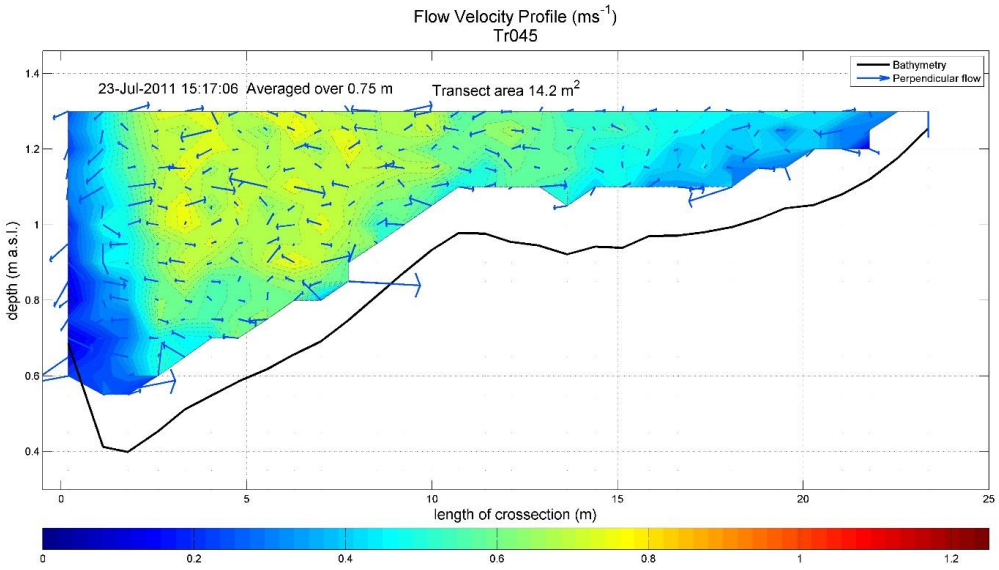
Flow Velocity Profile (ms-1)
Tr045
23-Jul-2011 15:17:06 Averaged over 0.75 m
Transect area 14.2 m2
Bathymetry
Perpendicular flow
depth (m a.s.l.)
length of crossection (m)

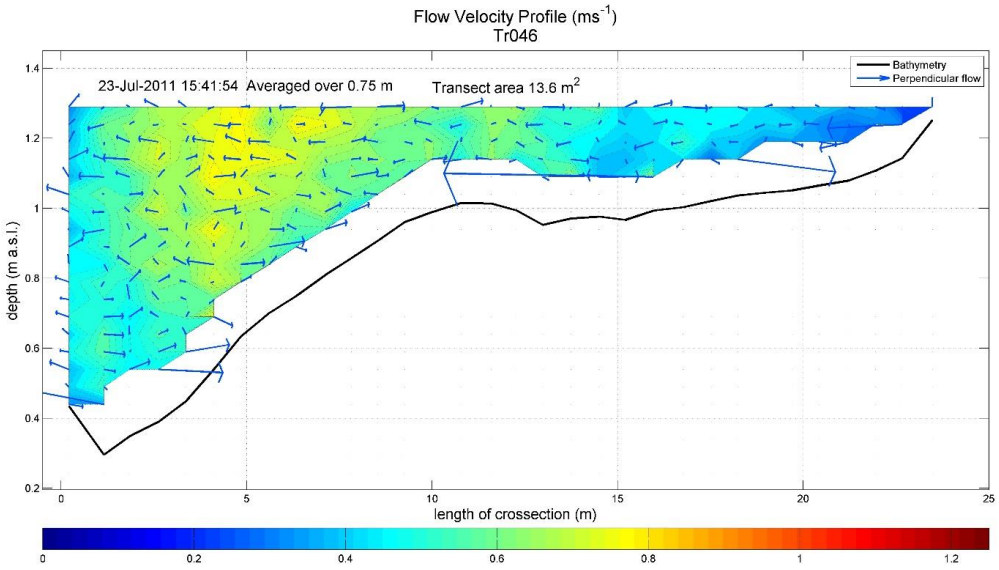
Flow Velocity Profile (ms-1)
Tr046
23-Jul-2011 15:41:54 Averaged over 0.75 m
Transect area 13.6 m2
Bathymetry
Perpendicular flow
depth (m a.s.l.)
length of crossection (m)

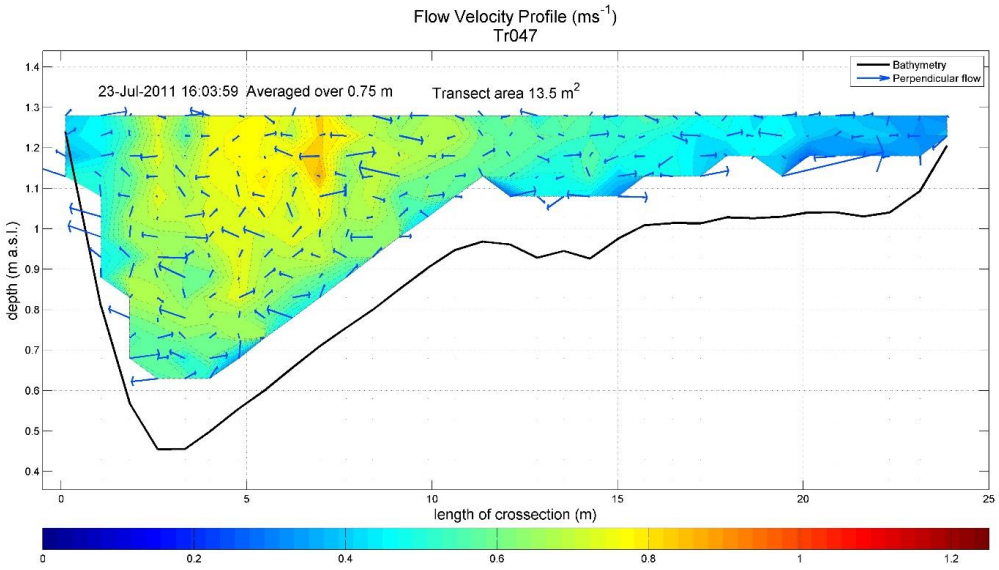
Flow Velocity Profile (ms-1)
Tr047
23-Jul-2011 16:03:59 Averaged over 0.75 m
Transect area 13.5 m2
Bathymetry
Perpendicular flow
depth (m a.s.l.)
length of crossection (m)

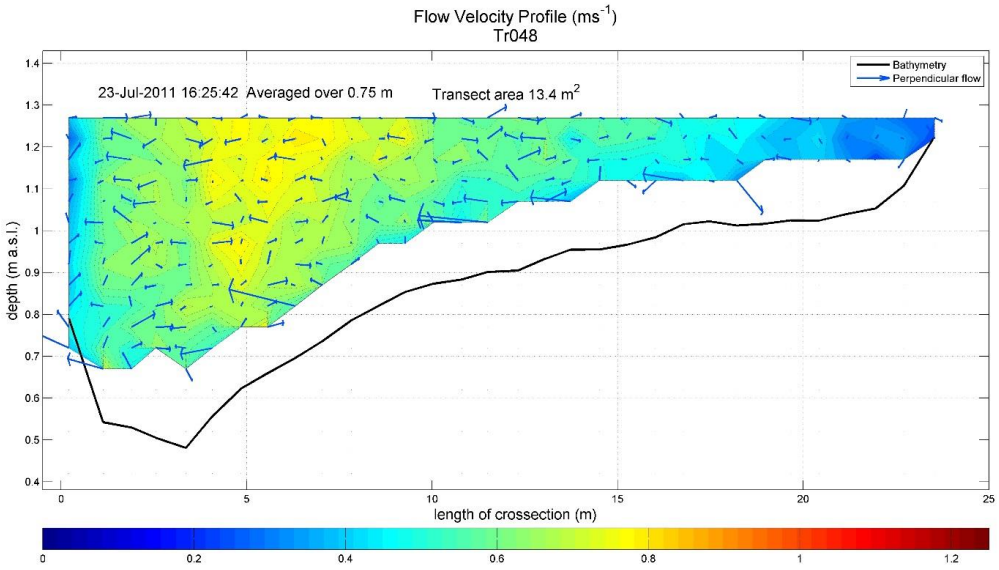
Flow Velocity Profile (ms-1)
Tr048
23-Jul-2011 16:25:42 Averaged over 0.75 m
Transect area 13.4 m2
Bathymetry
Perpendicular flow
depth (m a.s.l.)
length of crossection (m)

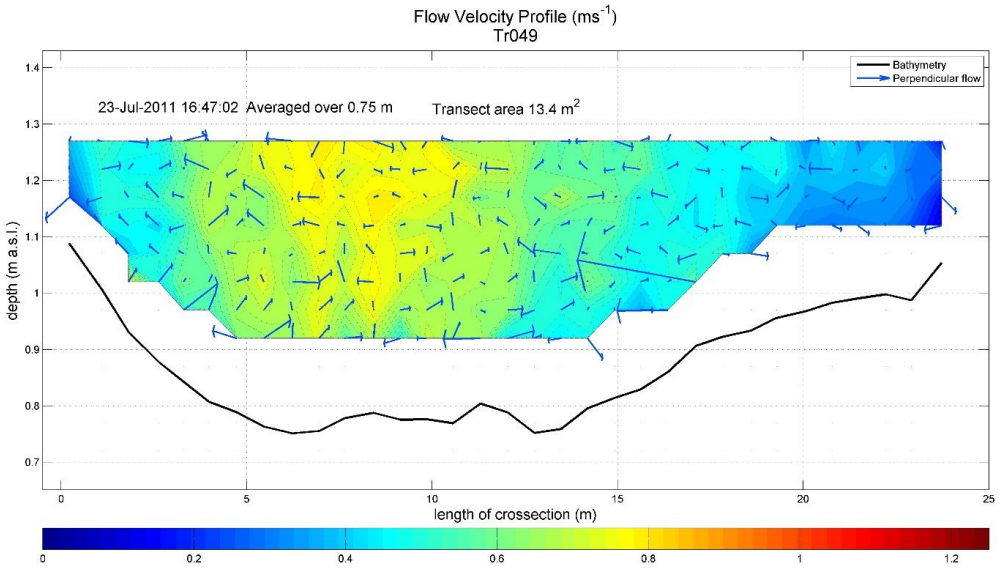
Flow Velocity Profile (ms-1)
Tr049
Bathymetry
Perpendicular flow
23-Jul-2011 16:47:02 Averaged over 0.75 m
Transect area 13.4 m2
depth (m a.s.l.)
length of crossection (m)

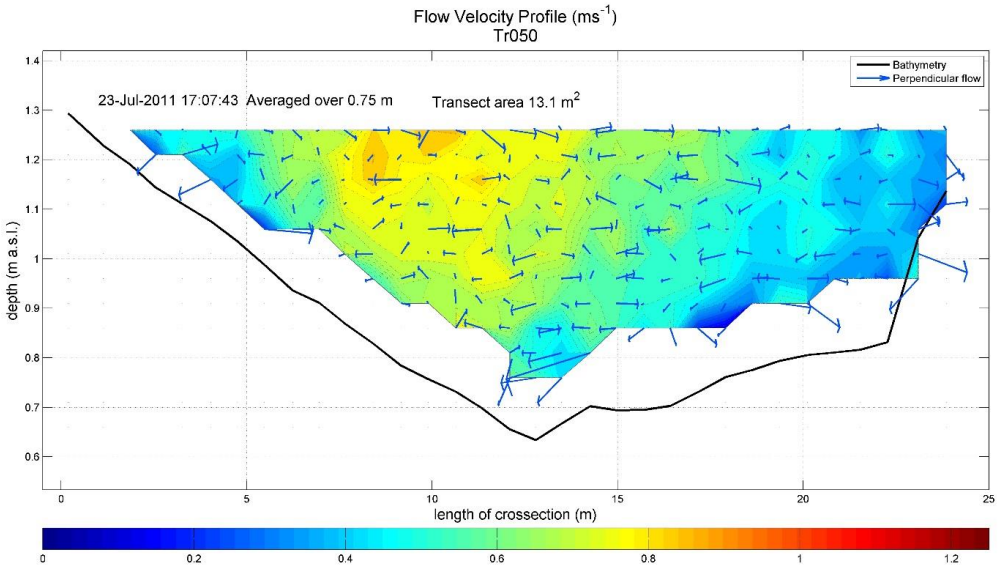
Flow Velocity Profile (ms-1)
Tr050
Bathymetry
Perpendicular flow
23-Jul-2011 17:07:43 Averaged over 0.75 m
Transect area 13.1 m2
depth (m a.s.l.)
length of crossection (m)

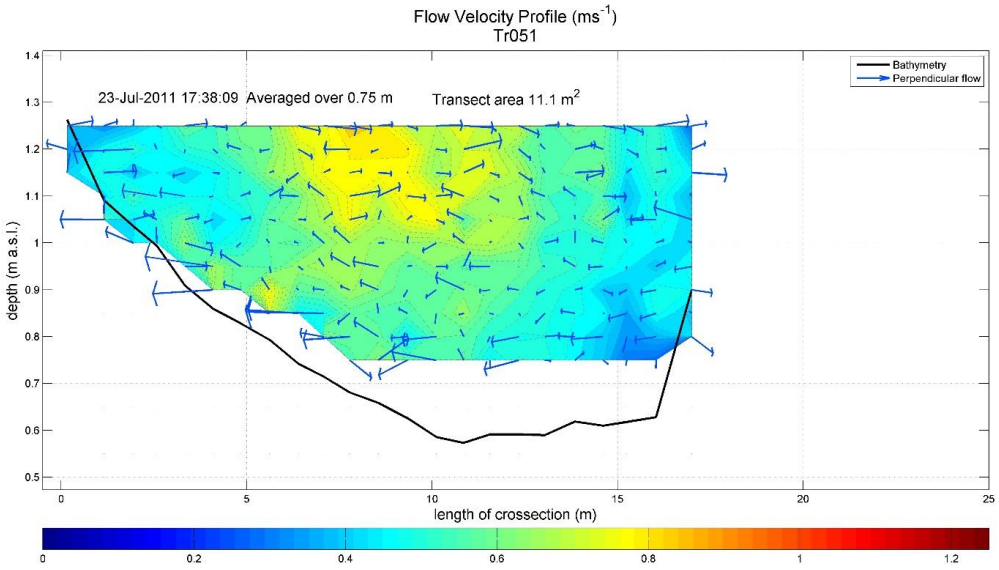
Flow Velocity Profile (ms-1)
Tr051
23-Jul-2011 17:38:09 Averaged over 0.75 m
Transect area 11.1 m2
Bathymetry
Perpendicular flow
depth (m a.s.l.)
length of crossection (m)

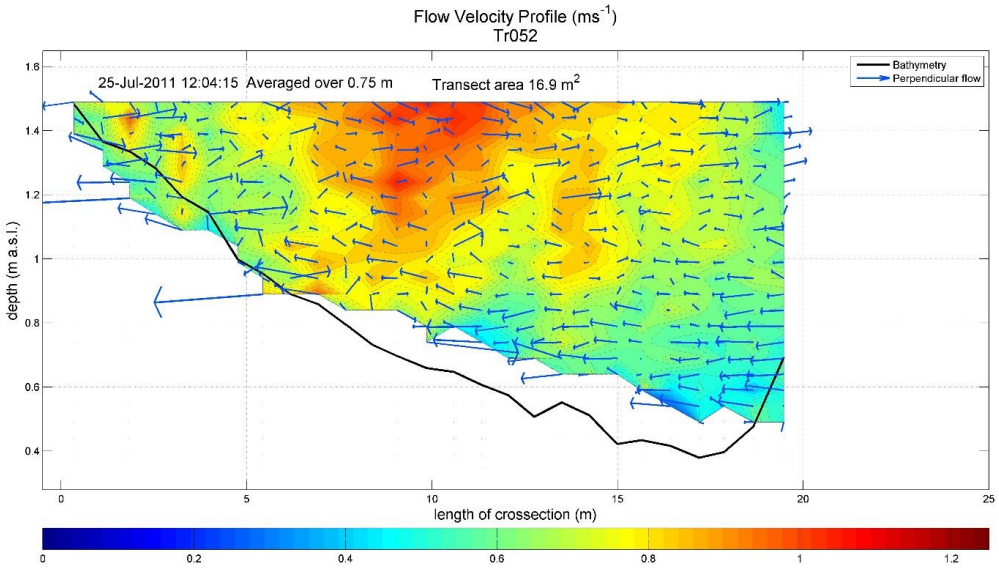
Flow Velocity Profile (ms-1)
Tr052
25-Jul-2011 12:04:15 Averaged over 0.75 m
Transect area 16.9 m2
Bathymetry
Perpendicular flow
depth (m a.s.l.)
length of crossection (m)

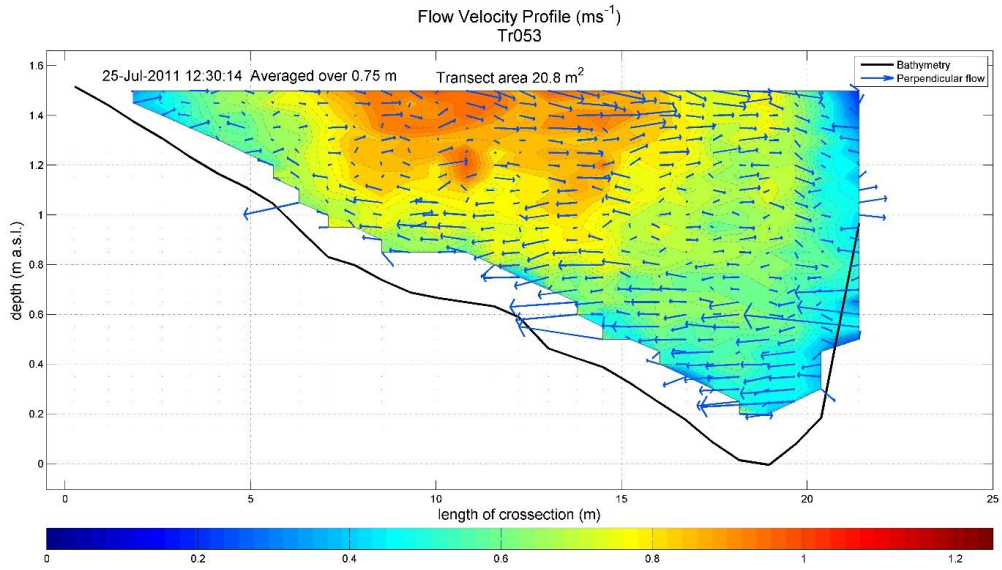
Flow Velocity Profile (ms-1)
Tr053
25-Jul-2011 12:30:14 Averaged over 0.75 m
Transect area 20.8 m2
Bathymetry
Perpendicular flow
depth (m a.s.l.)
length of crossection (m)

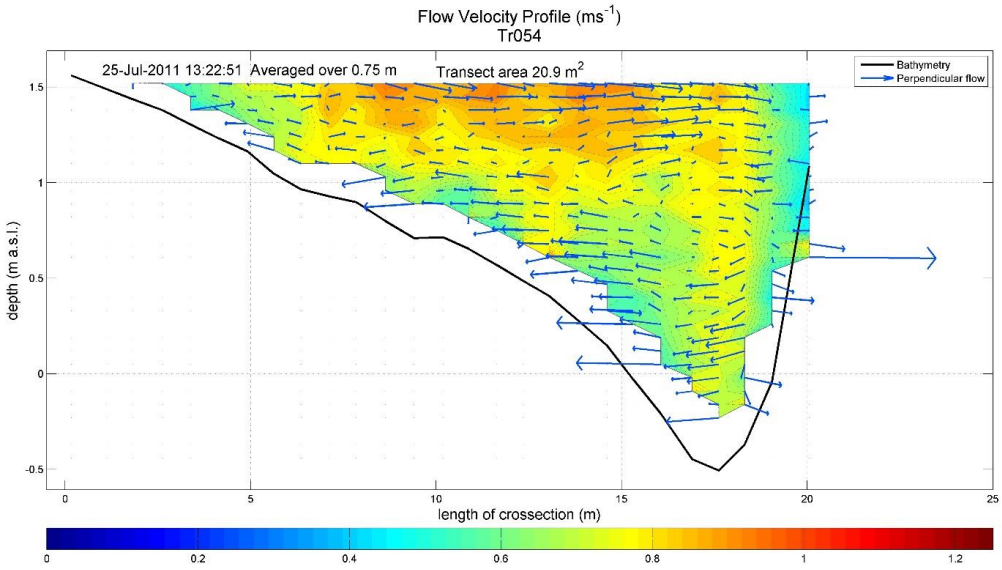
Flow Velocity Profile (ms-1)
Tr054
25-Jul-2011 13:22:51 Averaged over 0.75 m
Transect area 20.9 m2
Bathymetry
Perpendicular flow
depth (m a.s.l.)
length of crossection (m)

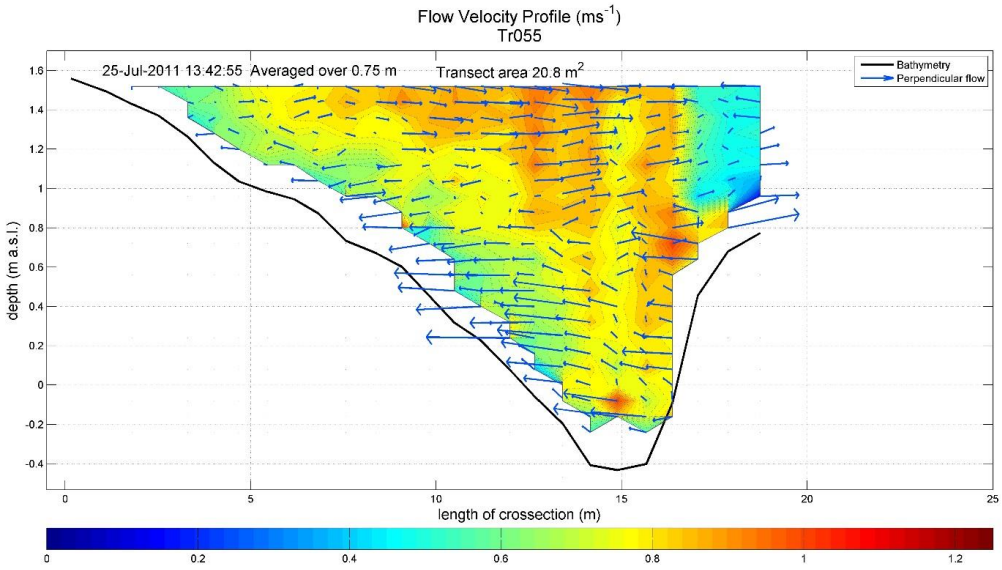
Flow Velocity Profile (ms-1)
Tr055
25-Jul-2011 13:42:55 Averaged over 0.75 m
Transect area 20.8 m2
Bathymetry
Perpendicular flow
depth (m a.s.l.)
length of crossection (m)

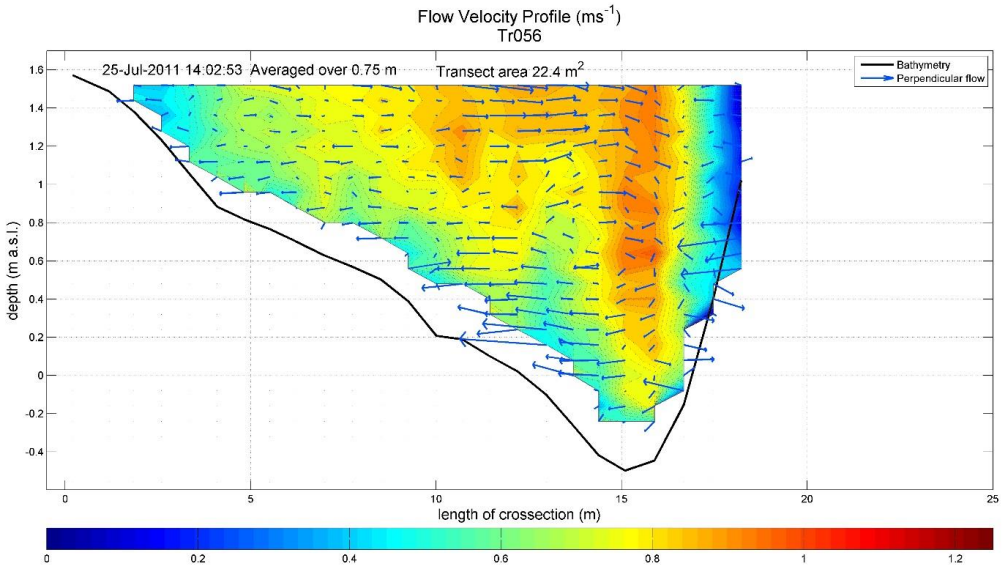
Flow Velocity Profile (ms-1)
Tr056
25-Jul-2011 14:02:53 Averaged over 0.75 m
Transect area 22.4 m2
Bathymetry
Perpendicular flow
depth (m a.s.l.)
length of crossection (m)

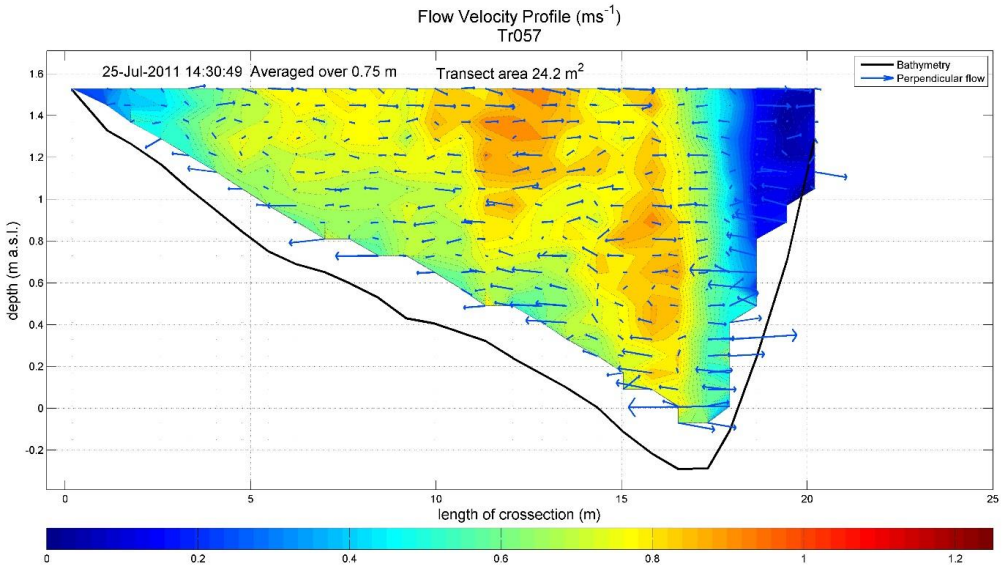
Flow Velocity Profile (ms-1)
Tr057
25-Jul-2011 14:30:49 Averaged over 0.75 m
Transect area 24.2 m2
Bathymetry
Perpendicular flow
depth (m a.s.l.)
length of crossection (m)

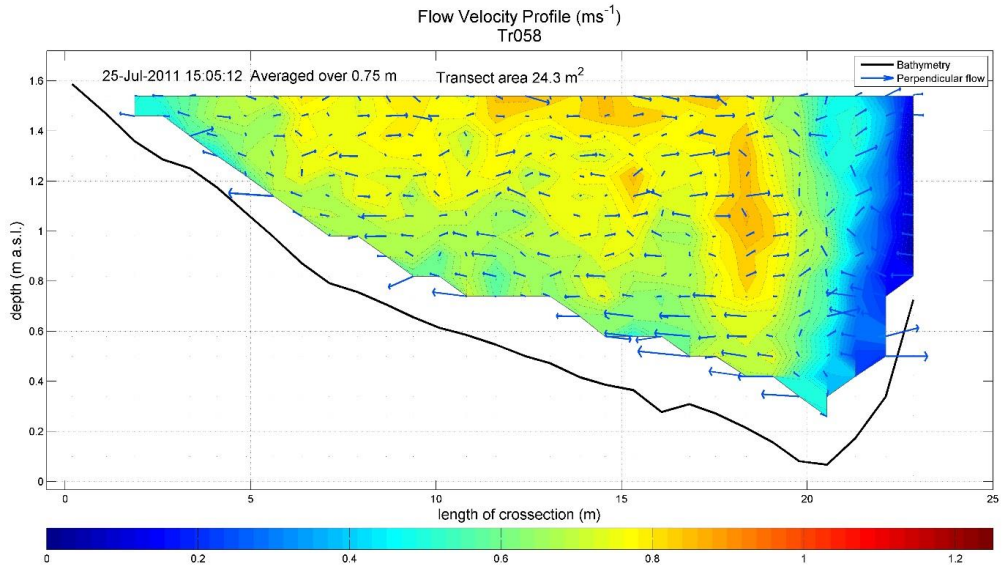
Flow Velocity Profile (ms-1)
Tr058
25-Jul-2011 15:05:12 Averaged over 0.75 m
Transect area 24.3 m2
Bathymetry
Perpendicular flow
depth (m a.s.l.)
length of crossection (m)

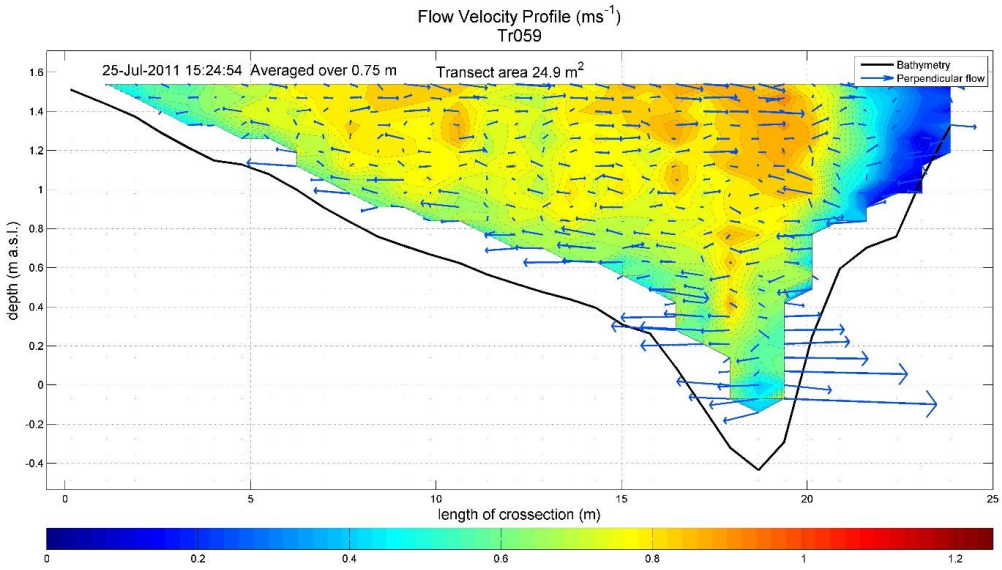
Flow Velocity Profile (ms-1)
Tr059
25-Jul-2011 15:24:54 Averaged over 0.75 m
Transect area 24.9 m2
Bathymetry
Perpendicular flow
depth (m a.s.l.)
length of crossection (m)

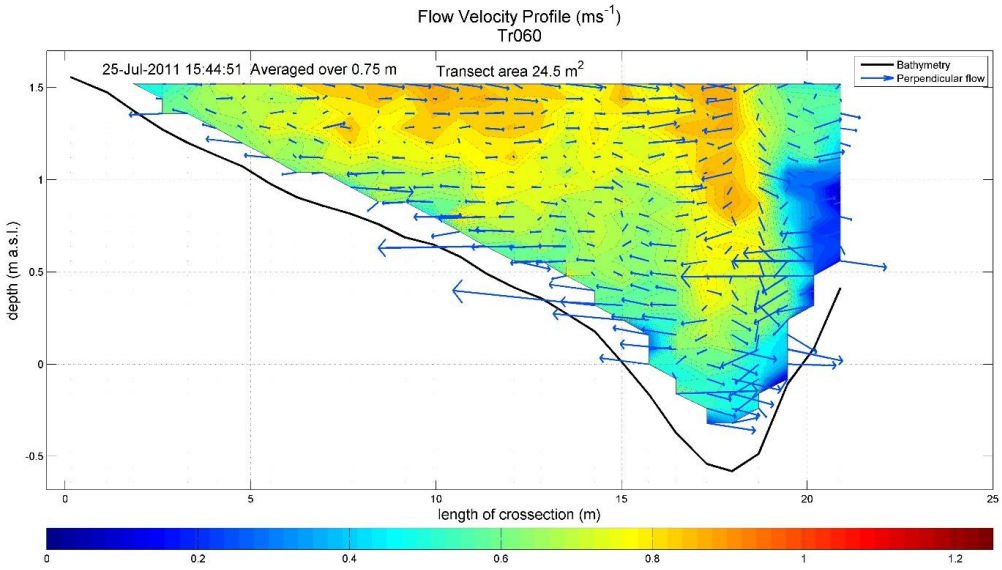
Flow Velocity Profile (ms-1)
Tr060
25-Jul-2011 15:44:51 Averaged over 0.75 m
Transect area 24.5 m2
Bathymetry
Perpendicular flow
depth (m a.s.l.)
length of crossection (m)

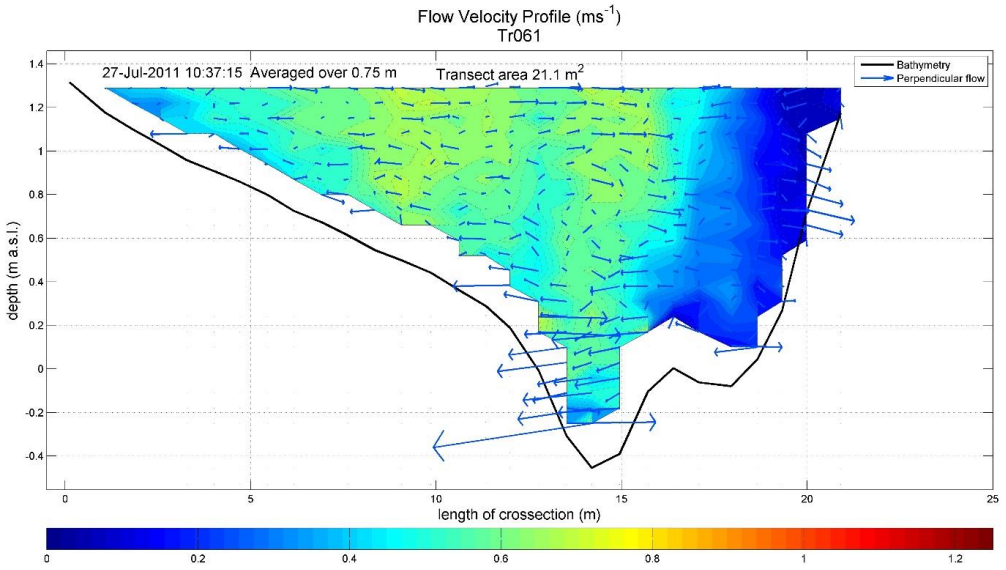
Flow Velocity Profile (ms-1)
Tr061
27-Jul-2011 10:37:15 Averaged over 0.75 m
Transect area 21.1 m2
Bathymetry
Perpendicular flow
depth (m a.s.l.)
length of crossection (m)

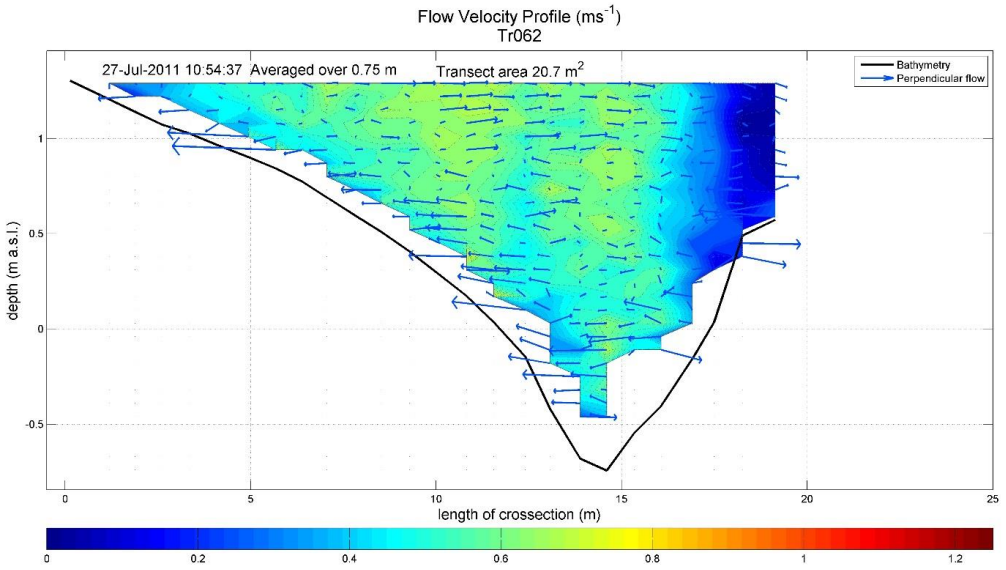
Flow Velocity Profile (ms-1)
Tr062
27-Jul-2011 10:54:37 Averaged over 0.75 m
Transect area 20.7 m2
Bathymetry
Perpendicular flow
depth (m a.s.l.)
length of crossection (m)

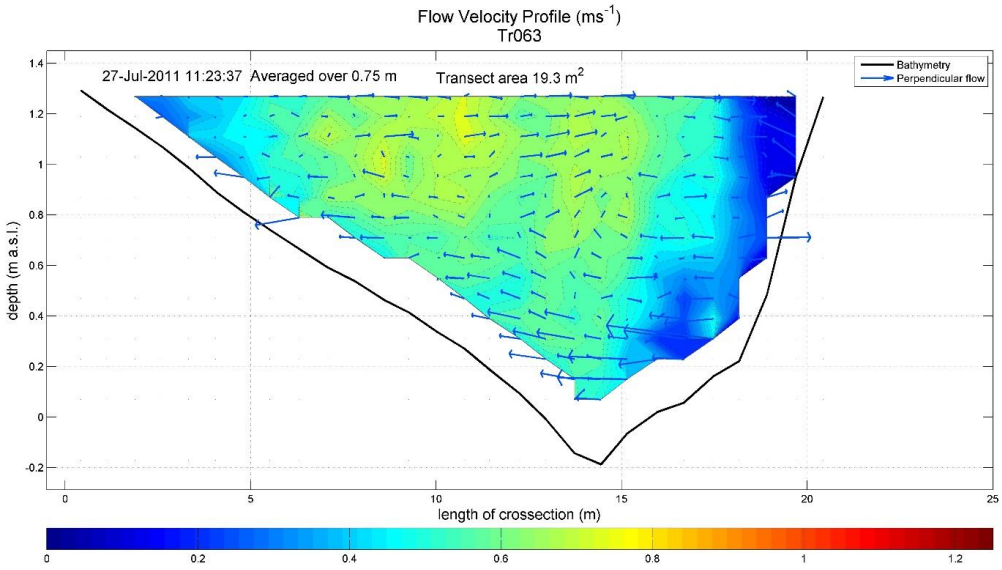
Flow Velocity Profile (ms-1)
Tr063
27-Jul-2011 11:23:37 Averaged over 0.75 m
Transect area 19.3 m2
Bathymetry
Perpendicular flow
depth (m a.s.l.)
length of crossection (m)

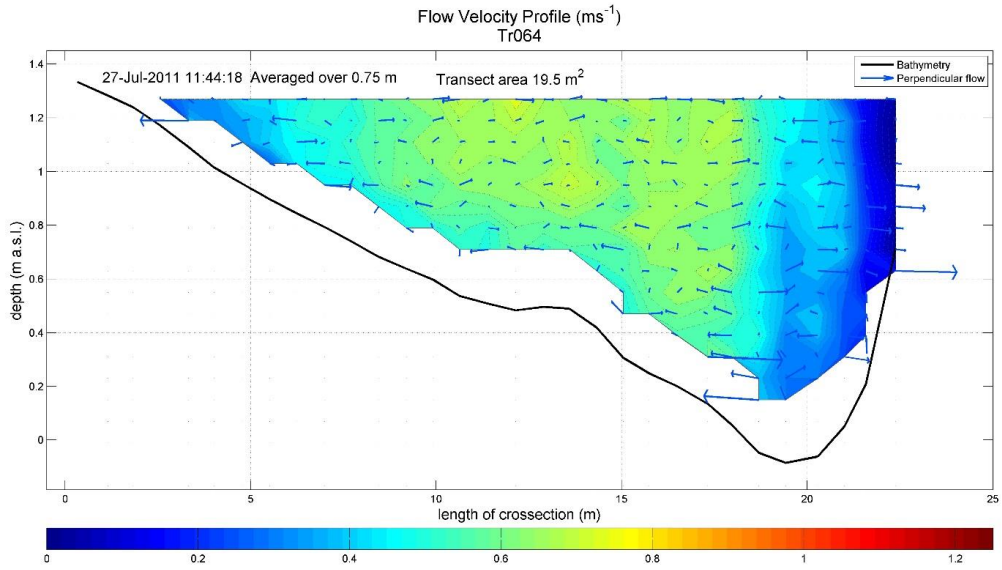
Flow Velocity Profile (ms-1)
Tr064
27-Jul-2011 11:44:18 Averaged over 0.75 m
Transect area 19.5 m2
Bathymetry
Perpendicular flow
depth (m a.s.l.)
length of crossection (m)

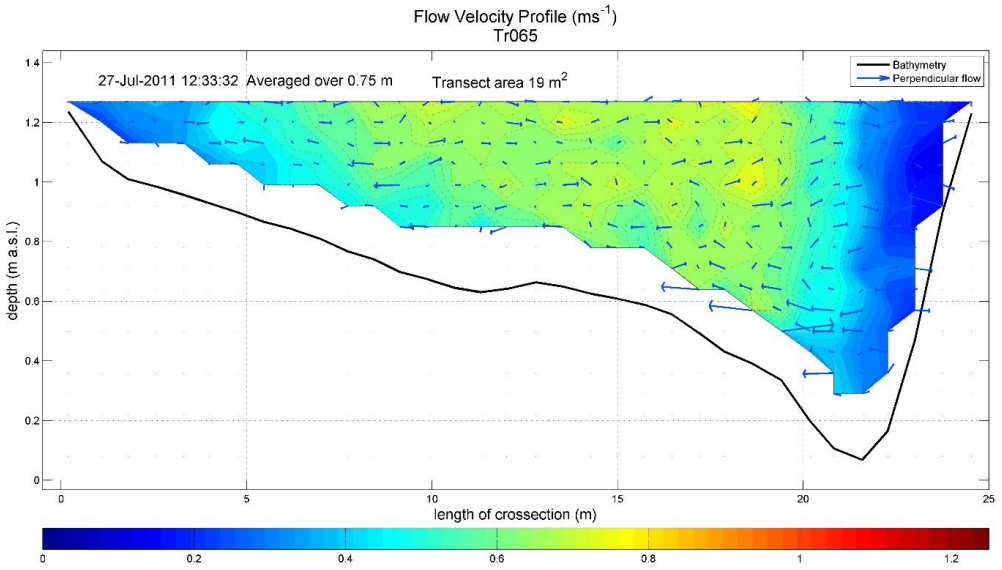
Flow Velocity Profile (ms-1)
Tr065
27-Jul-2011 12:33:32 Averaged over 0.75 m
Transect area 19 m2
Bathymetry
Perpendicular flow
depth (m a.s.l.)
length of crossection (m)

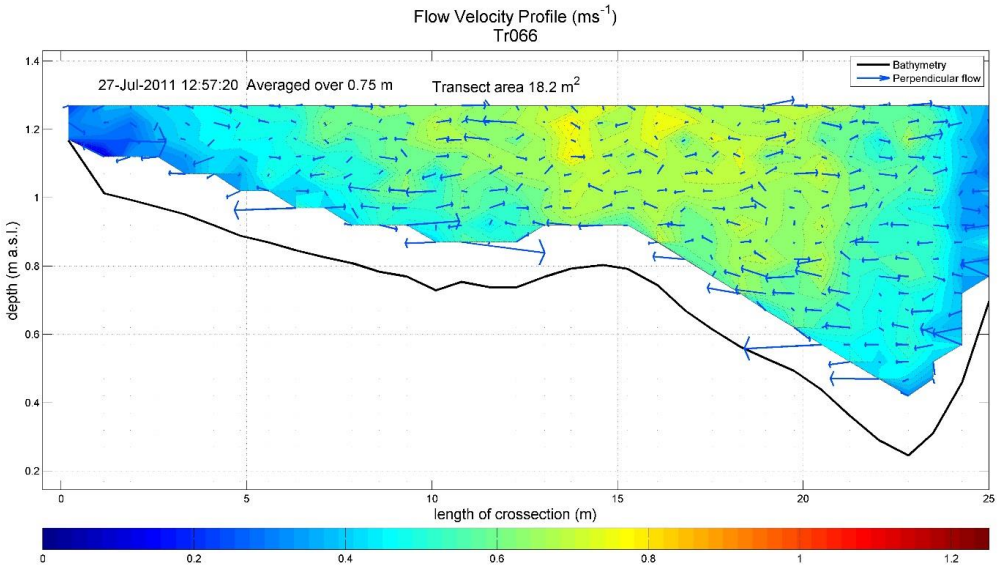
Flow Velocity Profile (ms-1)
Tr066
27-Jul-2011 12:57:20 Averaged over 0.75 m
Transect area 18.2 m2
Bathymetry
Perpendicular flow
depth (m a.s.l.)
length of crossection (m)

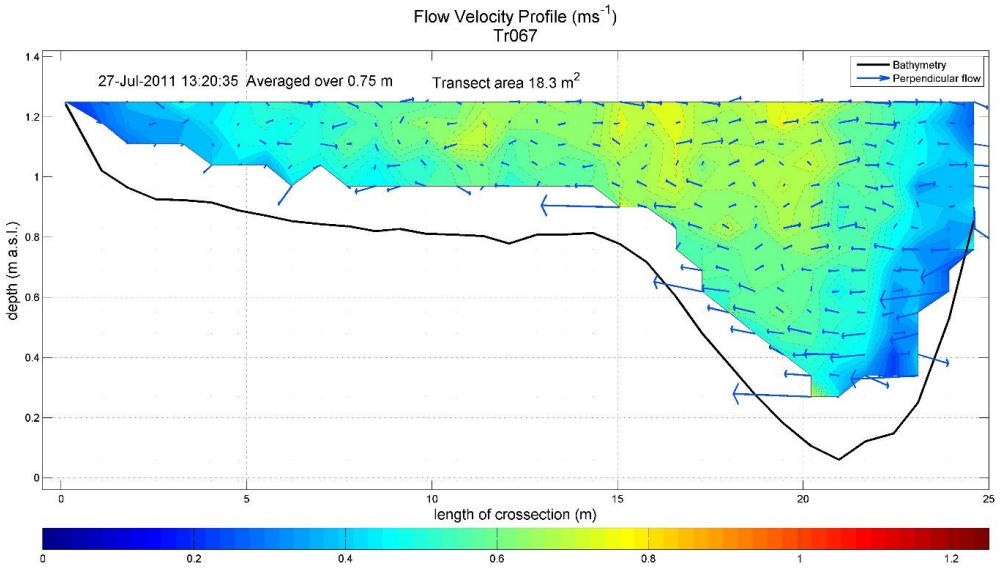
Flow Velocity Profile (ms-1)
Tr067
27-Jul-2011 13:20:35 Averaged over 0.75 m
Transect area 18.3 m2
Bathymetry
Perpendicular flow
depth (m a.s.l.)
length of crossection (m)

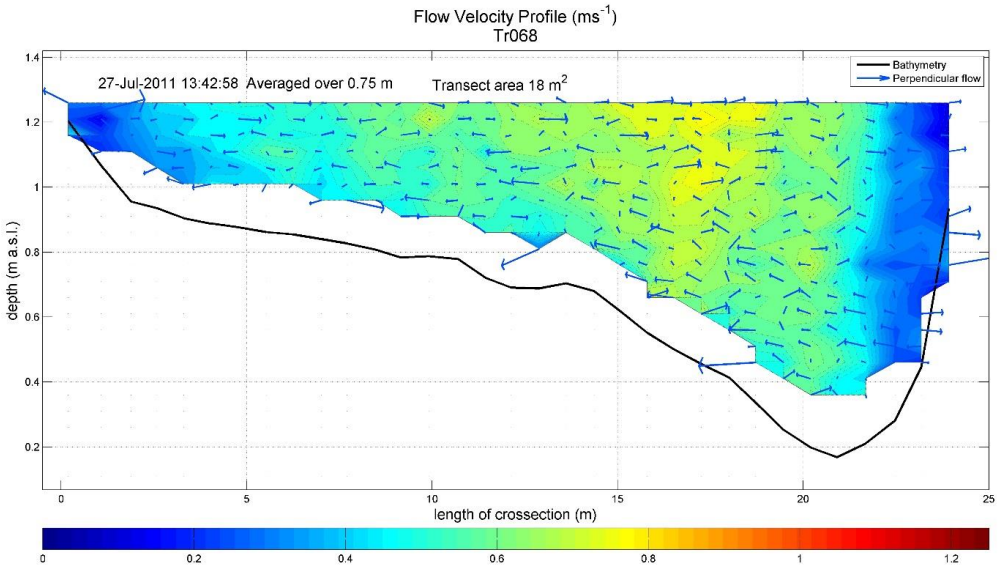
Flow Velocity Profile (ms-1)
Tr068
27-Jul-2011 13:42:58 Averaged over 0.75 m
Transect area 18 m2
Bathymetry
Perpendicular flow
depth (m a.s.l.)
length of crossection (m)

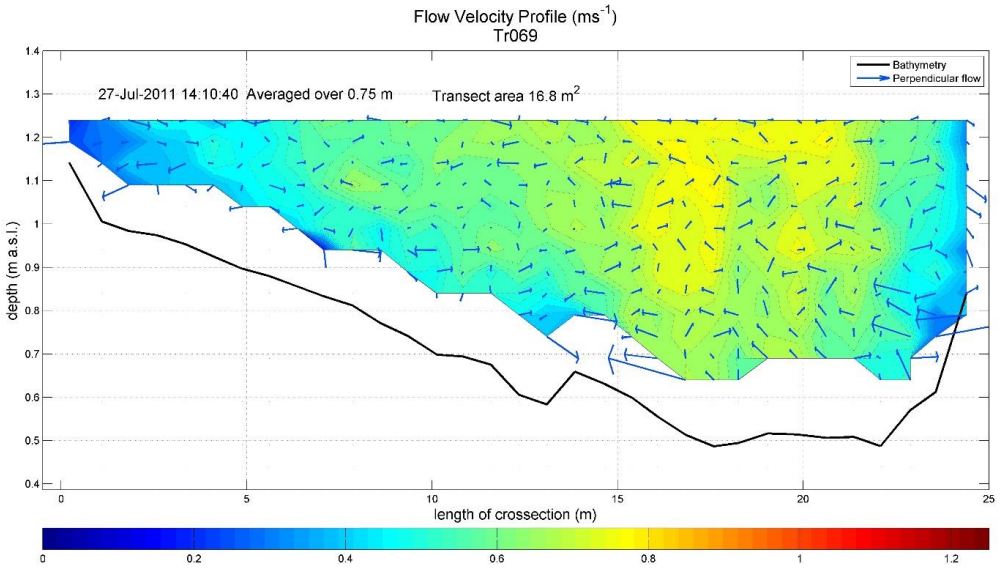
Flow Velocity Profile (ms-1)
Tr069
27-Jul-2011 14:10:40 Averaged over 0.75 m
Transect area 16.8 m2
Bathymetry
Perpendicular flow
depth (m a.s.l.)
length of crossection (m)

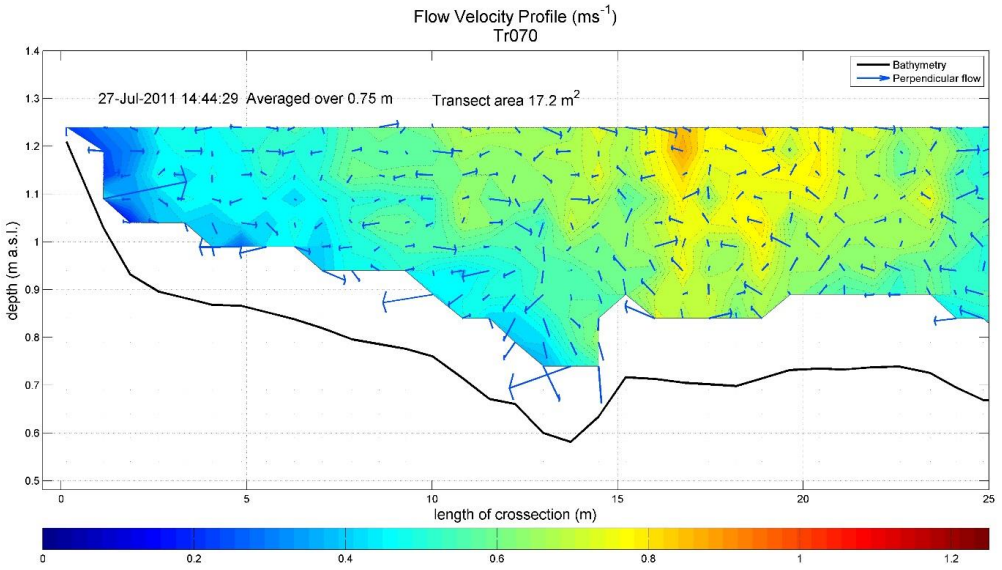
Flow Velocity Profile (ms-1)
Tr070
27-Jul-2011 14:44:29 Averaged over 0.75 m
Transect area 17.2 m2
Bathymetry
Perpendicular flow
depth (m a.s.l.)
length of crossection (m)

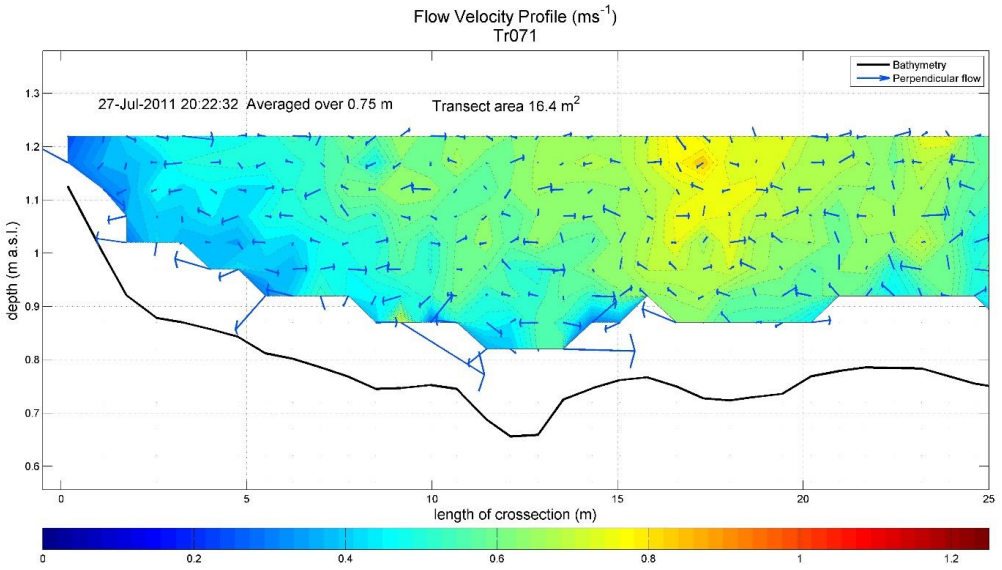
Flow Velocity Profile (ms-1)
Tr071
Bathymetry
Perpendicular flow
27-Jul-2011 20:22:32 Averaged over 0.75 m
Transect area 16.4 m2
depth (m a.s.l.)
length of crossection (m)

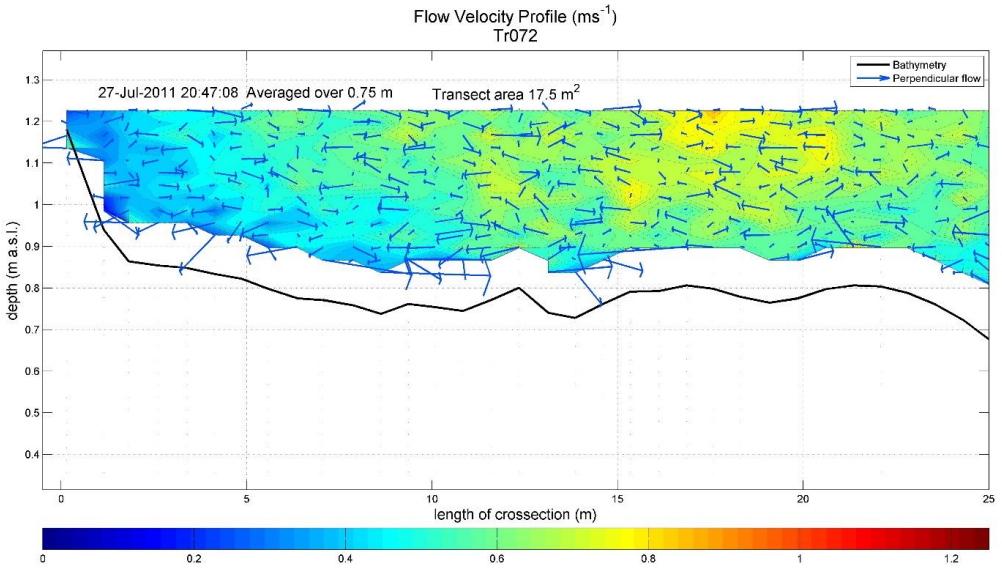
Flow Velocity Profile (ms-1)
Tr072
Bathymetry
Perpendicular flow
27-Jul-2011 20:47:08 Averaged over 0.75 m
Transect area 17.5 m2
depth (m a.s.l.)
length of crossection (m)

ISBN 978-82-326-3902-1 (printed version)
ISBN 978-82-326-3903-8 (electronic version)
ISSN 1503-8181

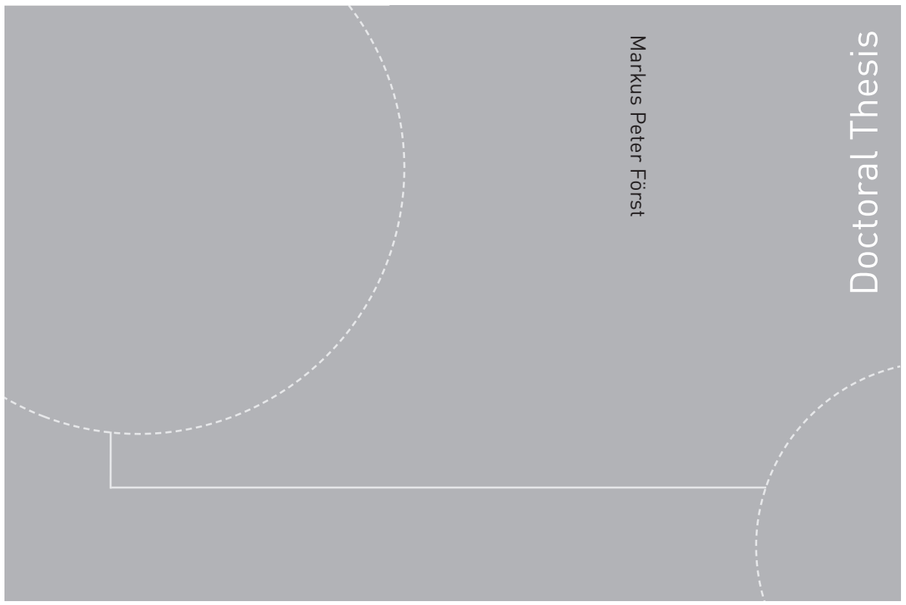

Doctoral theses at NTNU, 2019:152

Markus Peter Först

Effects of Flow Dynamics on Bank Erosion in Consecutive Meander Bends.

A Field Study

NTNU
Norwegian University of
Science and Technology
Faculty of Engineering
Department of Civil and Environmental Engineering

NTNU
Norwegian University of
Science and Technology

Doctoral theses at NTNU, 2019:152

NTNU

NTNU
Norwegian University of
Science and Technology